Seismic Vulnerability Analysis of Major Ethiopian Dams with Emphasis on Dam Safety Evaluation

Dissertation submitted to the School of Graduate Studies of Addis Ababa University in Fulfilment of the Requirements for a Doctorate Degree

Ali Aman

School of Graduate Studies

Addis Ababa University

Addis Ababa, Ethiopia

February 2020

Addis Ababa University

School of Graduate studies

This is to certify that the thesis prepared by Ali Aman, entitled: Seismic Vulnerability Analysis of Major Ethiopian Dams with Emphasis on Dam Safety Evaluation and submitted in fulfilment of the requirements for the Degree of Doctor of Philosophy in Geophysics (Engineering Seismology) comply with the regulations of the University and meets the accepted standards with respect to originality and quality.

Signed by the Examining committee:

Examiners: Prof. Gerald Zenz (Graz University of Technology, Austria)

Signature: Date: 23/7/2020

Dr. Ketsela Tadesse (Ethiopia)

Signature: Date: 23/7/2020

Advisors: Prof. Tilahun Mammo (Addis Ababa University, Ethiopia)

Signature: Date: 23/7/2020

Dr. Martin Wieland (ICOLD Chairman on seismic aspect of dam design, Switzerland)

Signature: Date: 23/07/2020

Chair of Department or Graduate program Coordinator

Abstract

Dams are critical facilities, which require special consideration to ensure their long-term safety. Among the safety concerns for large storage dams, seismic safety plays an important role, particularly for dams located close to the seismically active regions like the East African Rift System. Large dams in such seismically active regions must be capable of resisting severe earthquake ground motion expected at the dam site without uncontrolled release of water impounded in the reservoir. This can be achieved by conducting a comprehensive site-specific seismic hazard analysis, proper seismic design, adequate construction quality control, and appropriate operation and timely maintenance for upgrading any seismic deficiency, particularly for older dams. The main factor contributing to the risk of large storage dams is the water stored in the reservoir. Some of the reservoirs in Ethiopia are very large. In this dissertation, the seismic safety evaluation of large Ethiopian dams is analysed, which includes the review of previous works, site-specific seismic hazard evaluations, seismic risk analysis and detailed seismic safety analysis.

A review of the seismic design criteria used for large dams in Ethiopia shows that different criteria were considered and, in some cases, the poorly known seismic activity in the project region was ignored. In some dams, modern design and safety criteria were used whereas in other projects out-dated seismic design guidelines and codes were employed. As a result, the existing, under construction and planned dams require detailed seismic safety reviews to comply with modern seismic safety criteria.

The dam sites are located in variable geological and tectonic settings, which are responsible for the spatial variability of the seismicity at dam sites. The main tectonic structure in Ethiopia is the Main Ethiopian Rift (MER), which is characterized by its extensional tectonic nature, seismically active faults and major fractures that affect the safety of dams and may cause water losses from the reservoirs. This requires an extensive geological investigation beyond the footprint of the dam.

For the seismic hazard study, the seismogenic source zones were modelled by integrating the information developed from the regional geology, tectonics, seismic

energy release map, and observed seismicity. The seismic hazard analyses were conducted based on the probabilistic approach and a seismic hazard map is developed for the horizontal component of the peak ground acceleration (PGA) for a return period of 10,000 years. Six seismic zones are delineated in this map. In addition, for the different seismic zones, an estimation of the future power and irrigation potential of Ethiopia is made. Moreover, the dam sites are ranked according to the PGA-values for return periods of 10,000 years. These results are used as input for the seismic risk analysis.

The seismic risk of 30 large Ethiopian dams was evaluated. In the risk analyses, the levels of seismic hazard for which the dam is exposed, the vulnerability of the dam, and the consequences in the case of uncontrolled release of water from the reservoir were considered. Based on the risk analysis results, the following five dams Gibe III, GERD Saddle dam, Gidabo, Tendaho, and Tekeze dams were selected for detailed site-specific hazard evaluation and seismic safety analysis. In the site-specific seismic hazard analyses, multiple earthquake effects were taken into account. For the nonlinear stress, deformation and stability analyses acceleration time histories were used, which match the acceleration response spectra obtained from the seismic hazard analysis.

Gibe III dam is an RCC gravity dam with a height of 243 m. It is the world's highest RCC dam. The dam site is located at the border of the seismically active MER. Seismic stability analyses are carried out to check the response of the dam for the updated ground motion parameters of the safety evaluation earthquake (SEE). The static and dynamic analyses are performed using a two-dimensional (2D) plane stress finite element model of the highest cross-section of the dam. First, a linear-elastic dynamic analysis is carried out followed by the dynamic sliding stability analysis of different detached concrete blocks. The foundation rock is assumed massless, which implies that only the kinematic interaction effects are considered. The hydrodynamic pressure acting on the upstream face of the dam was represented by an added mass according to Westergard, assuming incompressible water in the infinite reservoir. The spectrum-matched acceleration time histories are used as input in the dynamic

analysis. All dynamic analyses are done by direct time integration of the equations of motion.

Grand Ethiopian Renaissance Dam (GERD) is the largest hydropower station currently under construction in Africa. The main dam is a 145 m high roller compacted concrete (RCC) gravity dam. It will create a reservoir with a volume of about 74 km^3. Besides the RCC dam, there is a 5.2 km long saddle dam with a maximum height of 65 m and a volume of 17 Mm^3. It is one of the longest concrete-faced rockfill dams (CFRD) in Africa. The seismicity in the project area is assumed to be low. However, the information on historical seismicity is scarce in the region.

Because of the size and importance of the GERD project, the seismic stability of the saddle dam is checked for the ground motion with a return period of 30,000 years. The dynamic analysis of the saddle dam is carried out by the equivalent linear method using a 2D dam model of the highest cross-section. The results show that the dam is safe under the worst-case earthquake loading and the crest settlement is insignificant compared to the available freeboard.

Gidabo dam is a central core earth-fill dam with a height of 27 m. The project includes an intake tower supported by a pile foundation in the upstream part of the dam, which is connected with a diversion conduit laid on a weak compressible foundation passing through the dam body. During dam construction (2016), the conduit that was laid on the soil foundation settled, creating a vertical offset of more than 50 cm at the joint between the pile-supported intake tower and the conduit due to the static loads from dam construction. Moreover, the dam site is located in the seismically active MER with several destructive earthquakes recorded in the past. The seismic stability analysis was conducted to determine the maximum deformation of the dam and settlement of the conduit when it is subjected to the SEE ground motion with 10,000 years return period. The total settlement estimated during SEE is tolerable. The dam is safe against overtopping, as sufficient freeboard is provided. However, cracking of the clay core along the conduit due to differential settlement may lead to internal erosion. Moreover, the offset of the conduit will increase and the conduit may not be adequate for lowering of the reservoir after the SEE.

Tendaho dam is one of the largest irrigation dams located in a region of high seismicity in Ethiopia. Movements along tectonic faults and other discontinuities in the footprint of the dam that can be activated by strong earthquakes close to the dam are expected to be the worst-case seismic effects for the dam. The present study aimed to check the seismic safety of the dam when it is subjected to both ground shaking and tectonic fault movements. The dynamic analyses were carried out by a 2D model of the highest cross-section using the equivalent linear analysis method. The results of the dynamic analyses show that the maximum loss of freeboard is 1.89 m due to slope movement, seismic densification of the embankment and fault displacement in the footprint of the dam that can be accommodated by the available freeboard of 3 m. Seepage along the fault in the dam foundation due to damage of the grout curtain and erosion along the dam-abutment contact due to seepage are possible.

The 188 m high Tekeze dam is the highest arch dam in Africa. The project area is characterized by undulating topography with steep slopes and deep valley, which is different from the other dam sites. Therefore, mass movements into the reservoir that generate impulse waves are possible during strong earthquakes. The seismic stability of the critical slopes is checked for the horizontal component SEE ground motion with a conventional pseudo-static procedure. The landslide is modelled as a solid mass and three-dimensional (3D) free radial propagation of the impulse wave was considered for estimating the wave generation and wave propagation parameters. The parameters controlling the impulse waves on dams were computed and the size of resulting impulse waves in the reservoir was determined. The maximum wave run-up and the possibility of dam overtopping were estimated. The results show that the maximum wave run-up under worst earthquake action can be accommodated by the freeboard allowance of 5 m adopted in the design. As a result, there is no overtopping risk expected from landslides generated impulse waves. However, the overall result of the present study highlights the importance of reviewing the seismic safety of the dam for the increased level of earthquake ground motion.

Acknowledgements

First of all, I would like to praise the Sovereign Lord, who provides me His strength and protection during the present research work.

I would like to express my deepest feelings of gratitude to my advisor Prof. Tilahun Mammo for his close supervision, consistent encouragement and guidance at every stage of this work. His motivation strongly supported me in completing the present research work in this manner.

Word cannot express my feelings of gratitude to my advisor Dr. Martin Wieland for his unlimited support and guidance in the course of this work. Without his input, this thesis would not be completed in this way.

I would like to express my sincere gratitude to current and previous higher officials of the Ministry of Water, Irrigation and Energy (Dr. Seleshi Bekele, Dr. Abraha Adugna, Motuma Mekessa, Alemayehu Tegenu) who provided time and resources for the present research work.

I would like to thank the Research and Development Directorate, Ministry of Water, Irrigation and Energy, for partly funding this research work.

I would like to thank the President of GEO-SLOPE International Ltd, Paul Grunau, for providing the software license free of charge for this research work.

I would like to convey my special thanks to World Bank staffs: Xiaokai L., Hayalsew Y., and Habab T., for all their limitless support during this thesis work.

I would like to express my thanks to ENTRO staffs particularly Michael Abebe and Frezer Zemdekun for all their support during this thesis work.

I would like to thank the School of Earth Sciences the supervisory committee members: Dr. Dessie Nadew and Prof. Tigistu Haile for their close follow-up, encouragements and suggestions to finalize this research work.

I would like to express my deepest gratitude to Dr. Tarun Raghouvanshi, Dr. Bayisa Regessa, Dr. Trufat Hailemariam, Prof. Bekele Abebe, Prof. Solomon Taddese, Prof. Gezehagn Yirgu, Dr. Worash Getaneh and Dr. Abera Alemu for their consistent encouragement and support.

I would like to express my feelings of gratitude to Dr. Balmwel Antanfu, Head of School of Earth Sciences, Dr. Mulugeta Alene Graduate research coordinator and all the staff for all their support.

I am thankful to the officials and staff of Construction Works Design and Supervision Cooperation for material support during this work.

I am also thankful to the officials and staffs of EEP at GERD, Gibe 3 and Tekeze project office for providing necessary data and technical support during field data collection.

I am also thankful to the staff of the Dam Safety Directorate in the Ministry of Water, Irrigation and Electricity: Getaneh Assefa, Addis Eshetu, Besrat Eshetu and Solomon Kenea for their kind assistance.

I am thankful to my friends: Assefa, Geremew, Meba, Haileyesus, Hailemichael and Dawit Nurie for their support and encouragement.

Finally, I have special thanks for my families and all friends who have helped me for the completion of this work.

Contents

List of Tables

Chapter 1

1 Introduction

1.1 Background Information

In recent years, dam safety issues have played an increasingly important role in Ethiopia due to: the design and construction of several large storage dams, the increase in population living downstream of dams, the rise in safety standards, and the economic development downstream of major dams. Currently, there are over 100 large dams in the country, including dams used for irrigation, hydropower and water supply purposes constructed by the federal or regional governments.

The storage volume of several large dams in Ethiopia is very large. For example, the reservoir capacity of Gibe 3 dam (15 km^3) is about 50% of that of all large dams in South Africa. Moreover, it is the highest RCC dam (243 m) in the world, commissioned in 2016. Likewise, the storage volume (74,000 Mm^3) of the reservoir of the Grand Ethiopian Renaissance Dam (GERD) is equivalent with the total storage volume of the ICOLD registered large dams in Spain, France and UK combined. Located on the Blue Nile River, GERD is the largest hydropower station (5,150 MW) under construction in Africa and in terms of concrete volume; it is the largest RCC dam in the world (10 Mm^3). One of the main factors contributing to the risk of large storage dams is the water stored in the reservoir. Thus, the construction of such large storage dams requires special consideration to ensure their long-term safety.

Among the safety concerns for large storage dams, seismic safety plays an important role, particularly for the dams affected by the seismically active East African Rift System (running for about 6000 km from Mozambique to the Dead Sea) that transects the country into two. The location map of dam sites in different basins is shown in Figure 1.1. The spatial distribution of the dams with respect to the seismic zone is

variable from basin to basin. The dams in the Awash and Rift Valley basins are located in high seismic hazard zones. Up to now these dams have not experienced significant earthquakes. In contrast, dams in Baro Akobo and Blue Nile basins are among dams in low to moderate seismic hazard zones of Ethiopia, which includes GERD dam.

The main tectonic phenomenon which has been a major concern for dam designers since long time is the ground shaking (Wieland and Brenner, 2008), which is addressed in all seismic codes, regulations and guidelines. It causes stresses, deformations, cracking, sliding, overturning, liquefaction, etc. However, recent observations have demonstrated that major earthquakes are multiple hazard events, which can affect large dam projects in different ways. These hazards include ground shaking, fault movements in the dam foundation, mass movements in the reservoir and at the dam site, liquefaction of dam materials and dam foundations, and others. For this reason, important dams require a comprehensive safety assessment for multiple seismic effects to minimize the potential risks in the downstream region of large reservoirs.

For this purpose, the following tasks were carried out:

1) Review of the international state of practice on seismic design and lessons learned from the observed performance of dams from past earthquakes;
2) Evaluation of seismic hazard assessment and seismic analysis reports conducted for various dams in Ethiopia and identification of main gaps in the hazard assessment and seismic analysis and design of large dams;
3) Assessment geological and seismotectonic setup and related hazards at dam sites;
4) Initial seismic hazard evaluation at 110 planned, under construction and existing dam sites based on modified source zone model developed by integrating geology, tectonics, seismic energy release map and observed seismicity;
5) Development of reference seismic zoning map for dams based on the probabilistic hazard analysis approach for earthquake return period of 10,000 years as per ICOLD recommendation for large dams;

6) Seismic risk analysis for 30 existing and under-construction dams based on current seismic hazard analysis results and using Bureau (2003) method;

7) Site-specific seismic hazard analysis at five selected dam sites for detailed seismic safety evaluation;

8) Deaggregation of the hazard result, spectral matching and development of acceleration time histories for the selected dam sites for detail analysis;

9) Two-dimensional (2D) seismic stability analysis of 4 dams for SEE ground motion;

10) Stability analysis of abutment and reservoir slopes under earthquake loading and analysis of impulse waves generated by earthquake-triggered mass movement into the reservoir and possible risks on the safety of the dam.

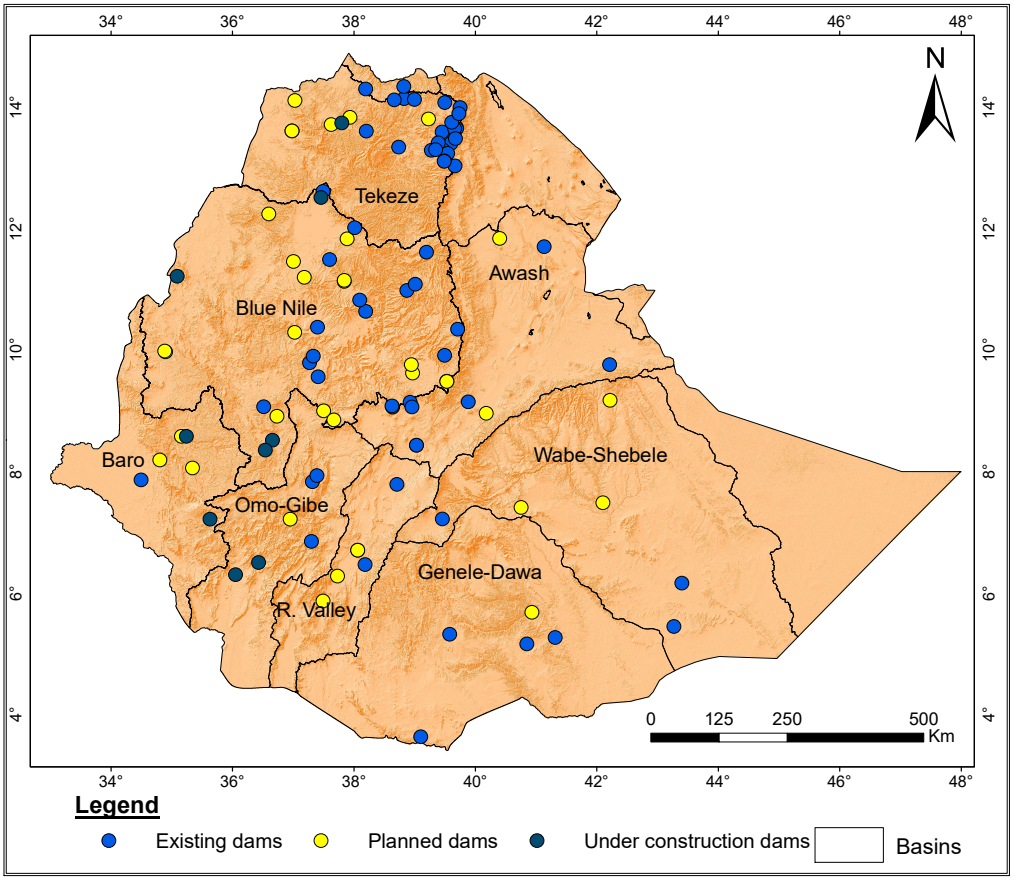

Figure 1.1: Location map of existing, under construction and planned large dam sites in different river basins in Ethiopia

1.2 Objectives

The main objective of the present study is to perform seismic safety evaluations of large dams with high consequence classes.

The specific objectives are:

- To identify the existing problems with the seismic hazard evaluation and design consideration for dams in Ethiopia.
- To evaluate the seismotectonic situation in the region and at various dam sites;
- To conduct initial seismic hazard assessment at existing and planned dam sites;
- To prepare a seismic hazard map for the horizontal peak ground acceleration (PGA) with a return period of 10,000 years, which can be used for preliminary seismic safety evaluation of dams;
- To conduct an analysis of the total seismic risk of 30 existing and under-construction dams to identify high-risk dams;
- To carry out a comprehensive seismic safety evaluation of selected high-risk dams, to analyse their dynamic response during the SEE ground motion and to identify potential failure modes; and
- To recommend possible intervention measures to be taken by dam owners or regulators to improve the safety of dams.

1.3 Problem

Several damaging earthquakes have occurred before the start of major dam construction in Ethiopia. These include: Dobi Graben earthquake of 1989 (M 6.3), Serdo earthquake of 1969 (M 6.1), Kara Kore earthquake of 1961 (M 6.3) and Langano earthquake of 1906 (M 6.8). The seismic hazard is assumed to be fairly constant with time and to follow the same pattern at a global scale. However, the earthquake risk of dams is rising with time due to the increase in new constructions, aging of existing structures and their foundation, inadequate designs, poor

construction quality controls and occupation of less favourable regions by people as well as population growth. In all these, only a few large dams have experienced significant earthquake ground motions. From these dams, some were damaged under earthquake shaking less than what is considered in their design. In other dams, the recorded level of ground shaking greatly exceeded the corresponding seismic design values and the dams withstood the earthquake loadings without significant damage.

The life-span of a dam is as long as it is safe and operable; it can be less than a few years or hundreds of years. Properly designed and constructed dams like Cornalvo and Proserpina dams in Spain built about 2000 years ago by the Romans are still in service. Dams can withstand severe loading condition like Lower Crystal Springs gravity dam in California (USA). The dam survived the 1906 San Francisco Earthquake of M 8.3 and the 1989 Loma Prieta Earthquake of M 7.1 without any cracks, while the main fault rupture was located at a distance of about 180 m from the dam during the San Francisco Earthquake. On the other hand, poorly designed or built dams can fail during construction or during the first year of impounding like Teton dam in Idaho (USA) that failed in 1975 during the first reservoir impoundment and failure of Xe-Pian Xe-Namnoy saddle dam in Laos that failed shortly after completion during a heavy rainfall in 2018.

The seismic hazard is one of the major hazards from the natural environment for which the dams have to be designed. It is of main concern for Ethiopian dams located in the seismically active MER. However, the seismic hazard was not given proper attention in the design and safety assessment of large dams in Ethiopia and it was also not well understood. In addition, the seismic design criteria used at the time of construction of dams do not correspond to today's recommended state of practice (ICOLD, 2016). Also, the quality of dam construction works is not properly documented, which makes it difficult to assess the condition of dams. This applies in particular to embankment dams used for irrigation and water supply.

Moreover, there are no guidelines or any regulatory framework in place, which enforce a specific set of design criteria to be followed during the design. As a result, the design consideration shows high degree of variability and do not follow a consistent methodology. Some designers use current state-of-the-art guidelines for

dam design; the others use codes which are obsolete today, showing a high degree of inconsistency in the seismic study and/or the seismic design and safety criteria. Therefore, the seismic safety of the existing dams may not be satisfactory if the current seismic design and safety criteria would be applied. It may not comply with the seismic hazard at the dam site or the dam type or the consequence class of the completed dam and reservoir. Instead, it is strongly influenced by the consultants' choices and their methodology followed without any guiding rule.

A number of embankment dams have safety problems under normal operational condition such as leakage, seepage, settlement, development of excess pore water pressure and others. Under seismic action the situation becomes more severe, which may endanger the safety of the dams and downstream communities. Due to this observation, the present research has been proposed with the objectives discussed in the previous Section. To achieve the listed objectives, systematic methodologies have been followed.

The present seismic hazard analysis result can be used for safety review and update of existing, under construction and planned dams. It helps the regulatory entity to develop seismic safety guidelines for dams, to prioritize dams based on their risk class for further actions and to provide information on the seismic safety status of the dams selected in the present work. The results can also be used for planning purposes by dam designers and developers and may give justification and encouragement for the support of future researchers work on dam safety and/or seismic hazard in Ethiopia.

1.4 Organization of the Thesis

The dissertation is sub-divided into seven main chapters. The first chapter deals with the general introduction. The second chapter discusses different aspects of the seismic hazard from the review of previous studies and identifies possible gaps. It also includes the evaluation of seismic hazard studies previously done for various dams. In chapter 3, the geological and seismotectonic features of the region are discussed. Chapter 4 covers the seismic hazard evaluation done based on the probabilistic

approach and the seismic zoning of the PGA developed for a return period of 10,000 years. Chapter 5 discusses the seismic risk analysis of 30 existing and under-construction dams. Chapter 6 includes the detailed site-specific seismic hazard evaluations and seismic safety analysis conducted for five large dams subjected to multiple earthquake effects during the SEE. In the final chapter, the overall conclusions of the study and recommendations for further works and studies are given.

Chapter-2

2 Dams and Seismic Hazard

2.1 General

Large dams were among the first structures, which were designed for earthquake loading (Wieland, 2008a). The failure of dams due to earthquake is dated back to 1886 with the first Augusta dam failed during the 1886 Charleston earthquake in South Carolina USA (Nuttli et al., 1986). The first dynamic analysis of an earth dam was made by Mononobe et al. (1936). However, a milestone in the seismic analysis of dams was the 1971 San Fernando earthquake in California, where damage was caused to the San Fernando embankment dams and also to Pacoima arch-gravity dam (Wieland, 2006).

In general, dams that behaved poorly during earthquakes were primarily tailings and hydraulic fill dams. According to USCOLD (1992), the current performance record of dams under earthquake loading appears outstanding with limited number of failures. However, the excellent performance is mainly related to the fact that only few dams have been shaken by earthquakes of magnitude and duration sufficient to jeopardize dams' structural integrity (USCOLD, 1992).

Good lessons have been learnt from the observed performance of various dams under earthquakes loading (M 8.3 April 18, 1906 San Francisco earthquake; M 6.5 February 9, 1971 San Fernando earthquake of USA; M 8 March 8, 1985 Chilean Earthquake, M 8.1 September 17, 1985 Michoacán earthquake of Mexico; M 6.9 October 17, 1989 Loma Prieta Earthquake of USA; M 7.7 January 26, 2001 Gujarat earthquake of India; M 7.9 May 12, 2008 Wenchuan earthquake of China; M 8.8 February 7, 2010 Maule earthquake of Chile; M 9 March 11, 2011 Tohoku earthquake in Japan and others). Details about these earthquakes and their effect on dams are available in

different publications. These earthquakes affected dam projects to various levels and the reasons for the observed damage may be due to the design standard adopted, construction quality control followed during dam construction, and the level of seismic hazard to which the dam was exposed.

In this Section, earthquakes having significant impact on dams and the performance of different dams subjected to earthquake ground motion are selectively reviewed and discussed along with the possible explanations for their good or weak performance. After that, a review of earthquake hazards in Ethiopia, previous seismic hazard studies for dams, and design considerations are discussed with the objective to identify the gaps or limitations. Lastly, design earthquakes and current seismic safety requirements for dams are explained.

2.2 Effects of Earthquakes on Dams

Records of damages from earthquakes in the past show that one earthquake can affect several large dams at a time. According to ICOLD (2010), 1803 dams and reservoirs and 403 hydropower plants suffered damages during the May 12, 2008 Wenchuan Earthquake (M 7.9) of China. Similarly, about 245 earthen dams were damaged by the Bhuj earthquake (M 7.7) of January 26, 2001 in Gujarat of India (Wieland, 2006). On October 17, 1989 the Loma Prieta Earthquake (M 7.1) affected the San Francisco Bay Region and induced strong ground motion in several embankment dams. Over 100 dams of different sizes, mainly embankment dams were situated within 100 km from the epicentre (USCOLD, 1992). This earthquake witnessed the capability of well-designed dams to withstand severe ground vibration hazard. The strong phase of shaking during that earthquake lasted less than eight seconds at rock and firm soil sites in the epicentral area, a relatively short duration for a magnitude greater than 7.0. During the San Francisco earthquake of 1906 (M 8.3), 30 dams at a distance of less than 50 km of which 15 were at a distance of less than 5 km from actual fault rupture (USCOLD, 1992). These dams survived the earthquake shaking without significant damage and confirmed that well-designed embankment dams can withstand the effect of strong ground shaking.

After the March 11, 2011 Mw 9.0 Tohoku earthquake of Japan, more than 400 dams had to be inspected and the dams performed well with minor damage. One exception was Fujinuma embankment dam (Yamaguchi et al., 2102), which failed and the reservoir was released catastrophically killing 8 people in the downstream area. The dam was completed in 1949 with a storage volume of 14 Mm^3.

2.3 Dams Subjected to Earthquake Loading

Dams under earthquake loading commonly show highly variable performance. The dynamic behavior is controlled by the intensity of shaking, duration of earthquake ground motion, site condition, dam size, dam type, design standards, construction quality and others. Few case studies are reviewed in the subsequent part.

From past observations, it is concluded that concrete dams are more vulnerable to cracking and less susceptible to catastrophic failure during earthquake loading as compared with embankment dams. The common seismic failure modes of concrete dams are mainly cracking and foundation failures. For embankment dams the main seismic failure modes are overtopping followed by progressive dam body erosion, internal erosion, foundation failure and liquefaction.

The performance of Aratozawa rockfill dam in Japan during the Miyagi earthquake (M 7.2) of June 2008 with epicentral distance of 15 km is an example for the excellent performance of a well-designed and well-constructed embankment dam under seismic loading (Fig. 2.1). Aratozawa dam was subjected to strong ground shaking with a PGA-value of 1.03 g recorded in the foundation gallery (Hinks et al., 2012). Despite the very strong earthquake shaking, the dam suffered only minor damage and a maximum crest settlement of 40 cm. During the 1985 Michoacán earthquake of Mexico (M 8.1) La Villita dam (60 m high earth-rock dam) and El Infiernillo dam (148 m high central core rockfill dam), located close to the earthquake epicentre experienced no significant damage. They have been shaken by five earthquakes with magnitude greater than 7.2. Total settlements from these earthquake events amounted to 1% of dam height for La Villita dam and the deformations remained small and consistent from one event to the next for El Infiernillo dam (USCOLD, 2000).

Lower Crystal Springs dam, a 43 m high concrete gravity dam, completed in 1890, survived the 1906 San Francisco earthquake of M 8.3 without any crack (USCOLD, 1992). The main fault rupture was located at a distance of less than 180 m from the dam. After 98 years of its service, the dam was shaken for the second time during the 1989 M 7.1 Loma Prieta earthquake at an epicentral distance of 75 km. The dam performed well again without any cracks.

Figure 2.1 : Upstream view of Aratozawa rockfill dam in Japan (left) (Hinks et al., 2012) and Lower Crystal Springs gravity dam that survived the 1906 M 8.3 San Francisco earthquake and M 7.1 Loma Prieta earthquake of 1989) (right) (USCOLD, 1992).

Contrary to the positive examples discussed before, there are few dams known for their weak seismic performance during relatively small earthquakes. Earlsburn embankment dam in Scotland failed after the 23 October 1939 earthquake (M 4.8, estimated PGA of 0.04 g) that occurred at an epicentral distance of 32 km (Musson, 1991) cited by (Hinks et al., 2012). Paiho dam in China was damaged during the 1976 Tangshan earthquake at low peak ground acceleration of 0.05 g recorded at the base of the dam. Similarly, Sharredushk dam in Albania was severely damaged and the freeboard reduced from 2 m to 0.1 m during an earthquake of M 4.1, with an estimated PGA of 0.07 g in 2009. This indicates that poorly designed or constructed embankment dams can be severely affected by relatively small earthquakes at close distance. The above examples clearly show that well-designed and constructed dams can withstand very high levels of ground shaking; however, poorly designed and constructed dams will fail at low levels of ground shaking. Additional case studies are listed in Table 2.1.

Table 2.1: Summary of observed performance of dams subjected to significant earthquake shaking

No.	Dam (type, year)	H (m)	Earthquake	Country	Dist. (km)	PGA (g)	Remarks
1	Lower Crystal Springs (CG, 1890)	43	M8.3 San Francisco Apr 18,1906	USA	0.4	0.68 E	No the slightest crack
			M7.1 Loma Prieta Oct 17,1989		75		No damage
2	Pacoima (CA, 1929)	113	M6.6 San Fernando Feb 9, 1971	USA	5	0.7 B, 1.25 LA	No damage and no cracks in arch dam only open Joint between arch and thrust block.
			M6.7 Northridge Jan 17, 1994		18	1.76 LA	
3	Koyna (CG, 1963)	103	M6.3 Koyna Dec 11, 1967	India	3	0.63	Cracks on both faces
4	Williams (CG, 1895)	21	M7.1 Loma Prieta Oct 17,1989	USA	9.7	0.6 E	No damage
5	Gohonmatsu (CG, 1900)	33	M7.2 Kobe Jan 17,1995	Japan	1	0.83	No damage
6	Shih-Kang (CG, 1977)	21.4	M7.6 Chi Chi Sep 21,1999	Taiwan	0	0.51 h 0.53 v	Vert. disp. of 9m Rupture of concrete.
7	Kasho (CG, 1989)	46.4	Western Tottori Oct 6, 2000	Japan	3.0-8.0	0.54	Cracks in control building at crest
8	Takou (CG, 2007)	77	M9 Tohoku Mar 11, 2011	Japan	109	0.38	Cracking of gate-house walls at crest.
9	Ambiesta (CA, 1956)	59	M6.5 Gemona Friuli May 6, 1976	Italy	22	0.36	No damage at all on the dam and 13 other dams in the area despite 965 death and 2.8 B USD econ. loss
10	Rapel (CA, 1968)	111	Santiago Mar 3, 1985	Chile	45	0.31	Damage to spillway and intake tower.
			Maule Feb 27, 2010		232	0.302	Dam performed well. Cracked pavement.
11	Techi (CA, 1974)	185	Chi Chi Sep 21, 1999	Taiwan	85	0.5	Local cracking of curb at dam crest.
12	Shapai (CA, 2003)	132	Wenchuan May 12, 2008	China	20	0.50 E	No Damage
13	Zipingpu (CFRD, 2006)	156	Wenchuan May 12, 2008	China	7		Joint crack, 76 cm crest settlement (0.5%)
14	Aratozawa (RF, 1991)	78	M7.2 Iwate Miyagi June 2008 (PGA 4g)	Japan	15	1.03	Minor damage with crest settlement of 40cm (0.5%)
15	Sharredushk (EF)	24	M4.1 Mar 2009	Albania	9.5	0.07	Severely damaged
16	Hsinfengkiang (CB, 1959)	105	M6.1 Reservoir induced, 1962	China	1.1	0.54	Horiz.. cracks in top part of the dam
17	Sefid Rud (CB, 1962)	106	M7.7 Manjil Jun 21,1990	Iran	Near	0.71 E	Horiz. cracks near crest, minor blocks disp.

Note: B – base, C – crest, CA - concrete arch, CB - concrete buttress, CG - concrete gravity, disp.- displacement, Dist. - distance, E – East, EF - earthfill, est.- estimated, h - horizontal, ht.- height, M - Moment Magnitude, PGA - Peak Ground Acceleration, RF - Rockfill, V – Vertical

2.4 Dams and Seismic Hazard in Ethiopia

The construction of dams started in Ethiopia in the late 1930s with the First Aba Samuel dam, commissioned in 1939. After that, several large dams were constructed with the first large hydropower dam (Koka) commissioned in 1961 and the construction of dams substantially increased after 2010 (Fig. 2.2). About thirty large dams have been constructed by the Federal Government of Ethiopia and over seventy large dams by the Regional States.

Figure 2.2: Year of construction of large dams in Ethiopia by the Federal Government

2.4.1 Strong Earthquakes in Ethiopia and Effects on Dams

Damaging earthquakes of significant magnitude were recorded in Ethiopia and the surrounding regions of the East African Rift system. In general, the instrumental and historical earthquake records contain relatively few strong earthquake events. Although casualties were reported from some of these earthquakes; none of the dams has experienced ground shaking from significant magnitude earthquakes (Fig. 2.3). M

6.8 Langano earthquake (1906), M 6.3 Kara Kore earthquake (1961), M 6.1 Serdo Earthquake (1969) and M 6.3 Dobi Graben earthquake (1989) are among the major earthquakes recorded in the past in Ethiopia. During the M 6.8 Langano earthquake (1906) in central Ethiopia, there was no dam in the country at all. During the M 6.3 Kara Kore earthquake (1961) and M 6.1 Serdo earthquake, there were only two dams (12 m high Aba Samuel commissioned in 1939 and 23 m high Koka gravity dam commission in 1961). Both dams are at epicentral distances of more than 200 km. In the case of the M 6.3 Dobi Graben earthquake of 1989 in the Afar region, there were about ten major dams in Ethiopia. However, none of them was within an epicentral distance of 300 km. At present, several large storage dams are either under construction or in the planning stage in this seismic active zone (Fig. 2.3). Particularly, dams in the MER and Afar are located at close distances to the major earthquakes recorded. These dam projects have to be able to withstand strong earthquakes.

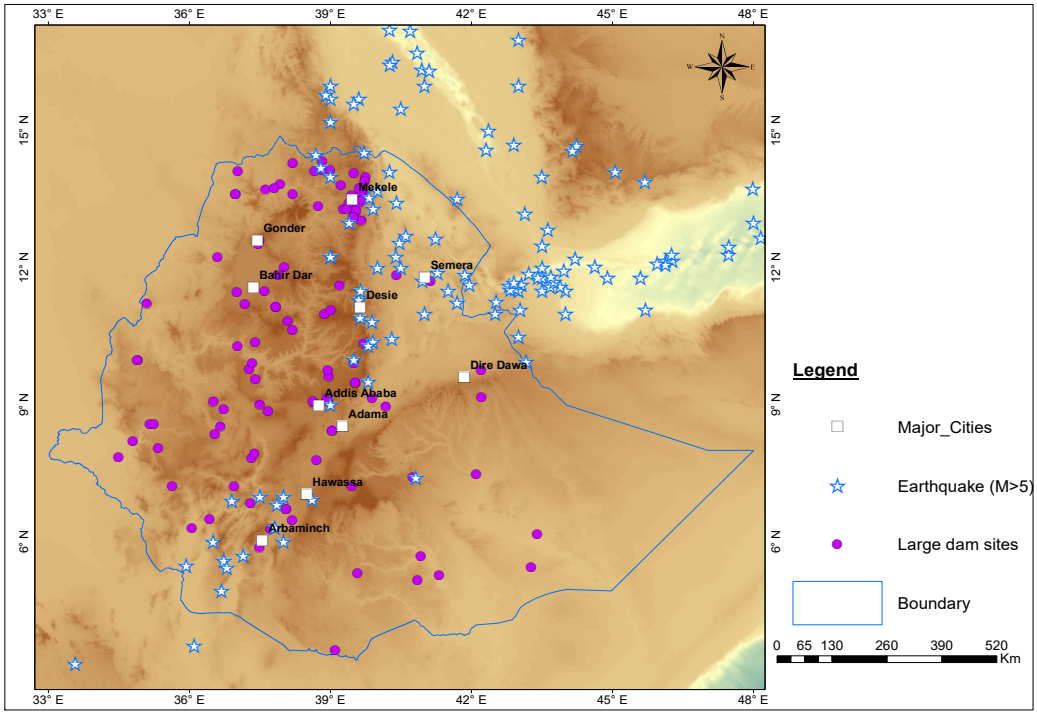

Figure 2.3: Major earthquakes recorded in the past with M>5 (1900 - 2018) and location of main dam sites in Ethiopia.

2.4.2 Seismic Design Considerations

The seismic hazard evaluation reports and seismic design analysis used for various dams are reviewed and existing gaps are identified. According to ICOLD classification, all dams considered during the present study are classified as large dams with high consequences in case of failure. High consequences include loss of life, injuries, social, economic and environmental impacts. The seismic hazard evaluation conducted during the design is summarized in Table 2.3 and Fig. 2.4. The horizontal PGA-values on the rock surface given in the seismic hazard assessment report vary from 0.03 g for Tekeze dam to 0.7 g for Gidabo dam. However, the PGA-value of 0.7 g proposed in the seismic hazard assessment report was not taken into account in the seismic design of Gidabo dam.

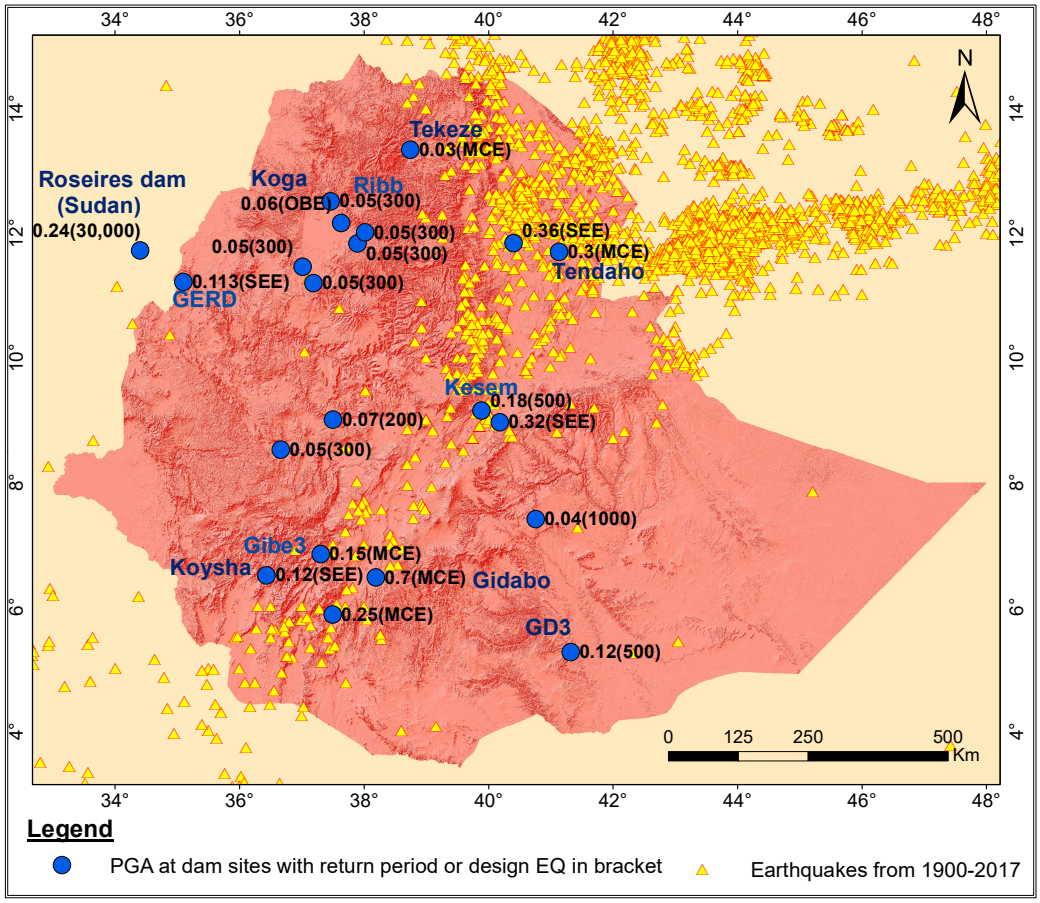

Figure 2.4: Seismic design parameters used for large dams in Ethiopia plotted over epicentral map of earthquake recorded from 1900 to 2017: the peak ground acceleration at dam sites is labelled with corresponding design earthquake/return period in the brackets.

Table 2.2: Seismic design parameters used for large dams in Ethiopia

No.	Dam Name	PGA (g)	Return Period (years)	Methodology	Status	Design Year
1	Arjo	0.05	300	SZM	UC	2007
2	GD3	0.12 MDE	500	Probabilistic	E	2009
3	GERD	0.113	10,000	Probabilistic	UC	2012
4	Gibe-3	0.15	MCE	Deterministic	E	2007
5	Gidabo	0.7	MCE	Assumption	E	2009
6	Gilgel Abay	0.05	300	SZM	P	2010
7	Gololcha	0.07 Sa@0.2s	1000	Probabilistic	P	2011
8	Goyisha	0.12	10,000	Probabilistic	UC	2017
9	Gumera	0.05	100	SZM	P	2009
10	Jema	0.05	300	SZM	P	2010
11	Karadobi	0.073 MDE	200	Probabilistic	P	2006
12	Kesem	0.32 Sa@1s	500	Probabilistic	E	2005
13	Koga	0.06 OBE	145	Probabilistic	E	2004
14	Logia	0.78 Sa@0.2s	10,000	Probabilistic	P	2016
15	Lower Segen	0.25	MCE	Deterministic	P	2008
16	Megech	0.05	300	SZM	UC	2009
17	Middle Awash	0.69 Sa@0.2s	10,000	Probabilistic	P	2016
18	Ribb	0.05	300	SZM	E	2009
19	Sego	0.25	MCE	Deterministic	P	2010
20	Tekeze	0.03	MCE	Deterministic	E	2001
21	Tendaho	0.3	MCE	Deterministic	E	2005
22	Upper Guder	0.2 Sa@0.2s	10,000	Probabilistic	P	2016

Note: PGA – Peak Ground Acceleration, MCE - Maximum Credible Earthquake, MDE – Maximum Design Earthquake, Rp – Return Period, SZM – Seismic Zoning Map, E – Existing, UC – Under construction, P – Planned, Sa – spectral acceleration, s – structural period in second

2.5 Design Earthquakes and Current Seismic Safety Requirements

2.5.1 Design Earthquakes

The terminology used for earthquakes required for the analysis and design of large dams varies among different countries; however, the terms used in revised guidelines

of the International Commission of Large Dams (ICOLD) Bulletin 148 (2016) are discussed as follows:

Safety Evaluation Earthquake (SEE) is the maximum level of ground motion a large storage dam should be analyzed and designed with a statistical return period of 10,000 years or for the maximum credible earthquake. Damage can be accepted, however, there shall be no catastrophic release of water from the reservoir.

Operating Basis Earthquake (OBE) is the level of ground shaking where no structural damage to the dam and appurtenant structures should occur. The dam body, appurtenant structures and equipment should remain functional with easily repairable damages. The recurrence period of the OBE specified by ICOLD (2016) is 145 years (i.e. 50% probability of not being exceeded in 100 years).

Maximum Credible Earthquake (MCE) is the largest reasonably possible earthquake that is considered along a recognized fault or within a defined tectonic domain, under presently known or presumed tectonic framework. The most severe ground motion due to worst-case earthquake scenario for a specific dam site is called MCE ground motion. Estimation of the MCE ground motion parameters is generally done using a deterministic hazard analysis, in which the MCE scenarios for each known fault and tectonic province are considered.

Reservoir-triggered seismicity (RTS) has been observed after filling of the reservoir. It is more likely to occur in reservoirs with the water depth exceeding 100 m and/or reservoirs with about a storage volume of over 500 Mm^3 and in dams and reservoirs located in tectonically active areas or areas with very high tectonic stresses.

Based on the dam location and prevailing seismotectonic situations, the strongest RTS events may represent ground motion less than or equal to SEE or greater than the OBE ground motion. However, in no case RTS ground motion should be greater than the SEE ground motion. Therefore, for a dam designed for SEE, RTS is not a problem apart from other structures in the dam and reservoir region that are constructed without any seismic considerations. From previous cases of RTS the highest magnitude was 6.3.

2.5.2 Seismic Safety Criteria for Dams

The basic seismic loads for the design of new dams or for the safety evaluation of existing structures are derived from the SEE and OBE. Depending on the applicable conditions, a dam may be evaluated for one or both of these basic seismic loads. The primary requirement for the earthquake-resistant design of dams is to protect public safety, property and environment. Hence, large dams must be capable of resisting severe earthquake motion or fault movement at the dam site without uncontrolled release of the water stored in the reservoir. It is also important that the spillway and bottom outlets should be operational after the earthquake. In the case of the SEE, damage to the dam, even extensive, may be acceptable as long as no catastrophic release of water from the reservoir occurs.

The spillway has to be able to release moderate floods even after an earthquake. In addition, the bottom outlets should allow for lowering the reservoir after an earthquake in case of major damage to the dam. Concerning the reservoir, the effects of impulse waves caused by mass movements into the reservoir triggered by earthquakes have to be investigated. Overtopping of the crest of embankment dams is the main concern. The factors governing the level of seismic safety evaluation at a particular site include: the seismic hazard of the dam site, the type of dam, the functional requirements, the consequence rating of the completed dam and reservoir and the consequences of underestimating or overestimating the risk (ICOLD, 2016).

2.6 Conclusions

The first dam that failed during an earthquake was Augusta dam, which failed during the 1886 Charleston earthquake. It was recognized that the catastrophic release of reservoirs due to dam failure will have severe consequences; therefore, large dams were among the first structures designed systematically for earthquake loading. The observed damages from earthquakes in the past show that one earthquake can affect several large dams at a time. Dams under earthquake loading commonly show highly variable performance. The seismic performance of dams is mainly controlled by the

level of earthquake ground motion (amplitude, duration and predominant period) to which the dam was exposed, site condition, dam size, dam type, design standards and construction quality.

From previous observations, it can be concluded that concrete dams are more vulnerable to cracking and less susceptible to catastrophic failure during earthquake loading as compared with embankment dams. As a result, particular emphasis should be given for embankment dams constructed in MER and Afar affected by extensional tectonics. No concrete dams so far reported, which were exposed to a strong earthquake and violated the SEE criterion (there was no uncontrolled release of reservoir water).

From the case studies reviewed, well-designed and well-constructed dams can perform well even under very strong earthquake loading greatly exceeded the corresponding seismic design values like Lower Crystal Springs dam that survived the 1906 San Francisco Earthquake of M 8.3 without any crack while the main fault rupture was located at a distance of less than 180 m from the dam. Minor damage such as settlement and cracks on the crest may be possible. Leakage may also increase temporarily due to opening of cracks and washing out of fine particles from joints or fissures. On the contrary, poor construction quality is the main reason for the seismic failure of dams under earthquake shaking less than what is considered in their design like in the case of Sharredushk and Tikves dams.

The seismic safety of large dams in Ethiopia is very important, because a failure of such structures, storing large reservoirs, may have disastrous consequences on life, property and economic activity in the downstream region. Several damaging earthquakes have occurred in the MER and surrounding region in the past. However, none of the dams experienced damage due to their large epicentral distances. During the present study, the seismic hazard evaluation and seismic stability analysis reports used for various dams are reviewed and existing gaps identified. A key observation is that the reports show high degree of variability and do not follow a consistent methodology. Some use the current state-of-the-art; others use codes and guidelines, which are out-dated today. Therefore, the seismic safety of these dams is not known,

some may even be deficient. Therefore, in a first step, a seismic reassessment of all large dams is recommended, a recommendation that was also made by ICOLD‘s seismic committee as far back as 1999. Sometimes, the return periods of the design earthquakes and confidence levels of the ground motion parameters do not comply with ICOLD guidelines. This is the case for the majority of dams in Ethiopia.

Chapter 3

3 Geological and Seismotectonic Background at Dam Sites

3.1 General

Knowledge of the geological and tectonic background of a region is a key component for the dam safety and seismicity. Geological factors can impose major constraints on the design, construction and long-term safety of large dam projects. Thus, understanding of the geological and tectonic background of the dam sites before the design phase is vital. The proper characterization of the site conditions is required for the design of any large storage project. To achieve this, adequate site investigations must be carried out. Dam failure due to geological, geotechnical and seismotectonic hazards include uncontrolled seepage, formation of cavities due to dissolution of materials, differential settlement, slope instability, sliding, rock fall, uplift pressures, changes in ground water table, piping in the foundation, hydraulic fracturing, shearing, faulting, and related seismic activity. Several of these problems have been observed at dam sites in Ethiopia. Thus, a complete understanding of the geologic conditions is crucial for the long-term safety of dams. It helps to implement proper remedial measures at the initial stages, since any treatment measures after dam construction or impoundment of the reservoir are costly and may also not be practical. Besides, costs and time of dam construction are directly related to the geologic conditions at dam sites.

The dam sites in Ethiopia are in variable geological and tectonic settings ranging in age from Precambrian to recent Quaternary. The on-going geologic and tectonic processes in the region strongly influence the safety of dams and reservoir water tightness, sometimes with hazardous consequences. However, proper attention has not been paid to the existing and newly planned dams located in tectonically active regions.

In this section, the geological and seismotectonic condition of dam sites is reviewed with emphasis on the seismic safety of dams and reservoir water tightness. The distributions of earthquakes are discussed. Furthermore, the effects of tectonic structures on the safety of dams and reservoir water tightness are highlighted and recommendations on further studies needed to reduce the risk are given.

3.2 Case Studies of Dam Failures due to Geological Problems

ICOLD (2005) has recorded several cases of dam incidents due to geological defects in the dam foundation. Similarly, data on failures and incidents to dams in the United States confirm that nearly 60 percent of dam failures are related to the geologic conditions in the foundation (Flagg, 1979).

There are several inherent uncertainties associated with the properties of geological conditions in the foundation. Some dam failures related to geological factors include: Tigra dam (1919, India) failed after reservoir filling due to uplift and sliding of the foundation rock; St Francis dam (1928, USA) due to geological instability in the abutment slope; Borga dam (1951, Sweden) due to piping through a sand layer in foundation during first filling; Goczalkowice dam (1956, Poland) due to excess pore water pressure in the foundation, Lake Invernada dam (1958, Chile) sinkholes appeared in the foundation during reservoir filling; Baldwin Hills dam (1963, USA) due to fault movement in foundation that led to rupture of asphalt lining of the reservoir and under drains; Vajont dam (1963, Italy) due to mass movement into the reservoir that led to overtopping; Kedarnala dam (1964, India) and Laguna dam (1969, Mexico) due to piping through weathered volcanic tuff; Bastusel dam (1972, Sweden) leakage led to sinkhole; Tarbela dam (1974, Pakistan) failed during first filling due to sinkholes formed in upstream impervious blanket through gravel foundation; Three Sisters dam (1974, Canada) due to internal erosion into a gravel foundation; Keban dam (1975, Turkey) cavity in karstic foundation; Teton dam (1976, USA) piping through the foundation; Beaver dam (1984, Alaska USA), due to karstic foundation; Camara dam (2004, Brazil) smooth foliation surfaces left untreated in the foundation led to a foundation failure upon first filling; Oroville dam spillway failure (2017, USA) due to spillway design and construction weaknesses

together with poor bedrock quality; Xe-Pian Xe-Namnoy saddle dam (2018, Laos) seepage through weathered foundation; and others. Thus, the geological conditions must be thoroughly investigated and characterized to reduce the risk of dam failure. Some of the classic examples of dam failure cases due to geological problems are given in Fig. 3.1.

Earthquake is one of the main hazards for large dam projects. The problematic geological situations that caused the above-listed dam failures under normal operation are expected to worsen under earthquake excitation. Therefore, proper evaluation of the geological and tectonic settings is important for new dams as well as for existing dams.

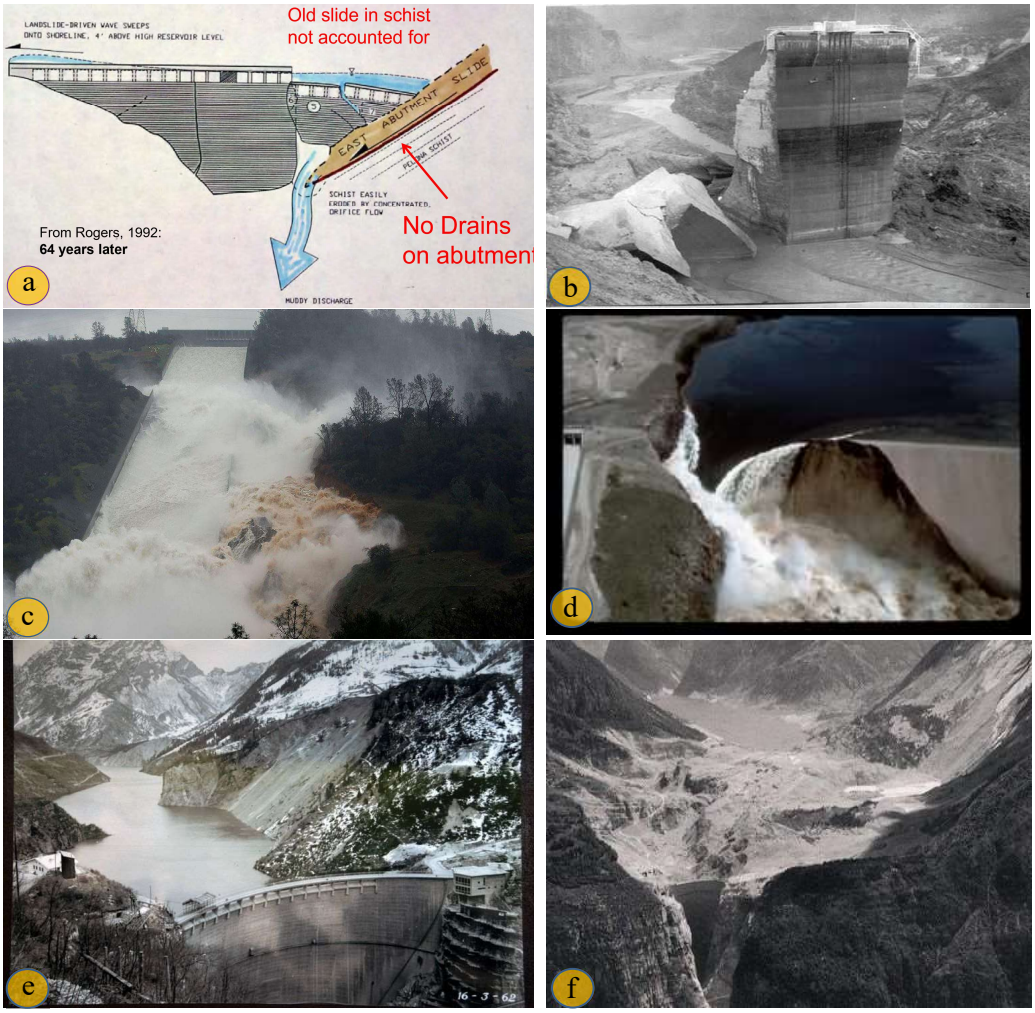

Figure 3.1: Dam failure cases due to geological problems: (a) and (b) St. Francis dam failure, 1928, (c) spillway failure of Oroville dam, 2017, (d) Teton dam failure, 1976, (e) and (f) Vajont dam, 1963.

3.3 Seismotectonic Background of Ethiopia

The Afro-Arabian Rift system comprises the southern Red Sea Rift, the Gulf of Aden Rift and the East African Rift. These Rifts intersect each other forming an about 400 km wide triple-junction zone of the Afar Depression (Fig. 3.2). The Main Ethiopian Rift (MER), which is the part of East African Rift System (EARS), is one of the few areas in the world where on-going processes of continental break-up and the present-day ongoing extensional tectonics activities can be observed on land, particularly in Afar depression (Manighetti et al. 1997). The volcanism, recent faulting, and shallow earthquakes are evidence for the ongoing extensional deformation in the region. The Main Ethiopian Rift (MER) is generally the NE-trending sector of the East African Rift system that includes a series of Rift segments that extend from the Afar Depression at the Red Sea-Gulf of Aden junction to the Kenya Rift.

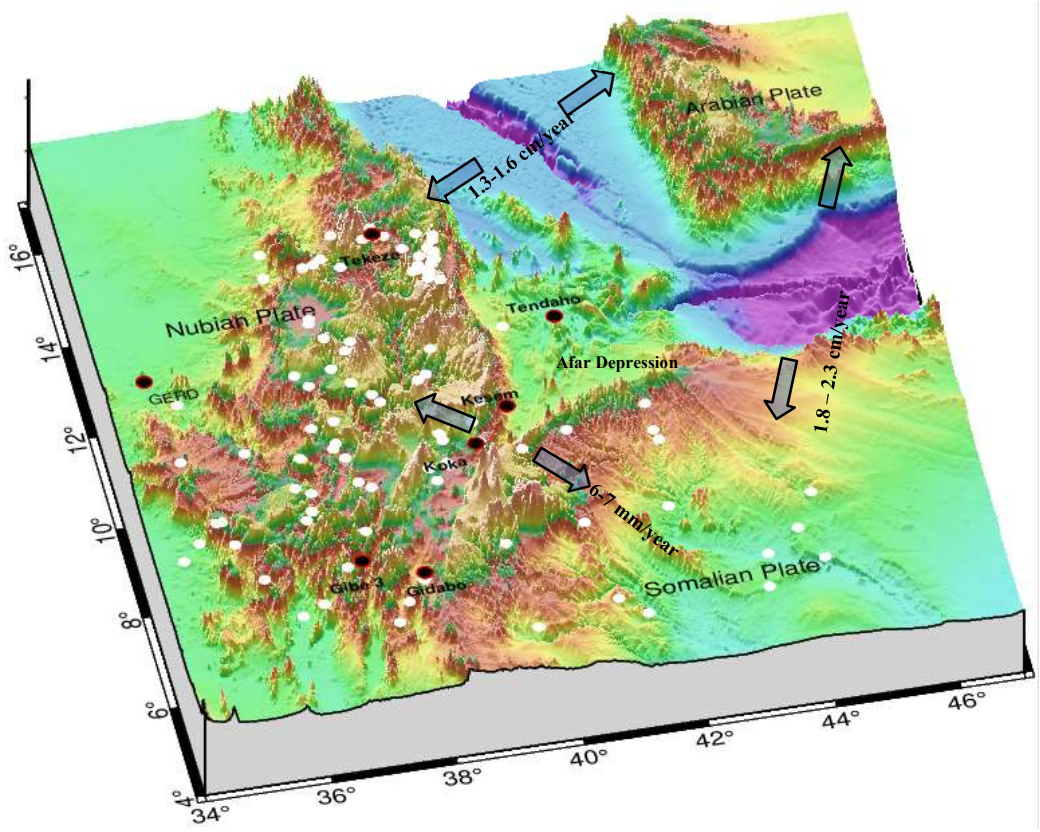

Figure 3.2: Large dams in Ethiopia (white and black dots) and slip rates and extension directions of Gulf of Aden Rift, Red Sea Rift and Main Ethiopian Rift forming the Afar Depression (seismically active triple rift junction).

The MER is characterized by active extensional tectonic movements between the African and Somalian plates with extension of 6-7 mm/year (Fig 3.2). The Ethiopian Plateau is separated into the Eastern and Western Plateau by the Afro-Arabian Rift System. The Western Escarpment of the Ethiopian Plateau has a north-south decrease in crustal thickness, allowing division into Northwestern Ethiopian and Southwestern Ethiopian Plateau at the YTVL (Figs. 3.2 and 3.3). The eastern Escarpment is referred to as a southeastern Ethiopian plateau. Both the eastern and western plateaus are characterized by east-west trending transverse lineaments constituting shield volcanoes. These lineaments are marked by Adigrat-Adwa Lineament (AAL), Yerer Tullu Wellel Volcano-Tectonic Lineament (YTVL), and Goba-Bonga Lineament (GBL) from north to the south.

Earthquakes in the region are of shallow crustal origin mainly following the extensional tectonics of the East African Rift system. Magmatic assisted rifting, associated with normal faulting, is the main source of seismic activity in this region. The largest earthquake recorded in the area is the M7.2 earthquake that occurred in South Sudan in May 1990, about 400 km from the Ethiopian border. Focal mechanisms of recorded earthquakes are dominated by the presence of normal mechanisms related to the extension of the Main Ethiopian Rift (MER). Few earthquakes show a strike-slip faulting mechanism, which is usually accomplished by the presence of faults perpendicular to the MER. Different studies show that the seismicity in the Ethiopian Rift varies spatially within the rift and its margin. Seismicity in the Northern Main Ethiopian Rift (NMER) occurs in the magmatic segments and along the rift-boundary faults, while the seismicity in the Central Main Ethiopian Rift (CMER) is localized only near the Eastern Rift Margin (Keir et al. 2006).

3.4 Tectonic Setup

The tectonic development of the Precambrian of Ethiopia is represented by subduction-accretion processes between arc terranes of the Arabian-Nubian Shield and predominantly gneissic terranes of the Mozambique Belt. It involves a plate

tectonic cycle spanning 350 Ma (million years), beginning about 900 Ma with rifting and continental break-up and ending about 550 Ma with convergence between East and West Gondwana continents (Tefera et al., 1996).

Late Paleozoic to Cretaceous tectonics is related to early rifting of Africa from East Gondwana that led to the formation of multiple rift basins and deposition of terrestrial and marine sediments in central and eastern Africa. The Abay, Ogaden and Mekele Basins are presumed to be intracontinental rift basins, formed as a result of extensional stresses induced by the break-up of Gondwana in Late Paleozoic (Kazmin, 1972). The Cenozoic tectonics is represented by the Afar Depression, the Main Ethiopian Rift, and the Ethiopian Plateau. The MER has been usually differentiated into three main segments, i.e. the Northern (NMER), the Central (CMER), and the Southern (SMER), representing different stages of the extension process, from early rifting in the Southern MER to more evolved stages in the Central and Northern MER preceding the incipient seafloor spreading in Afar. Two main distinct fault systems exist in the MER. These are the N300E to N400E-trending Miocene, steep, segmented border faults, and the Quaternary N-S to N200E-trending rift floor faults and aligned eruptive centres of the Wonji Fault Belt (WFB) (Mohr, 1967; Boccaletti et al., 1998). The latter ones began to develop around 1.6 million years ago. The Quaternary faults and associated eruptive centres along the rift floor constitute the youngest part of the MER (Mohr 1967, 1987; Boccaletti et al., 1998).

The Main Ethiopian Rift (MER), which is characterized by dominantly NNE-SSW trending normal faults, consists of zones of Quaternary tectonic and magmatic activity (Mohr, 1967). There are several indications that the MER and Afar are tectonically and seismic active at present. These include the recorded seismicity, the physical appearance of the faults (prominent, sharp and fresh scarps), and geothermal manifestations. The Quaternary faults in the MER, Afar and surrounding regions comprise more than 98% of the recorded earthquakes. The remaining earthquakes (2%) are related to the reactivation of the earlier rifts, mainly the Mesozoic rift.

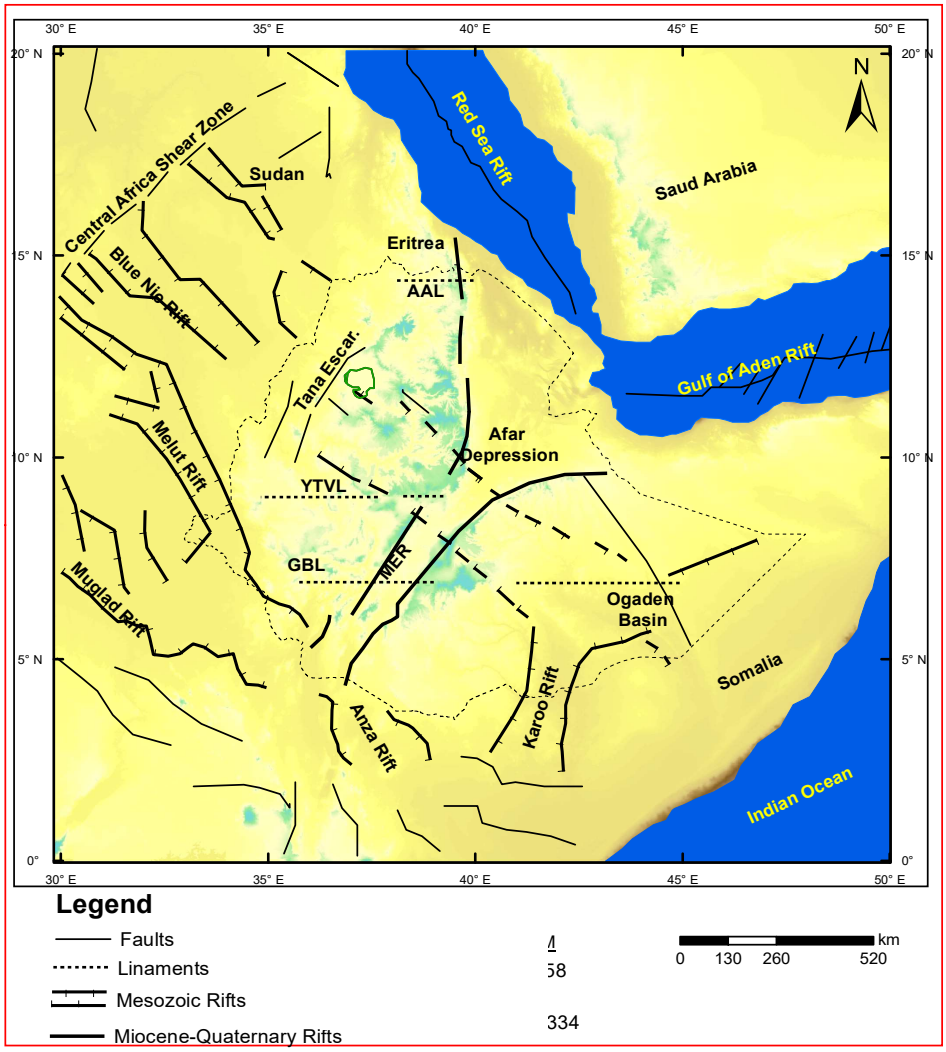

Figure 3.3: Tectonic features of East Africa showing major rifts and fault systems varying in age from Mesozoic to Quaternary which can cause significant earthquake hazards in the region.

3.5 Geological Setup

Ethiopia lies in the northern part of the East African Rift System; the geological setup is highly variable, ranging in age from Precambrian to recent Quaternary sediment. Rocks of Precambrian age underlie major parts of western and northern Ethiopia. Mesozoic and Cenozoic sediments are widely available in the eastern, central, and northern parts of the country. The Rift valley area is covered with relatively young volcanic and lacustrine deposits.

The Precambrian metamorphic and associated intrusive igneous rocks comprise 25% of the country's landmass (Fig. 3.4). These are exposed mainly in the northern, southern and western parts of the country (Kazmin, 1972). The high-grade gneisses and migmatites are referred to as Lower Complex is part of the Mozambique Orogenic Belt (Kazmin, 1972). The low-grade volcano-sedimentary rocks with associated mafic to felsic intrusives, which are referred to as Upper Complex, have an age ranging from 900 to 500 Ma with few exceptions (Kazmin, 1972; Kazmin et al., 1978).

Paleozoic–Mesozoic sedimentary rocks in the country are represented by three distinct sedimentary basins comprising about 25% of the country's landmass. These include the Ogaden Basin, the Blue Nile Basin, and the Mekele Basin (Tefera et al., 1996). The thick sediments of the Ogaden Basin consist of non-marine to deep marine clastics, very thick, shallow-to-deep marine carbonates and evaporites. The Blue Nile Basin consists of Paleozoic and Mesozoic sedimentary succession. The Mekele Basin comprises thick sediments ranging from fluvio-lacustrine to shallow and deep marine types.

Cenozoic volcanic and sediments cover 50% of the country's landmass, and range in age from the late Eocene up to historical times (Fig. 3.4). Volcanism started during the Eocene-late Oligocene with the eruption of flood basalts (Mohr, 1983). The earliest flood basalts forming the Ethiopian Plateau erupted in a rather short time interval (<5 Ma) with the greatest eruption rates occurring 31 to 28 Ma ago (Hoffman et al., 1997). This strong eruption was associated with the onset of continental rifting in the Red Sea-Gulf of Aden systems 29 Ma ago (Wolfenden et al., 2004). The second episode of flood basalt volcanism has been described in southern Ethiopia at 18-11 Ma and in the MER-Afar transition zone at about 11-10 Ma. Time correlative basaltic units are widespread both in the western (Wollega and Lake Tana basalts, 11-9 Ma) and in the southeastern Ethiopia Plateau at about 10.5-9 Ma. After these episodes of widespread flood basalts and subordinate silicic volcanics, volcanism is closely associated with the tectonic development of the MER. Rifting in the various MER sectors was characterized by volcanism with fundamentally bimodal character. Widespread late Miocene-Pliocene rhyolitic ignimbrites (~7-3 Ma) with intercalated

minor mafic lavas occur throughout the Northern and Central MER. In the Quaternary (<1.6-1.8 Ma), bimodal volcanic rocks (lava, pyroclastics and volcanoclastic strata) were generally closely associated with Wonji Fault Belt affecting the Rift floor.

3.6 Dam sites in Different Geological Setups

Among the 110 large dam sites considered in the present study, about 60% are in volcanic terrain of which nearly 25% in the Quaternary and 35% in the Tertiary and are distributed mainly in the central, north and western part of Ethiopia (Fig. 3.4). The development of any dam project in the Quaternary and adjacent Tertiary environment needs particular attention due to active geological processes in the region such as volcanism, tectonic movements and seismicity. The remaining 40% are nearly equally shared between the sedimentary and metamorphic environments, which are less active in terms of present-day ongoing geological processes (Fig. 3.4). In general, the majority of large dams is located in seismically less active zones, with few exceptions in the MER and Afar.

Metamorphic rocks and associated intrusives are more suitable for dam sites as compared to igneous and sedimentary rocks. However, there is a high variability in the types of rocks and rock properties due to the geological processes that the rocks underwent. The presence of unfavorable geological structures (folding, faulting, shear zones and joints) and inter bedding of strong rocks with weak layers or weak metamorphic rocks such as phyllite, slate and talc can create major safety problems in the dam foundation like inadequate sliding stability of concrete dams. Moreover, folds and faults can develop several fractures and crushing of rocks that are responsible for settlements, uplift and leakage on dams.

The suitability of sedimentary rocks for dam and reservoir sites greatly differs based on their composition and material properties. Soft sedimentary rocks like mudstone and shale are not suitable for massive concrete dam structures (inadequate bearing capacity, large deformations, etc.) Sandstone inter-bedded with shale or claystone can cause sliding problems. Thin layers of shale or claystone between layers of sandstone

dipping towards the downstream or the valley side may cause slope stability problems. Volcanic rocks such as unwelded tuff and volcanic breccia in the presence of paleo soils or volcanic ash layers can affect dam stability and cause leakages.

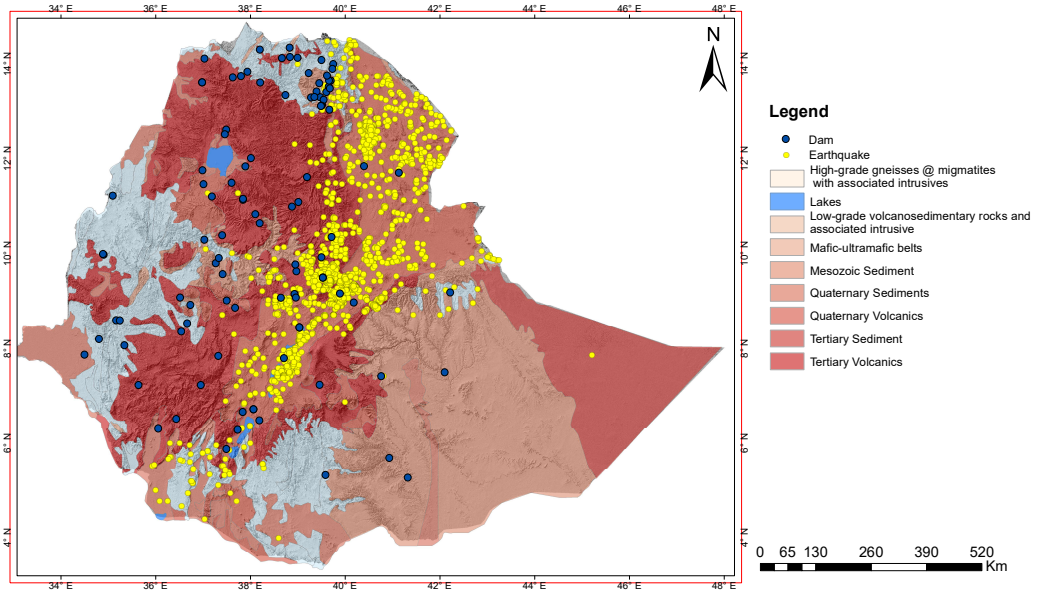

Figure 3.4**:** Plot of dam sites and earthquake epicenters over generalized geological map of Ethiopia. Yellow and blue circles represent earthquake epicenters and dam sites, respectively.

3.7 Seismicity in Relation to the Geological Setup

A general assessment has been made considering the seismicity link with the geology and tectonics in the region. A plot of earthquake epicenter over the generalized geological map of Ethiopia show that about 90% of the epicenter of recorded earthquake falls in the Quaternary and adjacent Tertiary geological setup that found in the central part of Ethiopia (Fig. 3.4). As a result, the dam sites found in these zones are relatively in a higher seismic risk zone. In addition, unconsolidated alluvial and lacustrine sediment of Quaternary and Tertiary age have major problems of high settlement and liquefaction under seismic loading. These types of deposits in the seismically active zone of the Rift can significantly amplify earthquake ground vibration hazards. As a result, the dams on these soils can be subjected to an increased level of ground motion than at rock sites. For the dam sites found in a sedimentary

environment, the seismicity is moderate to low for the Blue Nile and Ogaden Basins and relatively high for the Mekelle Basin. The seismic hazard in the metamorphic terrain like GERD and GD3 dam sites are assumed to be relatively lower.

3.8 Tectonic Impacts at Major Dam and Reservoir Sites

Geological structures such as faults, major fractures, joints and shear zones can affect large dam projects in different ways. Active faults can generate strong ground motions at dam sites. In addition, large earthquakes very close to a dam site may cause movements along secondary faults or pre-existing discontinuities in the dam foundation. Such features can greatly reduce shear strength in the foundation and abutment slopes. Seepage through a fault or major joint/fracture zone can later lead to piping or uplift if proper treatment was not made. Faults can create connections to deep-seated groundwater under high pressure and temperature, which can affect foundation preparation, grouting and construction works.

Moreover, the extension direction of the MER is assumed to be E-W (roughly perpendicular to the EARS trend) (Boccaletti et al., 1998, 1999) and NW-SE. The water-tightness of the reservoirs that are aligned parallel to MER and EARS is controlled by the tectonic structures and is one of the major challenges for reservoirs water tightness. Presently, there is a significant water loss observed from these reservoirs such as Kesem, Koka and Tendaho. This might have safety and economic impacts. During an earthquake, the situation will become even worse due to the opening of the cracks and damage of the grout curtain or cutoff walls in the dam foundation.

For this purpose, the importance of water tightness study for major reservoirs is highlighted as a priority area for the next phase of works (Fig. 3.5). Among these reservoirs, those in the MER and Afar have a leakage problem through faults and major fractures. Some of these leakages are well observed on the surface and the others are hidden but they are also recharging the groundwater in the region.

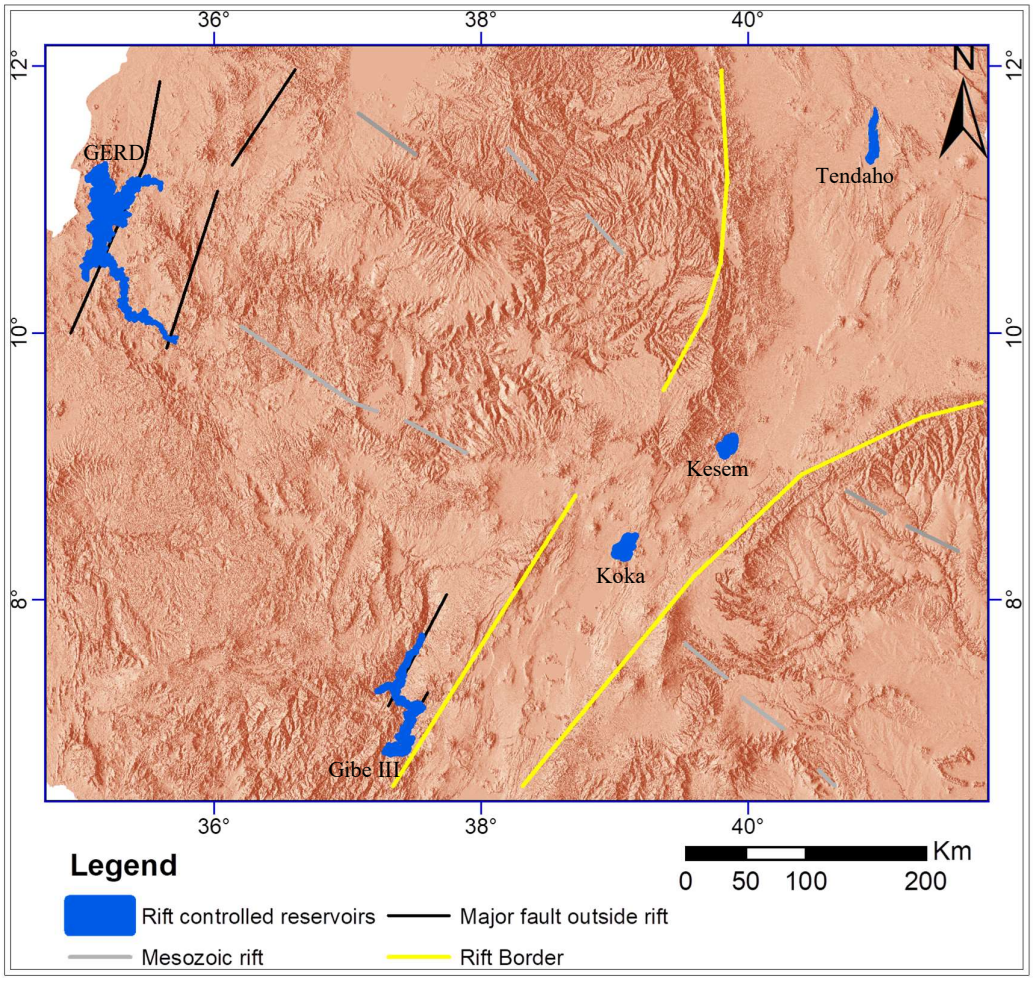

Figure 3.5**:** Five major reservoirs controlled by rift structures and major faults which can affect the reservoirs water tightness: Tendaho reservoir in the tripe rift junction; Kesem and Koka reservoirs in the MER; Gibe III reservoir in the margin of the MER; and GERD reservoir in the Mesozoic Blue Nile Rift.

3.9 Conclusions

Ethiopia is situated in a seismically and tectonically active part of the East African Rift. The dam sites are located in variable geological settings ranging in age from Precambrian (metamorphic terrain) to recent Quaternary sediment. In terms of geology, nearly 25% of the dam sites considered in the present study are located in Quaternary volcanic, 35 % in Tertiary, and 20% each in sedimentary and metamorphic terrains. The geological factors take the leading causes or contributory

factors for several dam failures reported in the past. Thus, understanding of the geologic conditions at dam sites is crucial at the initial stage of project development since any treatment measure after dam construction or impoundment of the reservoir is very expensive and may also not be practical.

Regarding the seismicity in relation with the geological setup, about 90% of the recorded earthquakes in Ethiopia have occurred in Quaternary and surrounding Tertiary geological settings. Thus, existing and planned dams in this domain require particular attention for the safety of dams, particularly with respect to the seismic safety. Moreover, the reservoirs in the MER are strongly affected by faulting and major fractures, which have caused major leakage problems observed in several dams. Preventive measures against leakage like proper grouting or cutoff walls are necessary. The current water loss through leakage will become critical as water stress increases in the basins with time. Thus, an integrated geological, structural and geophysical study of the dam sites is crucial to improve the safety of the dams and minimize water loss through leakage. For dams in the planning stage in this zone, it is recommended to thoroughly study the impact of structural tectonics in the project areas and the way to minimize water loss from the reservoir through dam foundation and abutment slopes before defining the dam type.

In addition, faulting in dam foundations and at close distance to dam site would be a major safety concern for dams. It is essential to characterize these faults in terms of age to identify their activity.

Chapter 4

4 Seismic Hazard Analysis

Seismic hazard analysis involves the quantitative estimation of ground motion at a particular site of interest taking into account the effect of source, path, and local site conditions. This is necessary for the purpose of working out the earthquake-resistant design of new structures or for evaluating the safety of existing ones such as buildings, dams, nuclear power plants, and others. With the consideration of geology, tectonics, seismicity recorded, and attenuation characteristics of the seismic waves, seismic hazard analysis is commonly done to provide an estimate of site-specific design ground motion in the area of interest.

There are two methods of seismic hazard analysis, i.e. deterministic and probabilistic hazard analyses. A deterministic seismic hazard analysis (DSHA) is carried out, when an earthquake for a well-known source expected to cause damage at the site of interest. In the deterministic hazard evaluation, procedures for selecting seismic evaluation parameters such as magnitude and distance should be ascertained by identifying earthquake scenarios. These are commonly related to active faults, which show signs of movements in Holocene (last 11,000 years), large faults with evidence of movements in Late Pleistocene (11,000 - 35,000 years ago) or major faults that show evidence of repeated movements in Quaternary or in the last 1.8 million years (ICOLD, 1992). The capability of the faults must be determined using well-established methods such as a rupture length-magnitude relationship or fault movement-magnitude relationship proposed by Wells and Coppersmith (1994). The distance to these faults and their estimated rupture length are critical parameters in these empirical relations.

The goal of seismic hazard analysis for any structure is to ensure that the structure can withstand a given level of ground shaking while maintaining a desired level of

performance. However, there are a number of uncertainties about the location, size, and resulting magnitude of ground shaking of future earthquakes. A probabilistic seismic hazard analysis (PSHA) aims to quantify these uncertainties and combine them to produce an explicit description of the distribution of future earthquake shaking that may occur at a site. The basic methodology is based on Cornell (1968). A PSHA quantifies numerically the contributions to the seismic ground motion of all sources and magnitudes larger than a designated minimum to the maximum magnitude in the earthquake catalogue. The possible occurrence of each magnitude earthquake at any part of a source including the closest location to an area of interest is directly incorporated in the PSHA.

The seismic hazard is one of the major concerns for Ethiopian dams located in the seismically active East African Rift zone. However, until recently the seismic hazard was not given proper attention in the design and safety assessment of large dams and it was also not well understood. In addition, the seismic design criteria used at the time of construction of dams do not correspond to today's recommended state of practice (ICOLD, 2016). Moreover, there is no guideline or regulatory framework in place, which enforces a specific set of design criteria to be followed during the design. As a result, the design consideration shows a high degree of variability and does not follow a consistent methodology.

The present seismic hazard evaluation aimed to analyze earthquake hazard for major dam sites in Ethiopia and to develop reference seismic hazard maps for return periods of 10,000 years as per ICOLD recommendations for large storage dams (ICOLD, 2016). The seismic hazard analysis is based on the probabilistic approach using earthquakes recorded from 1600 to 2017. To attain the objectives, the following tasks have been done:

(1) Review of the previous studies in the region and at dam sites to identify the gaps;
(2) Compilation of the earthquake records in the region from different earthquake catalogues;
(3) Homogenization of the earthquake events collected from various sources to make uniform the magnitude of measurement and to remove duplicate events;

(4) Declustering of the catalogue to avoid foreshocks and aftershocks and completeness analysis for various magnitude ranges;

(5) Determination of the earthquake recurrence models and activity rate was worked out based on declustered catalog;

(6) Development of a modified seismic source zones model capable of generating strong ground motion was done by integrating the information obtained from regional geology, tectonics, seismic energy release map and observed seismicity;

(7) Selection of attenuation models for each source zone was performed on the basis of their compatibility to the specific regions

(8) The seismic hazard analysis and development of seismic hazard map for a return period of 10,000 years were done for each dam site. Based on the geology, tectonics, and seismicity, the region was divided into 6 seismic zones; and

(9) Finally, the hydropower and irrigation potential in each seismic zone was determined.

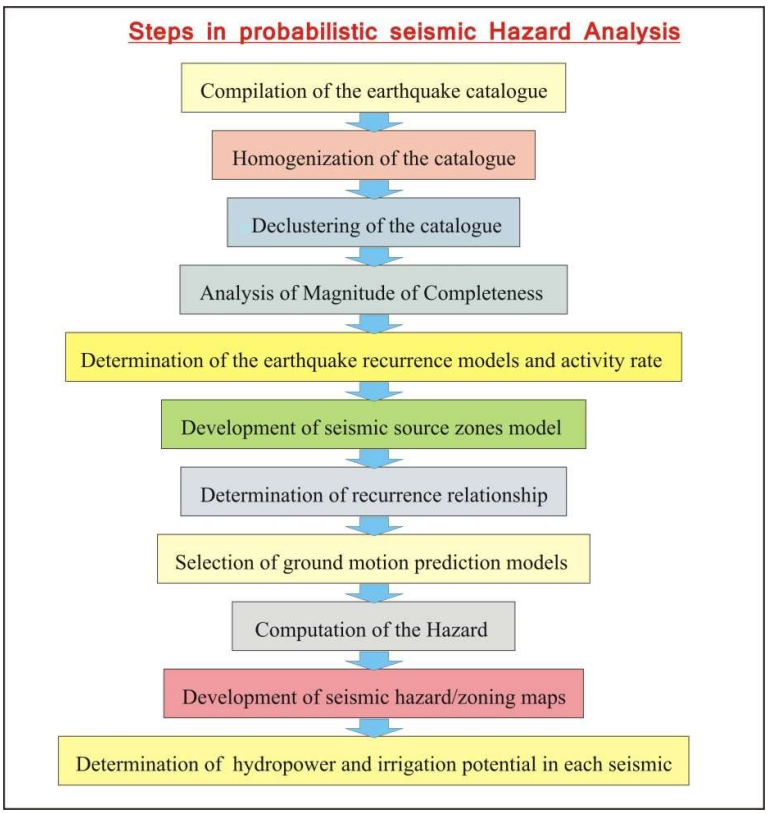

4.1 Previous Studies

Besides the site-specific seismic hazard analysis for various dams, a review of previous studies was made (Gouin, 1979; Kebede and Asfaw, 1996; Midzi et al., 1999; Hagos et al., 2006, Lubkowski, 2014; Ayele, 2016; Poggi, 2017). Gouin (1979) conducted the first and foremost extensive seismic hazard assessment and produced peak ground acceleration (PGA) maps for Ethiopia and Eritrea for a return period of 100 years (Fig. 4a). Following the work of Gouin, Kebede and Asfaw (1996) carried out the seismic hazard assessment for Ethiopia and developed a zoning map in terms of intensity scale (Fig. 4b).

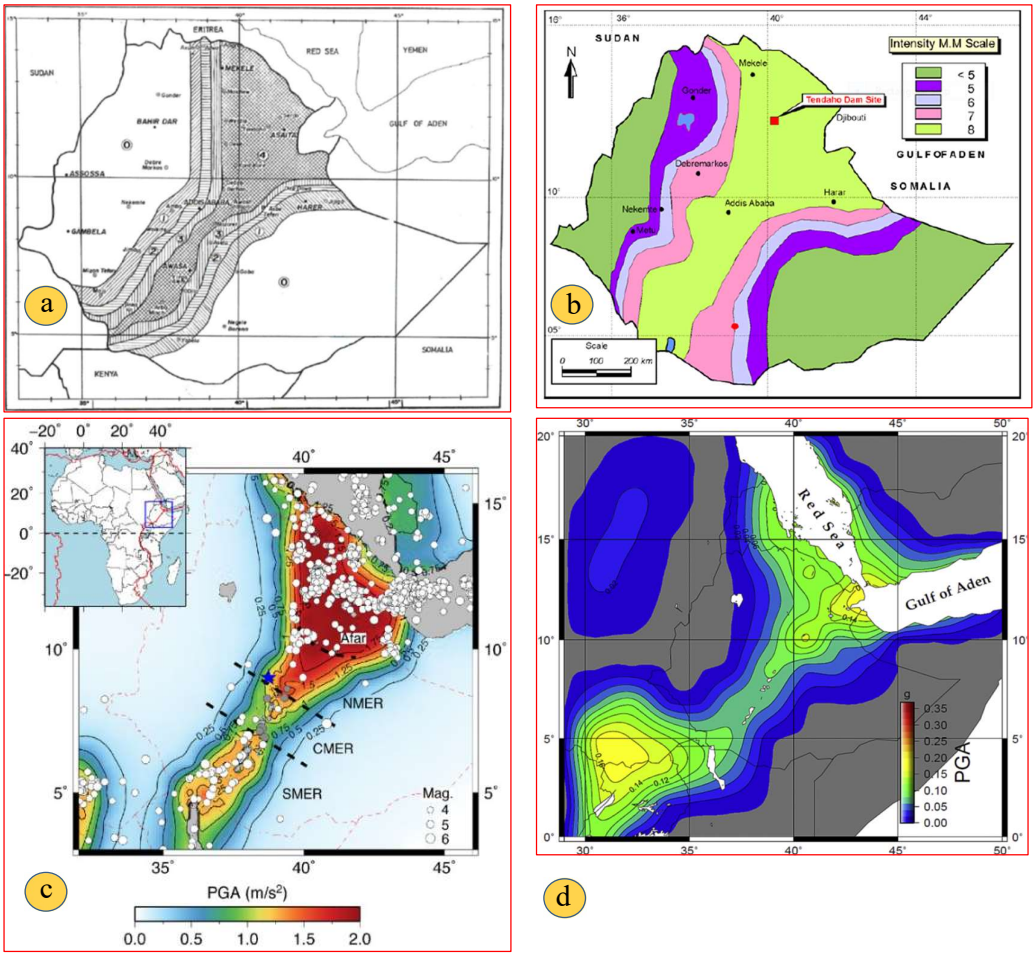

Figure 4.1: Seismic zoning map previously done: Gouin (1978)[a] based on PGA of 100 years RP, Kebede and Asfaw (1996)[b] based on Modified Mercali Intensity scale, Midzi et al., (1999)[c] based on PGA of 100 years RP and Ayele (2016) [d] based on PGA of 475 years RP

Midzi et al. (1999) conducted a generic type of PSHA over a wider area of eastern and southern Africa, as part of the Global Seismic Hazard Assessment Project (GSHAP) (Fig. 4c). Lubkowski et al. (2014) have done preliminary studies on the seismic hazard for East Africa. Aleye (2016) conducted a seismic zoning map of the region for the PGA with a return period of 475 years on which the current seismic building code of Ethiopia is based (Fig. 4d). Poggi et al. (2017) carried out a seismic hazard assessment of the East African Rift using new data and the Global Earthquake Model (GEM).

So far no studies have been made at a national or regional scale for return periods for dams (i.e. 10,000 years) except some project-specific studies that are reviewed in Chapter 2. In this thesis, the seismic hazard analysis is done for a return period of 10,000 years. The resulting seismic zoning map can then be used for large dams.

4.2 Compilation of Earthquake Catalogue

The development of an earthquake catalogue is the first step in the probabilistic seismic hazard analysis that is needed for the development of recurrence models (G-R Model) and source input parameters for hazard analysis. For this purpose, historical and instrumentally recorded earthquake catalogues are compiled from previous works in the region and international sources:

International Seismological Center (http://www.isc.ac.uk/iscbulletin/search/bulletin/), United States Geological Survey (http://earthquake.usgs.gov/earthquakes/search/), National Geophysical Data Center (https://www.ngdc.noaa.gov/nndc/struts/form), Global Centroid Moment Tensor (http://www.globalcmt.org/CMTsearch.html), and from Gouin (1979) and Ayele (1995). From these catalogues, earthquakes with magnitude above 3 recorded from 1600 to 2017 were compiled for further homogenization and declustering works.

4.3 Homogenization of the Catalogue

The complied earthquake events from different sources were merged and duplicate events were removed. However, the earthquake data found from various sources are in different magnitude scales including moment magnitude (Mw), surface-wave magnitude (MS), body-wave magnitude (mb), local magnitude (ML), and the earthquake intensity scale (I). Therefore, it is a prerequisite for a complete earthquake catalogue to have a uniform magnitude. This process involved converting all earthquake events into uniform magnitude type, i.e. the moment magnitude, which is the preferred scale used today. For the magnitude conversion, empirical equations developed by Scordilis (2006) and (Goitom et al., 2017) were used (Table 4.1).

Accordingly, the earthquake catalogue consisting of 5,583 events with Mw > 3 for the years 1631 - 2017 were homogenized for further declustering works.

Table 4.1: Conversion relationships used for magnitude homogenization

Magnitude Conversion	Relationship	Author
1. Mb to Mw	$Mw = 0.92 \times mb + 0.67$	Brehe et al. (2017)
2. MS to Mw	$Mw = 0.67(\pm 0.05)Ms + 2.07(\pm 0.03)$ $3.0 \leq Ms \leq 6.1$	Scordilis, E. M. (2006).
3. MS to Mw	$Mw = 0.99(\pm 0.02)Ms + 0.08(\pm 0.13)$ $6.2 \leq Ms \leq 8.2$	Scordilis, E. M. (2006).
4. ML to Mw	$Mw = 0.85 \times ML + 0.65$	Brehe et al. (2017)

4.4 Declustering of the Catalogue

Declustering of the earthquake catalogue is required before using it for the seismic hazard analysis. Declustering involves removing duplicate events, i.e. separating dependent events (foreshocks and aftershocks) from the independent event, the main shock. Declustering was made using Zmap program version 6 (Weimer, 2001). Three declustering algorithms by Uhrhammer (1986), Reasenberg (1985), and Gardner and Knopoff (1974) were chosen. Each algorithm considers different distances and time windows for declustering (Table 4.2). The catalogue consisting of 5,583 events was declustered using the algorithms by Gardner and Knopoff (1974) and Reasenberg (1985) and four window sizes by Gardner and Knopoff (1974), Gruenthal (1985),

Reasenberg (1985), and Uhrhammer (1986). The corresponding results are given in Table 4.3. The number of events obtained after declustering is the lowest for Gruenthal (1055 events) and the highest for Reasenberg (3267 events).

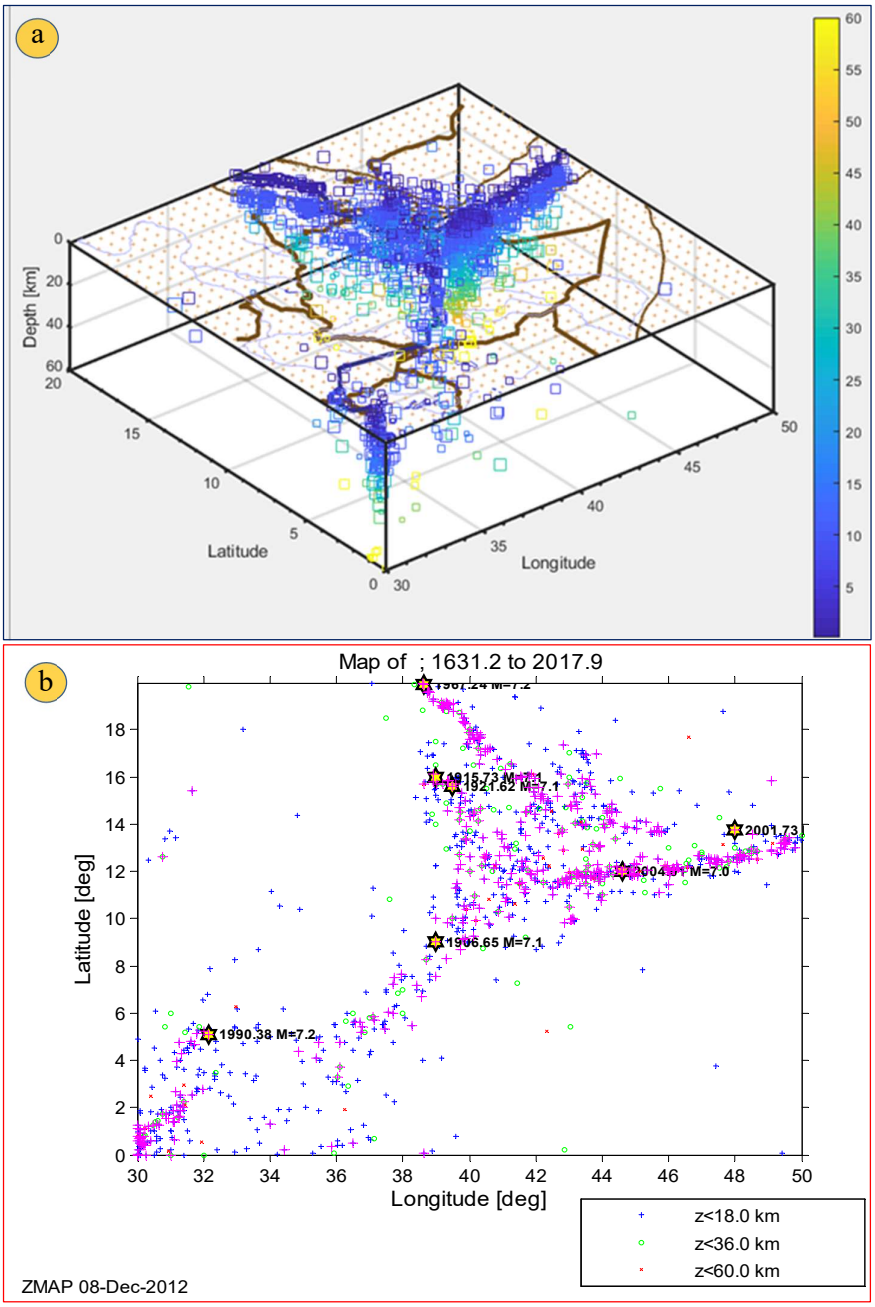

Figure 4.2: Earthquake catalogue after declustering with Gardner and Knopoff (1974) algorithm and window size: (a) hypocenteral distribution of declusterd earthquakes, and (b) epicentral map of declustered earthquakes.

Table 4.2: Windows sizes used for declustering proposed by previous researchers

No.	Algorithm Type	Distance-Window (Km)	Time-Window (D)
1	Gardner, 1974	$d = 10^{0.1238\times M+0.983}$	$t=\begin{cases}10^{0.032\times M+2.7389}, & if\ M\geq 6.5\\ 10^{0.5409\times M-0.5477}, & else\end{cases}$
2	Gruenthal, 1985	$d = e^{1.77+(0.037+1.02\times M)2}$	$t=\begin{cases}e^{-3.95+(0.804+17.32\times M)2}, & if\ M\geq 6.5\\ 10^{2.8+0.024\times M}, & else\end{cases}$
3	Uhrhammer, 1986	$d = e^{-1.024+0.804\times M}$	$d = e^{-2.8+1.235\times M}$

Finally, the result obtained from the algorithm by Gardner and Knopoff is used for the seismic hazard analysis due to similarity in tectonic conditions and the worldwide acceptance. The final catalogue, after the removal of the duplicate events, foreshocks, and aftershocks, consists of 1327 seismic events with moment magnitudes between 3 and 7.2 recorded from 1631 to 2017. The distributions of the hypocentres and epicentres of the declustered earthquake catalogue are shown in Fig 4.2.

Table 4.3: Input parameters for declustering algorithm by Reasenberg (Stiphout et al., 2012)

Parameter	Standard	Min	Max
τmin [days]	1	0.5	2.5
τmax [days]	10	3	15
P1	0.95	0.9	0.99
xk	0.5	0	1
xmeff	1.5	1.6	1.8
rfact	1.0	5	20

where τmin is the minimum value of the look-ahead time for building clusters if the first event is not clustered, τmax is the maximum value of the look-ahead time for building clusters, p1 is the probability of detecting the next clustered event, τ, xk is the increase of the lower cut-off magnitude during clusters: xmeff = xmeff + xkM, M is the magnitude of the largest event in the cluster, xmeff is the effective lower magnitude cutoff for the catalogue, rfact is the number of crack radii surrounding each earthquake within new events considered to be part of the cluster.

Table 4.4: Results of earthquake events (Mw > 3) after declustering with different Algorithms and Window size

Declustering Algorithms/Window/	Original No. Events	No. Clusters	Independent Event	
			No. (%)	% of Energy release
1. Gardner/Gruenthal/	5583	422	1033 (19)	53
2. Gardner	5583	456	1327(24)	56
3. Gardner /Uhrhammer/	5583	484	2191(39)	59
4. Reseanberg	5583	338	3267(58)	App >80

4.5 Analysis of Magnitude of Completeness

The analysis of the magnitude of completeness involves computing the time window for which the catalogue is complete. The most common method used for

completeness evaluation is the Visual Cumulative Method proposed by Mulargia and Tinti (1985). It is a graphical procedure based on the observation that earthquakes follow a stationary occurrence process. For a given magnitude range, the period of completeness is considered to begin at the earliest time when the slope of the cumulative fitting curve can be approximated by a straight line. Use of Zmap program is also an option for completeness analysis of the earthquake catalogue. In the present study, the completeness analysis is carried out by the Visual Cumulative Method and Zmap 6 program.

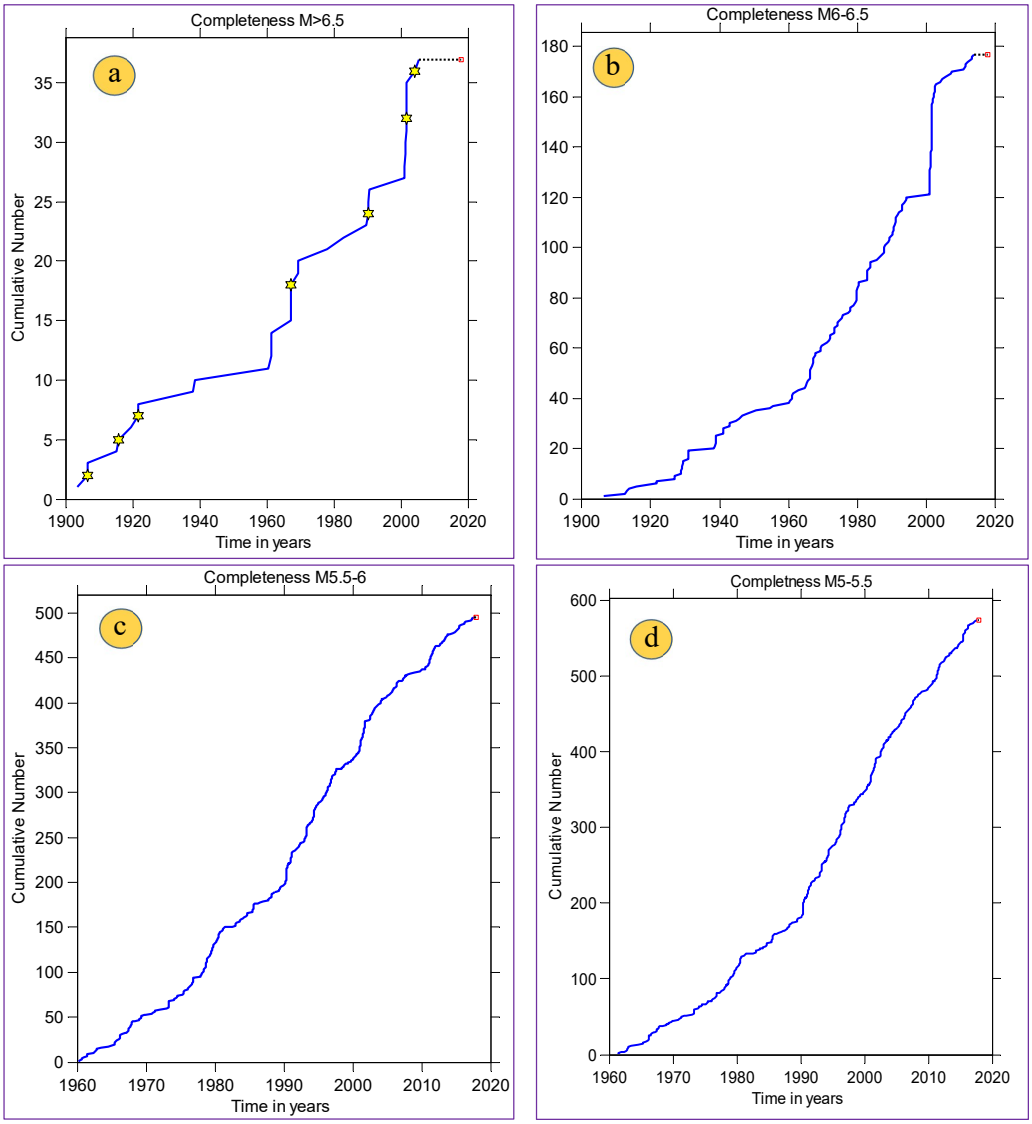

Figure 4.3: Completeness periods of the catalogue for magnitude above 5 [a]$M_{>6.5}$, [b]$M_{6\text{-}6.5}$, [c]$M_{5.5\text{-}6}$, and [d]$M_{5\text{-}5.5}$

The results are in agreement with each other. According to the result obtained, the magnitude of completeness varied with time, magnitude and space. The catalogue is complete since 1900 for Mw>6 and after 1960 for Mw>5 (Fig. 4.3). For magnitudes Mw<5, the catalogue is not uniformly complete for the entire region due to a sparse seismological network in the area.

4.6 Defining Seismic Source Zones

The seismic source zones represent areas where the seismicity is assumed to be homogenous and where there is an equal chance of earthquake occurrence at any point in that source. It can be a line (fault) source or an area source, depending on the available database. However, only area sources are normally recommended in Ethiopia, due to the lack of detailed data on active faults. Seismic hazard analyses are associated with large uncertainties when historical data are insufficient to define the rates of seismicity for the different source zones.

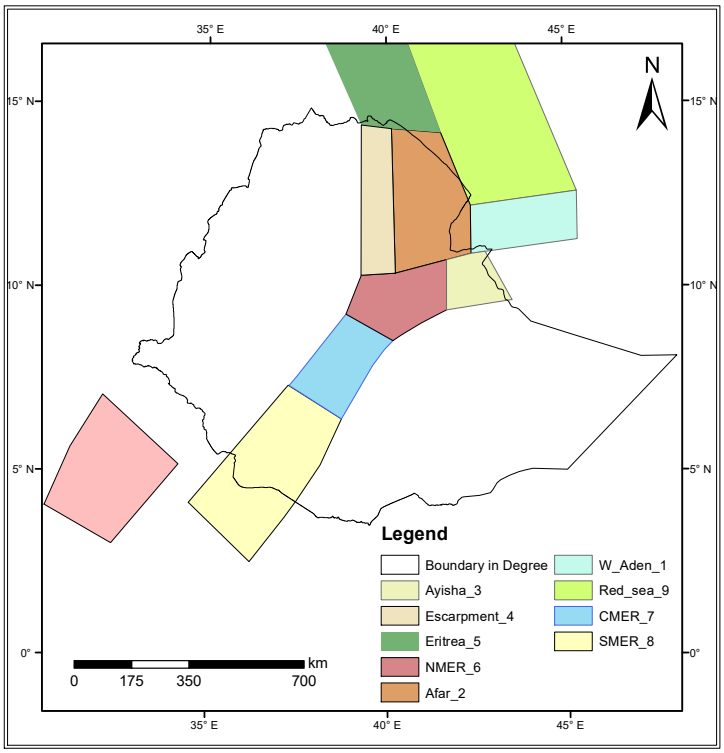

Figure 4.4: Model of seismogenic source zones used for the development of the seismic hazard maps of Ethiopia (modified from Goin 1979 and Hofstetter and Beyth (2003)) by integrating the information obtained from regional geology, tectonics, seismic energy release, and observed seismicity.

Such uncertainties may be decreased using geological data in areas where seismicity is shallow and produced by Quaternary faulting (Wesnousky, 1986). For this work, area source zones previously proposed by different researchers such as Gouin (1979), and Hofstetter and Beyth (2003) were modified (Fig. 4.4).

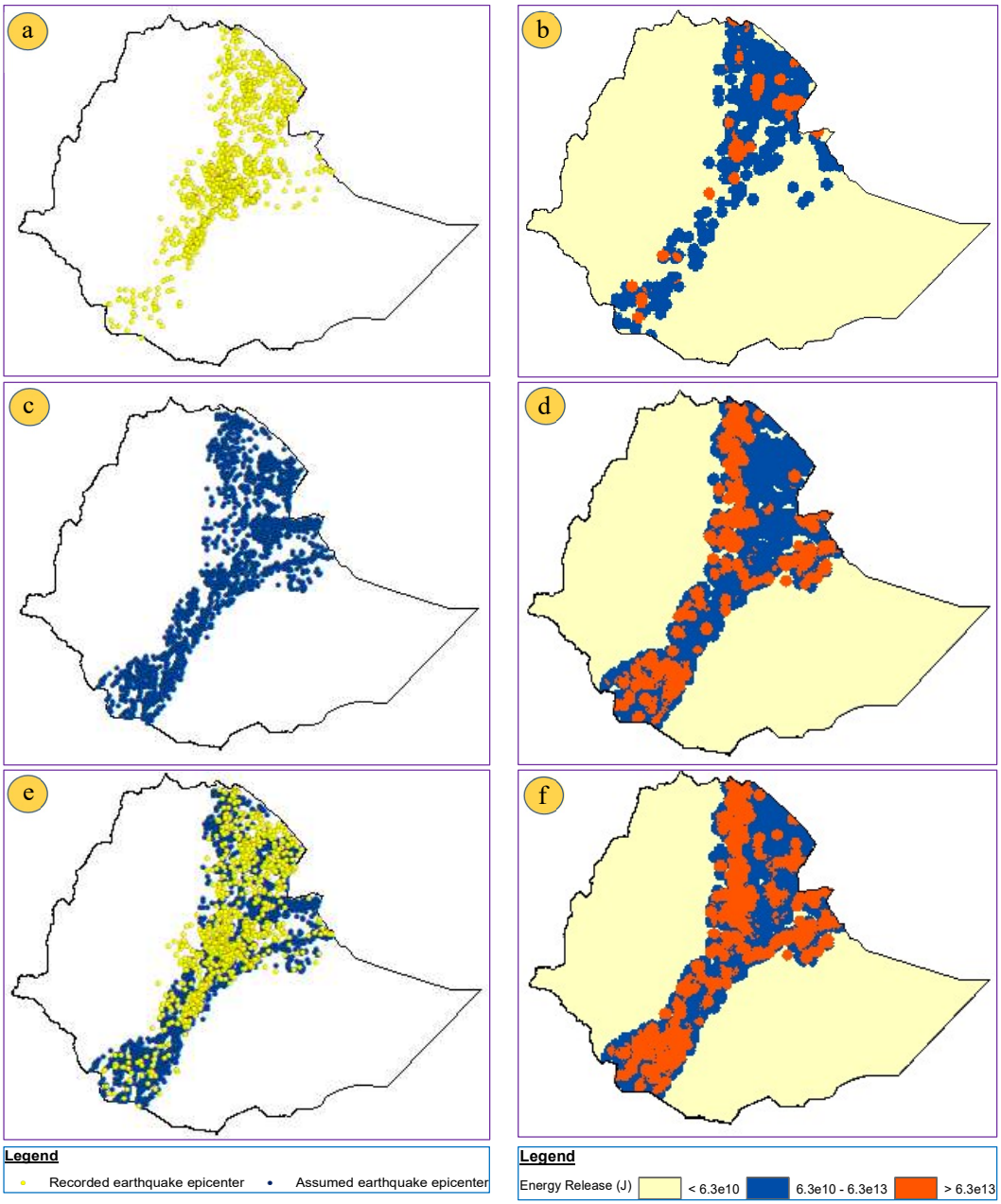

Figure 4.5: Comparisons made between earthquake epicentral maps (left) drawn from: (a) earthquake recorded from 1900 to 2017, (c) earthquake epicenter obtained from Quaternary fault back analysis (e) epicentral map of both a and c earthquakes merged with their corresponding energy release maps (b, d, f) in Jule (right).

The modification was made based on the present assessment that takes into account geology, tectonics, seismicity recorded, seismicity estimated from Quaternary fault back analysis and energy release map developed from both seismicity recorded and seismicity from fault back analysis.

Faults from active Quaternary geology and the surrounding region were mapped using ASTER DEM and existing geological maps. After that, the magnitudes of the earthquakes from faults were determined using the empirical relations developed by Wells and Coppersmith (1994). One-third of the entire length of the fault is assumed to be ruptured at a time (Bohnhoff et al., 2016). The epicenter is assumed as the center of the fault segment and the epicentral map was consequently drawn at the center point. The epicentral map from fault back analysis compared with the observed earthquake epicentral map and the results are in acceptable agreement (Fig. 4.5).

4.7 Recurrence Relationship

The seismicity at each seismic source zone can be characterized with the Gutenberg - Richter (G-R) recurrence relation:

$\log^{N} = a - bM$

Where N is the number of earthquakes having magnitude greater than M and “a” and “b” are constants specific to the source zones and are estimated by a regression analysis of the past seismicity data. “a” gives the rate of occurrence of earthquake events and “b” gives the relative distribution of small and large events. Each source zone supports different values of “a” and “b”.

The a- and b-values are determined by Z-map software (Wiemer, 2001) and the results are cross-checked with the regression method before using them for the seismic hazard analysis. In this process, the cumulative number of earthquakes of a specified magnitude and greater are identified from the declustered earthquake catalogue, which is normalized over the completeness period, to calculate the cumulative frequency. The cumulative frequency (logarithmic scale) is correlated

with the specified magnitude, a linear regression analysis is carried out and fitting to the data is performed to get the fitted trend equation. This provides an estimate of "a" and "b" parameter of the G-R model. Accordingly, the G-R model parameters are gained for all the seismic source zones. The determination of the focal depth is generally poor due to the very limited number of seismographic stations in the region. In the present work, an average focal depth of 10 km is assumed in the seismic hazard computation. The maximum magnitudes for different sources were also crucial for the hazard level and were determined after careful analysis of the earthquake catalogue in combination with the analysis of faults and the seismotectonic settings.

4.8 Ground Motion Prediction Models and Logic Tree Application

Among the critical elements required in the seismic hazard analysis is the choice of ground motion prediction equation (GMPE). This equation defines the reduction in peak ground acceleration (PGA) or intensity (I) with distance from the epicenter (R) for an earthquake of a given magnitude (M). Due to the lack of strong-motion data in Ethiopia, no attenuation equation is developed for the country. In such a situation, it is a very common practice to use worldwide attenuation relationships developed for similar tectonic and geologic conditions. Large numbers of such relationships are available as proposed by different authors for specific regions of the world. Some of these are commonly used for seismic hazard analysis in the region. Moreover, there are a number of uncertainties related to the estimation of the magnitude, location and depth of an earthquake, the magnitude recurrence rate and the attenuation of seismic waves, etc. Thus, to account for all the uncertainties in ground motion predictions, hybrid GMPE is adopted to allow the use of alternative models, each of which is assigned a weight factor that is interpreted as the relative likelihood of the model is correct (Bommer et al., 2005). To attain this, the best three next generation attenuation (NGA) models developed for shallow crustal earthquakes in active tectonic environments are chosen based on the criteria used by Delavaud et al. (2012) with the weight percentages shown in Fig. 4.6.

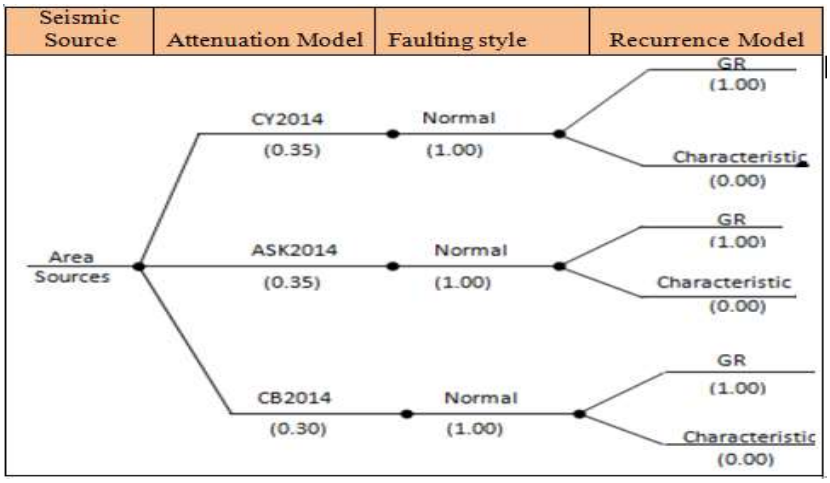

Figure 4.4: Hybrid GMPE used in the seismic hazard analysis. The weighting factors are indicated in brackets (CY2014 - Chiou and Youngs (2014); ASK2014 - Abrahamson, Silva and Kamai (2014), and CB2014 - Campbell and Bozorgnia (2014).

The NGA-West2 ground motion database comprises a very large set of ground motions recorded in worldwide shallow crustal earthquakes in active tectonic regimes. The database has one of the most comprehensive sets of meta-data, including various distance measure, different site characterizations, earthquake source data, etc.

4.9 Computation of the Hazard

The probabilistic seismic hazard analysis was performed using the Crisis 2018 seismic hazard analysis program (Ordaz et al., 2018). The parameters used for each seismic source zone include: a-values (rate of earthquakes occurrence in the source zones), b-values (relative ratio of small to large magnitude earthquakes), M_o (threshold magnitude), Mmax (the maximum magnitude expected in the region) and the seismicity rate.

Mmax for each seismic zone was determined based on maximum historical earthquakes recorded and earthquake magnitude obtained from Quaternary fault rupture length analysis. Input data for crisis needs the values of the mean annual rate of exceedance of a minimum specified I(Mo). It can be obtained from the G-R

relationship in the recurrence model. The input parameters used for the seismic hazard analysis are given in Table 4.5.

Table 4.5: Seismicity parameter used for the hazard analysis

Zone	Mo	Area (km2)	Mmax Observed	Mmax Assigned	β	N(M≥5)/yr
Southern Red Sea	5	164,454	7.2	7.5	2.34	1.05
Eritrea	5	75,022	7.1	7.4	1.96	0.68
Western Gulf of Aden	5	47,563	7.1	7.4	2.25	1.3
Escarpment	5	41,124	6.2	7.1	2.06	0.48
Afar	5	84,184	6.6	7.1	2.21	1.08
NMER	5	48,728	6.8	7.1	2.18	0.27
CMER	5	47,603	6.8	7.1	2.18	0.19
SMER	5	116,753	6.5	7.1	2.18	0.71
Ayisha	5	25,177	6.16	7.1	2.18	0.12
South Sudan	5	96,065	7.1	7.5	1.91	0.55

4.10 Development of Hazard Maps

From the seismic hazard analysis, the peak ground acceleration (PGA) of the horizontal earthquake component on rock outcrop is presented as hazard zoning map for a return period of 10,000 years (equivalent to 1% exceedance probability in 100 years) (Fig. 4.7). The hazard map is divided into six zones based on the PGA results: Zone 1 (0.1 g), Zone 2 (0.1 – 0.2 g), Zone 3 (0.2 - 0.3 g), Zone 4 (0.3 – 0.4 g), Zone 5 (0.4 – 0.5 g) and Zone 6 (> 0.5 g). The locations of dam sites are plotted on the isoseismal map (Fig.4.8).

The level of hazard is highest in Afar region with PGA-value exceeding 0.65 g in the area bordering Djibouti. The hazard map describes the aggregate hazards from the seismic sources and is composed of the respective contributions of all possible earthquakes from the sources that are potentially damaging. From the seismicity observed at various dam sites, the Main Ethiopian Rift controls the seismic hazard in the central and southern part of the country followed by the Escarpment Seismogenic Source Zone which governs the hazard at dam sites in the northern part of Ethiopia.

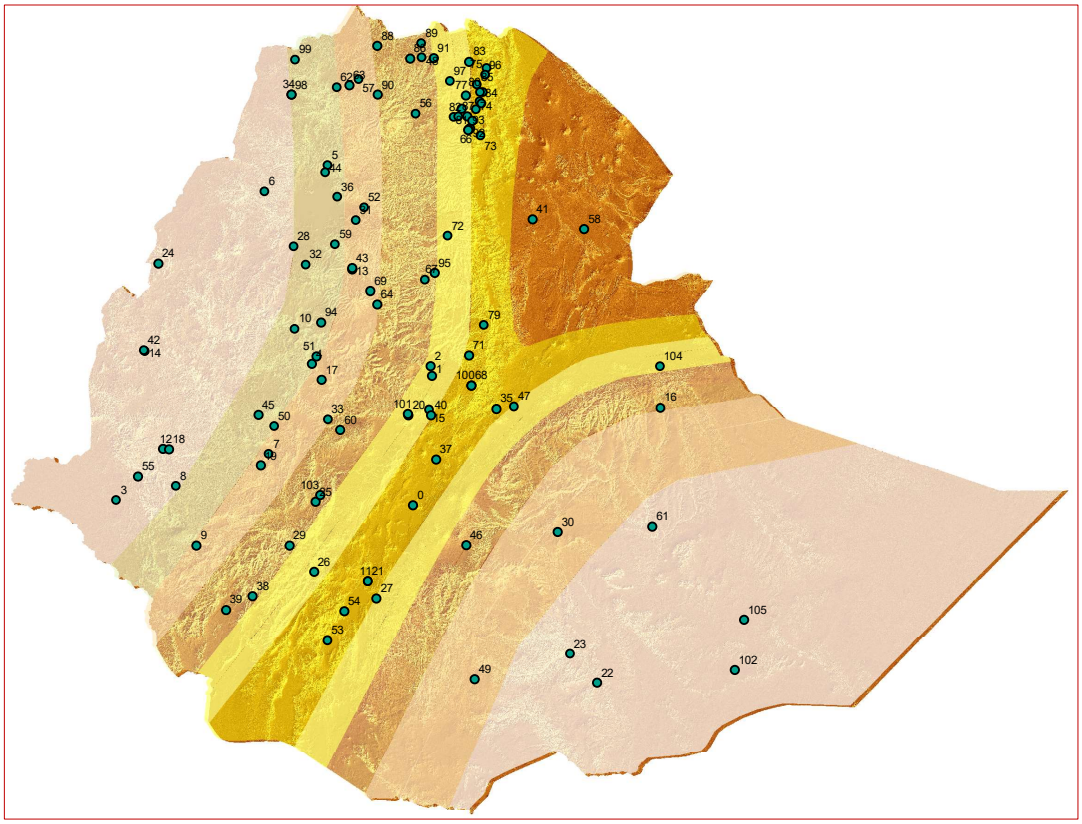

Figure 4.5: Seismic zoning map of Ethiopia for 10,000 years return period. Circles indicate the location of dam sites.

4.11 Hydropower and Irrigation Potential in Different Seismic Zones

Based on the seismic zoning map, the number of dams in different risk zones and estimated power and irrigation potential are summarized in Table 4.6. The estimation of power and irrigation potential is based on currently available data, which may vary with time due to new development plans or additional data from dam inventory currently ongoing. Out of 110 large dam sites considered in the present hazard analysis, 38 dam sites are found in a seismically high-risk zone, 45 dam sites are located in low seismic risk zone and 27 dam sites are located in a moderate risk zone.

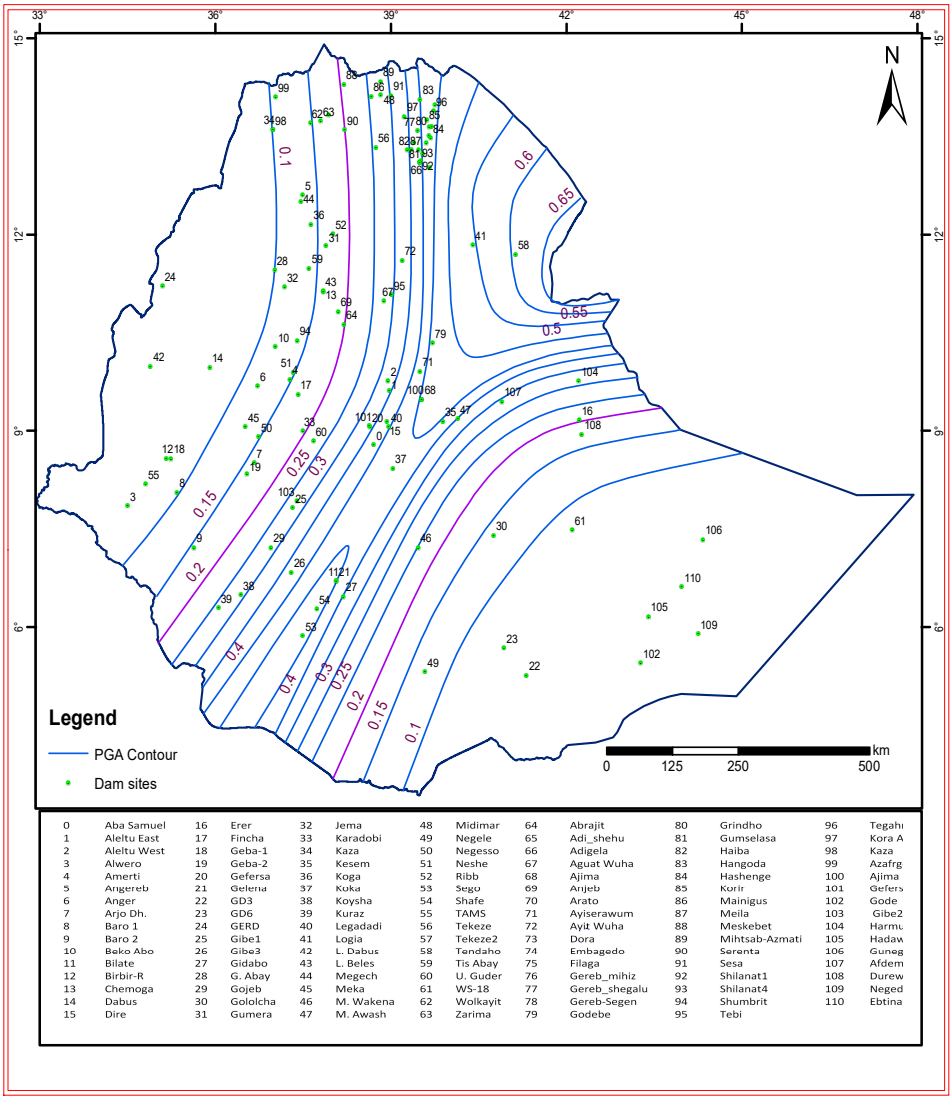

Figure 4.6: Seismic hazard map for PGA with return period of 10,000 years (horizontal earthquake component on outcropping rock and 5% damping) and location of dam sites.

The preliminary estimate of the hydropower and irrigation potential in various seismic zones was conducted. Accordingly, the majority of hydropower dams and potential dam sites are found in a seismically less active zone as compared to irrigation and water supply dams. The total percentage of power from large existing, planned and under construction hydropower dams located in the different seismic zones are estimated (Table 4.6). Similarly, the irrigation potential that depends on large dams is also estimated based on available data.

Table 4.6: Estimated hydropower and irrigation potential in different seismic zones (PGA for return period of 10,000 years)

Seismic Zone	PGA horizontal (g)	No. of dam sites		Estimated Hydropower Potential (%) (existing and planned)	Estimated Irrigation Potential (%) (existing and planned)
		Existing	Planned		
1	0.1	6	10	31	16
2	0.1 - 0.2	9	20	35	30
3	0.2 – 0.3	10	17	18	12
4	0.3 - 0.4	8	10	11	15
5	0.4 – 0.5	11	7	5	17
6	>0.5	1	1	-	10

According to Table 4.6, 66 % percent of hydroelectric generating capacity is located in zones of low seismic hazard with PGA of less than 0.2 g. 18 % is found in a moderate seismic hazard zone (PGA 0.2 – 0.3 g) and the remaining 16 % in a high seismic hazard zone.

In other words, 84% of Ethiopia's hydroelectric generating capacity is located in zones of low to moderate seismicity and 46% of the irrigation potential that depends on dams is located in a zone of a low seismicity, 12% is found in moderate seismic hazard zone and 42% in a high seismic hazard zone.

4.12 Conclusions

The East African Rift System (EARS) which includes the MER is a seismically as well as tectonically active region. It has experienced damaging earthquakes recorded in the past. Therefore, the seismic hazard is an important one that must be considered in the design of new dams and the safety evaluation of existing dams. The goal of a seismic hazard analysis is to ensure that the structure can withstand a given level of ground shaking while maintaining a desired level of performance. In this regard, the seismic hazard studies previously carried out for the dams in Ethiopia, discussed in Chapter 2, show high variability and don't comply with the current state of practise. The present study shows that they have to be revised for most dams. The seismic hazard analysis was conducted based on the probabilistic approach. The earthquake catalogue of Ethiopia, compiled from international and local earthquake catalogues, consists of more than 5583 events with Mw greater than 3 for the period 1600 to 2017. Homogenization of the earthquake catalogue was done followed by declustering and completeness analysis for various magnitude ranges. The catalogue compiled for this study is complete since 1900 for Mw>6 and after 1960 for Mw>5.

From compiled catalogue (1600 to 2017), an epicentral map of earthquakes in Quaternary geological setup and its periphery was drawn. Similarly, an epicentral map of earthquakes was also drawn from fault back analysis. Based on the two epicentral map, an energy release map was developed to obtain additional insight in seismogenic source zone delineation. Accordingly, the modified seismogenic source zone was modelled by integrating the information from the Quaternary geological and tectonic setup, seismic energy release, and observed seismicity.

Using the modified seismic source zone model, seismic hazard analysis was carried out to prepare a reference seismic zoning map for large dams with a return period of 10,000 years as recommended by ICOLD (2016). The horizontal PGA-values obtained for various dam sites for 10,000 years return period vary between 0.1 g and 0.61 g. The minimum is for the GERD dam and the maximum is for the Tendaho dam. According to the hazard map, six seismic zones were defined (zone 1 less than 0.1 g, zone 2 0.1- 0.2 g, zone 3 0.2 - 0.3 g, zone 4 0.3 – 0.4 g, zone 5 0.4 – 0.5 g, and zone 6 greater than 0.5 g). Accordingly, 38 dam sites are located in a seismically high-risk zone, 45 in low-risk zones and 27 dam sites in a moderate-risk zone. The results of the present probabilistic seismic hazard study show that in the past the seismic hazard has been underestimated in most dam sites; therefore, in the MER, Afar and its surrounding the seismic hazard and seismic safety criteria must be updated, followed by a seismic safety check of the dams.

The PGA-values for different dams can be estimated based on the seismic hazard map developed in this study. For the hazard analysis, Vs30 of 760 m/s is assumed as representative for average rock site in the dam foundation. Based on the site-specific geology and site conditions, the seismic hazard can be higher. This map is suitable for preliminary design and safety assessments of existing dams. However, for the detail design of large storage dams, a site-specific hazard assessment is highly recommended.

Chapter 5

5 Seismic Risk Analysis

5.1 Introduction

In any business, there is a risk and it is not possible to avoid at all, except to minimize it. Risk is the probability that some undesirable events to occur from manmade hazards or hazards from the natural environment. In the context of dam safety, the undesirable event is a dam failure which is an uncontrolled release of water from the reservoir (Wieland, 2019). Such undesirable event of dam failure results from a number of uncertainties that are involved in the safety evaluation of dams. Even when conservative assumptions are made, there will always be a probability that the performance of the dam during its lifetime may not be as predicted (Yegian et al., 1988). This indicates that large dams are critical facilities whose failure could produce important societal and economic consequences. Dam failures can lead to extensive life loss, economic or financial losses, environmental damage, damage to cultural heritage sites and other undesirable consequences. Consequences are a means of measuring the severity of a dam failure. Thus, a dam safety risk is measured not only by the probability of dam failure but also by the probability distribution of the consequences of the failure.

The risk (R) is defined as the probability of failure (pf) multiplied by the consequences (C). Besides, pf can be defined as the product of the hazard (H) times the vulnerability (V). Based on this, the basic factors of a risk analysis are H, V, and C. Risk analyses can be done for single projects or a portfolio of dam projects; for single hazards (floods and earthquake ground shaking) or for all possible hazards (natural hazards, man-made hazards and site-specific and project-specific hazards) (Wieland, 2019). However, risk analyses are only feasible for specific hazards such as flood hazard or seismic ground shaking hazard. The results of such specific hazards

analyses do not provide a complete picture of the risks of a large dam project (Wieland, 2019).

Table 5.1: List of large dams in Ethiopia used in seismic risk analysis

No.	Dam	Basin	Dam Type	Dam Height(m)	Reservoir Volume(Mm^3)	Purpose	Commissioned
1	GERD	Abay	RCC CG	145	74,000	H	UC
2	Gibe-4	Omo-Gibe	RCC CG	201	6500	H	UC
3	Gibe-3	Omo-Gibe	RCC CG	246	14,700	H	2016
4	Gibe-2	Omo-Gibe	CG	53	2.26	H	2010
5	Gibe-1	Omo-Gibe	AFRD	71	839	H	2004
6	GD3	Genale	CFRD	70	1,400	H	2019
7	Tekeze	Tekeze	ARCH	188	9,293	H	2009
8	Neshe	Abay	E	38	448	H	2011
9	Amerti	Abay	E	15	219	I	2009
10	Wakena	Wabe Sh.	ER	42	763	H	1990
11	Fincha	Abay	E	22	940	H	1970
12	Koka	Awash	CG	23	1,850	H	1961
13	A. Samuel	Awash	CG	22	35	H	1939
14	Zarima	Tekeze	ACRD	150	4,000	I	2019
15	Arjo	Abay	E	47	2,000	I	UC
16	Gidabo	R. Valley	EF	26	72	I	2018
17	Ribb	Abay	E	73	234	I	2017
18	Kesem	Awash	R	96	500	I	2012
19	Tendaho	Awash	ER	53	1,860	I	2009
20	Koga	Abay	E	21	83.3	I	2007
21	Alwero	Baro	E	14	75	I	1991
22	Kuraz	Omo-Gibe	R	30	30	I	2017
23	Megech	Abay	R	78	180	I/WS	UC
24	U. Guder	Abay	EF	40	57	I	UC
25	Angereb	Abay	E	23	5.29	WS	1992
26	Meqa	Abay	RF	18	11	WS	2010
27	Dire	Awash	E	41	19	WS	1995
28	Midimar	Tekeze	E	30	10	WS	1988
29	Gefersa	Abay	CG	110	2,570	H	2018
30	Legadadi	Awash	E, CG	44	44	WS	1978

ACRD – Asphalt Core Rockfill Dam; AFRD – Asphalt Face Rockfill Dam; CFRD – Concrete Face Rockfill Dam; CG – Concrete Gravity Dam, RCC CG – Roller Compacted Concrete Gravity Dam; E – Earthfill Dam; ER – Earth-Rockfill Dam; H – Dams used for Hydropower; I – Dams used for Irrigation: WS – Dams used for Water Supply; UC – Dams Under Construction.

Risk analysis for dam safety management can be done by qualitative, quantitative or empirical approaches. An empirical method was proposed by Bureau (2003) which is based on the statistical analysis of historical data. This method is used in the present study to evaluate the seismic risk of 30 large dams in Ethiopia (Table 5.1 and Fig. 5.1). Failure of a major dam in Ethiopia could impose severe economic loss. Both directly, through the loss of structures and the downstream damage, but also through loss of power production, irrigation, water supply and related consequences. This could last for years since such structures are not easily replaceable. Such an event could severely damage the good economic development that the country is currently experiencing or even bring it to a complete stop. The main objective of this risk analysis is to rank dams in terms of seismic risk and to prioritize dams with the highest risk class or highest consequences for detailed safety evaluation.

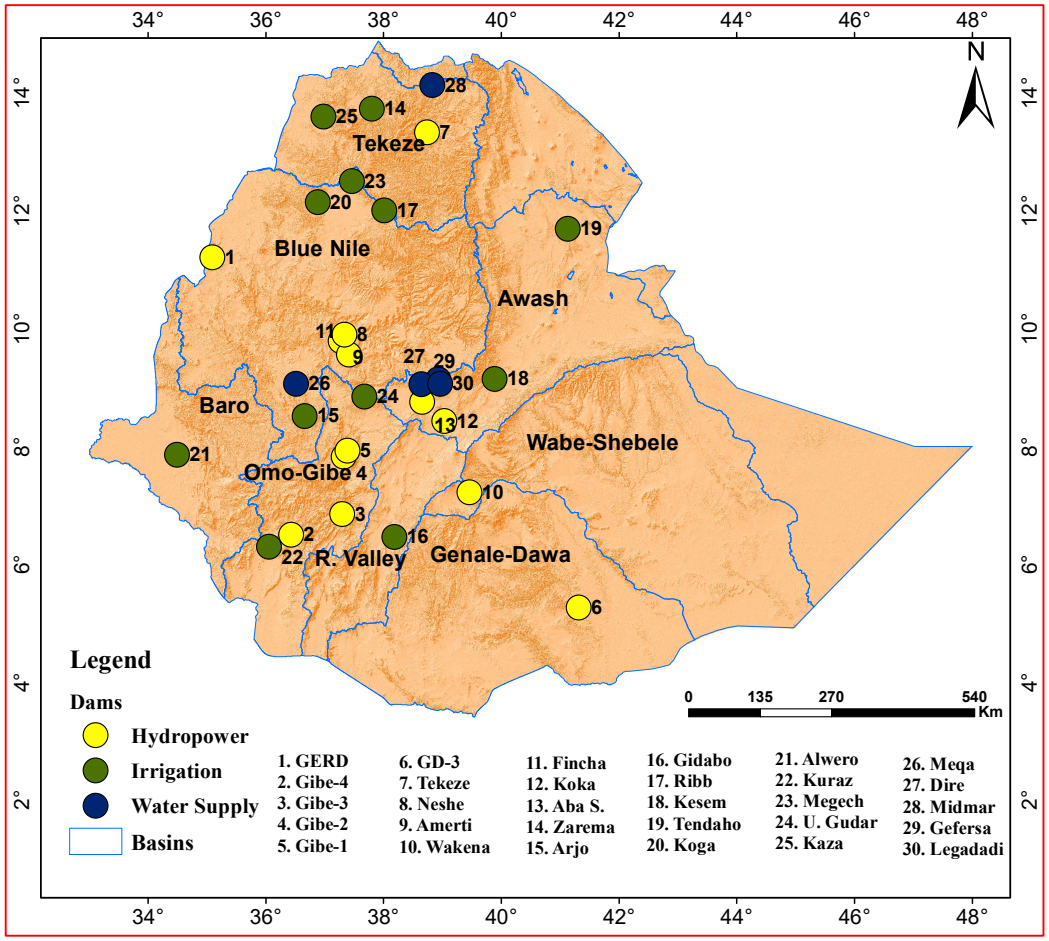

Figure 5.1: location map of thirty large dams in different basins of Ethiopia considered for seismic risk analysis.

For the seismic risk analysis, the results of the probabilistic seismic hazard analysis, discussed in Chapter 4, were used as input. The seismic hazard (different levels of ground motion), the seismic vulnerability of the dam and safety-relevant elements (seismic performance or probability of failure), and the consequences (loss of life and physical damage) in case of uncontrolled release of water from the reservoir, were considered. Based on this, the seismic risk classes of the 30 dams have been defined and their seismic vulnerability ranked. The result of the risk analysis combines available information on the level of the seismic hazard at dam sites, vulnerability, and consequences to prioritize the decision-making methodologies in dam safety. This is very important for planning of dam safety rehabilitation measures and the development and implementation of emergency preparedness plans for the priority dams.

5.2 Methods

There are different methods for the seismic risk assessment of large storage dams. Methods proposed by ICOLD (1989) and Bureau (2003) are the most common ones used for the seismic risk analysis of large dams. A seismic risk ranking method is given in ICOLD Bulletin 72 (1989). This risk ranking method consists of structural and socioeconomic components. The structural components depend on the storage volume and height of the dam. The socio-economic component depends on the number of people who need to be evacuated in case of dam failure and the potential downstream damage. This method gives higher weighting factor to dams with larger storages, posing larger evacuation requirements and causing higher potential downstream damage. The risk rating is subdivided into four risk factors, i.e. capacity risk factor, dam height risk factor, evacuation requirements risk factor, and potential downstream damage risk factor. Weights are given to the risk factors, which may be described as low, moderate, high or extreme. The Total Risk Factor (TRF) is the sum of the above four risk factors. Based on TRF four risk classes are defined: low (0 - 6), moderate (7 - 18), high (19 - 30), and extreme (31 - 36). According to the risk classification, the seismic design criteria are specified. Dams with high seismic risk

rating will require a detailed method of dynamic analysis and acceleration time histories as input. Simpler analysis methods of using response spectra or peak ground motion parameters may be acceptable for dams of low or moderate risk ratings.

The method proposed by Bureau (2003) is used for this study. It considers different risk factors and weights to measure the total risk factor (TRF) of a dam, which depends on the dam type, size, age, downstream risk, and vulnerability. The method was originally developed for general earthquake risk and loss estimation in the USA and subsequently modified by different researchers.

Accordingly, the total risk factor is defined as follows:

$$TRF = [CRF + HRF + ARF + DHF] \times PDF \quad \text{.....(5.1)}$$

CRF - Capacity Risk factor;

HRF - Height Risk factor;

ARF - age rating factor;

DHF - downstream hazard factor, and

PDF - predicted damage factor.

CRF, HRF and ARF measure the risk related to the dam and the reservoir. The DHF can be taken as the sum of the evacuation requirement factor (ERF), and the downstream damage risk index (DRI) as shown in Eq. (5.3).

ERF depends on the population at risk and DRI depends on the value of private, commercial, industrial and government properties in the potential flood path.

5.3 Analysis of the Results

The total risk analyses were conducted considering four risk factors. The first factor addresses risks related to the dam structure and the reservoir. The second one deals with downstream risks that comprise risks of life, property and environment

downstream of the dam. The third risk factor is related to the seismic vulnerability rating, and the last factor represents the seismic hazard (peak ground acceleration and maximum expected earthquake) at each dam site.

5.3.1 Dam Structural Risks

Dam structural risk (R1) can be taken as the sum of risks associated with dam height, storage volume and age of the dam, i.e.

R1 = CRF + HRF + ARF …….. (5.2)

Both the reservoir capacity risk factor (CRF) and the dam height risk factor (HRF) reflect that high dams or large storage reservoirs can cause significant flood damage in the downstream area of the dam. Whereas, the age rating factor (ARF) takes into account the decrease of dam safety with age due to natural processes and the lack of proper maintenance. Furthermore, the construction methods, equipment types and quality control methods have changed. The age risk factors given by Bureau (2003) are used in this risk analysis with minor modifications taking into account the age of dams in Ethiopia and the time difference during the development of this method. The criteria used for rating dam structural risk are given in Table 5.2.

Table 5.2: Definition of dam height and reservoir capacity risk factors (weighting factors are given in brackets)

Risk factor	Contribution to total risk factor (weighting points)			
	Low	Moderate	High	Extreme
Reservoir capacity [Mm^3] (CRF)	< 0.1 (6)	0.1 – 1 (4)	1 – 60 (2)	> 60 (0)
Dam height [m](HRF)	< 6 (6)	6-12 (4)	12-24 (2)	> 24 (0)

Table 5.3: Dam age risk factor (ARF)

Dam Age	<1920	1920 -1950	1950-1975	1975-2000	2000-2015	> 2015
ARF	6	5	4	3	2	1

5.3.2 Downstream Risk

Ethiopia has extensive densely populated low-lying areas and dams are usually constructed in mountainous terrain. The people affected by dam failure are living downstream in the flood plain. According to Bureau (2003), the downstream hazard factor (DHF) is given by the sum of downstream evacuation requirements factor (ERF) and the downstream damage risk index (DRI) that depends on the population at risk and the properties exposed to flood risk, respectively.

DHF = ERF + DRI……..... (5.3)

Table 5.4: Dam structural risk factors of Ethiopian dams

Dam	CRF	HRF	ARF	Dam	CRF	HRF	ARF	Dam	CRF	HRF	ARF
Aba Samuel	4	4	5	GERD	6	6	1	Legadadi	4	6	3
Alwero	6	4	2	Gibe-1	6	6	2	Megech	6	6	1
Amerti	6	4	3	Gibe-2	4	2	2	Midimar	4	6	3
Angereb	4	4	2	Gibe-3	6	6	1	Negele	4	4	3
Chara	6	2	3	Gidabo	6	6	1	Neshe	6	6	2
Arjo	6	6	1	Kesem	6	6	2	Ribb	6	6	1
Dire	4	6	2	Koga	6	4	2	Tekeze-1	6	6	2
Fincha	6	4	3	Koka	6	4	5	Tendaho	6	6	2
Gefersa	4	4	3	Koysha	6	6	1	Wakena	6	6	3
GD3	6	6	1	Kuraz	4	6	1	Zarima	6	6	1

In the present study, the assessment of the downstream evacuation requirement factor (ERF) and the downstream damage risk index (DRI) have been determined based on available reports, field observations and satellite images. However, these factors should preferably be obtained from dam breach analyses, inundation mapping, and economic studies. In addition, DHF should be updated periodically and whenever new information becomes available on downstream developments, or when the dam is repaired, modified, or raised.

Table 5.5: Evacuation requirement factor (ERF) and damage risk index (DRI) (after Bureau 2003)

	Extreme	High	Moderate	Low
Number of people	>1000	100 - 1000	1-100	0
Rate (ERF)	12	8	4	1
DRI	High	Moderate	Reduced	None
Rate (DRI)	12	8	4	1

5.3.3 Seismic Vulnerability Rating

The vulnerability rating is a function of the site-specific seismic hazard and observed performance of similar dams, as defined by a predicted damage factor (PDF).

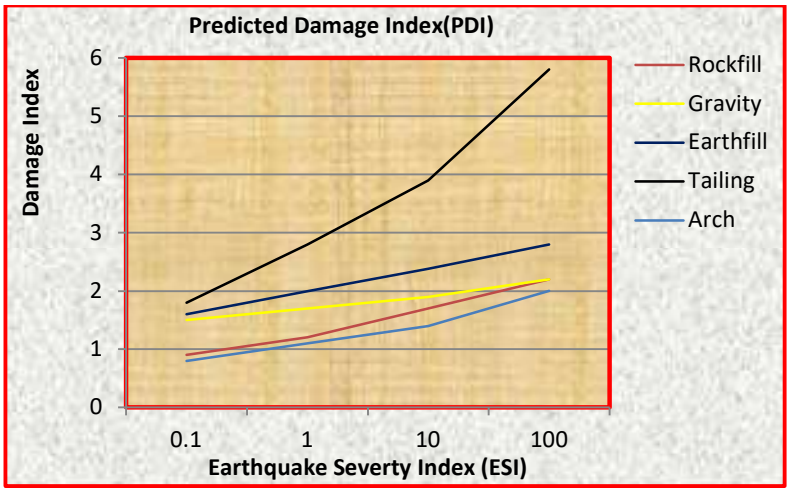

Figure 5.2: Predicted earthquake damage index (PDI) for various dams (after Bureau and Ballentine 2002). One means no damage and six means total collapse.

Dam vulnerability curves developed by Bureau and Ballentine (2002) from the observed seismic performance of dams during earthquakes were used to compute a predicted damage index (PDI). The PDI depends on the dam type and the site-specific seismic hazard. The expected ground motion at the dam site for the scenario earthquake considered is expressed by the earthquake severity index (ESI) defined by Eq. 5.4.

$$\mathrm{ESI} = \mathrm{PGA} \cdot (M - 4.5)^3 \quad \text{..... (5.4)}$$

Where PGA is the peak ground acceleration and M is the maximum possible earthquake magnitude.

5.3.4 Dam Risk Classes

Based on the results obtained for all risk factors (CRF, HRF, ARF, DHF and PDF), the total risk factor (TRF) is computed using Eq. 5.1. The results are given in Table 5.6.

Table 5.6: Ranking of total seismic risk of Ethiopian dams

Dam Name	Site Influence		Structural Influence			Downstream Influence		Vulnerability Rating			Risk		
	M_{max}	PGA	CRF	HRF	ARF	DRI	ERF	ESI	PDI	PDF	TRF	Class	Category
Tendaho	7.1	0.61	6	6	2	12	12	7.42	2.30	5.76	218.7	III	High
Kesem	7.1	0.44	6	6	2	12	12	5.35	2.24	5.61	213.1	III	High
Gidabo	7.1	0.40	6	6	1	12	12	4.87	2.23	5.56	205.9	III	High
Dire	6.8	0.38	4	6	3	12	12	4.62	2.22	5.54	205.0	III	High
Koka	7.1	0.43	6	4	4	12	12	5.23	2.04	5.11	194.2	III	High
A. Samuel	6.8	0.38	4	4	5	12	12	4.62	1.85	4.63	171.5	III	High
Gibe-3	6.8	0.34	6	6	1	12	12	4.50	1.85	4.63	171.2	III	High
Gefersa	6.8	0.34	4	4	4	12	8	4.14	1.84	4.60	147.3	III	High
GERD	6.0	0.10	6	6	1	12	12	0.34	1.58	3.96	146.4	III	High
Ribb	6.0	0.17	6	6	1	12	12	0.58	1.88	4.69	141.9	III	High
Legadadi	6.8	0.39	4	6	3	8	8	4.75	1.86	4.64	134.6	III	High
Midimar	6.0	0.28	4	6	3	4	8	0.95	1.95	4.88	121.9	II	Moderate
Fincha	6.0	0.17	6	4	4	4	8	0.56	1.87	4.67	121.5	II	Moderate
Neshe	6.0	0.15	6	6	2	6	6	0.49	1.85	4.63	120.3	II	Moderate
Gibe-1	6.5	0.27	6	6	2	12	8	2.16	1.41	3.53	120.1	II	Moderate
Tekeze	6.5	0.26	6	6	2	12	12	3.16	1.25	3.13	119.0	II	Moderate
Alwero	6.0	0.10	6	4	3	4	8	0.34	1.80	4.49	112.3	II	Moderate
Koga	6.0	0.14	6	4	2	4	8	0.47	1.85	4.61	110.7	II	Moderate
Arjo	6.0	0.16	6	6	1	12	12	0.54	1.18	2.96	109.4	II	Moderate
Angereb	6.0	0.16	4	4	3	6	6	0.54	1.87	4.66	107.3	II	Moderate
Meka	6.0	0.13	4	4	3	4	8	0.44	1.83	4.59	105.5	II	Moderate
Amerti	6.0	0.15	6	4	1	12	12	0.49	1.17	2.92	102.2	II	Moderate
Wakena	6.5	0.25	6	6	3	4	8	2.00	1.48	3.69	99.7	II	Moderate
U. Guder	6.0	0.10	6	6	1	4	8	0.34	1.58	3.96	98.9	II	Moderate
Megech	6.0	0.13	6	6	1	8	12	0.43	1.15	2.87	94.7	II	Moderate
Zarima	6.0	0.17	6	6	1	12	8	0.56	1.00	2.50	82.6	II	Moderate
Kuraz	6.5	0.26	4	6	1	4	8	2.08	1.41	3.52	80.9	II	Moderate
GD3	6.0	0.10	6	6	1	4	12	0.34	1.11	2.78	80.7	II	Moderate
Gibe-2	6.5	0.27	4	2	2	4	4	2.16	1.77	4.43	70.8	II	Moderate

Mmax – maximum earthquake magnitude (Mw), PGA – Peak Ground Acceleration (horizontal component of SEE), CRF – Capacity Risk Factor, HRF - Height Risk Factor, ARF - Age Risk Factor, DRI – Damage Risk Index, ERF – Evacuation Requirement Factor, ESI – Earthquake Severity Index, PDI – Predicted Damage Index, PDF – Predicted Damage Factor, TRF – Total Risk Factor

5.4 Discussion of Results

The analysis of the total seismic risk factor is conducted for 30 large dams in Ethiopia. According to the method proposed by Bureau (2003), the risk class of the dams are as follows: I (low) for the TRF less than 25; II (moderate) for the TRF from 25 to 125; III (high) for the TRF 125 to 250; and IV (extreme) for the TRF exceeding 250. The large dams considered in the present seismic risk analysis are classified in risk classes II and III, a moderate and high-risk rating and there is no dam having risk classes I and IV. The results of the total seismic risk analyses of the dams are given in Table 5.6. The TRF values range from 64.0 to 218.9 and the PGA from 0.1 g to 0.61 g (low to high hazard classes). There are eleven dams (36%) in risk class III and nineteen dams (64%) in risk class II. Among the 11 dams in risk class III (high risk), Tendaho dam in Afar region has the highest seismic risk with a TRF-value of 218.7 followed by Kesem, Gidabo, Dire, Koka, Aba Samuel, Gibe-3, GERD, Ribb, and Gefersa dams in decreasing order of TRF-value. A detailed seismic hazard and seismic safety analysis should be performed for these dams.

The seismic risk analysis depends mainly on the dam type and downstream consequences; earthfill dams have higher risk than concrete gravity, rockfill, and arch dams in decreasing order. Besides, one of the limitations of this method is aggregating different types of earthfill and rockfill dams. For example, central clay core has higher seismic risk as compared to concrete face, asphalt face or asphalt core rockfill dams, which is one of the limitations of the method. Furthermore, earthfill dams are also highly variable dam types and include hydraulic fill and zoned earthfill dams, which have again the same value. Thus, this limitation needs improvement to differentiate various types of rockfill and earthfill dams. In addition, the method only takes into account earthquake ground shaking. Other earthquake hazards like faults in the footprint of the dam or the reservoir, and rockslides, rockfalls and landslides at the dam site or in the reservoir are not considered.

The three Addis Ababa water supply dams (Dire, Legadadi, and Gefersa) are all high risk dams. Out of the three dams, two are also aging. The seismic design and safety criteria used for the design of these dams are either not known or are obsolete when

compared with modern criteria. These dams are vital for the water supply of Addis Ababa, a rapidly developing city. The seismic safety of these three dams must be checked with high priority (Fig. 5.3).

Figure 5.3: Addis Ababa City Aminstration dams and downstream flood risk zone: (a) Dire dam, (b) Gefersa gravity dam, (c) Legadadi dam, and (d). part of Burayu town in the flood zone of Geferesa dam

Similarly, a seismic hazard analysis and a detailed seismic safety evaluation shall be conducted for the oldest hydropower dams, i.e. Koka and Aba Samuel dams (Fig. 5.4). High population growth, economic development, and expansion of urbanization downstream of these dams, which were not available during the construction period, call for higher seismic safety standards. For example, during commissioning of Koka dam in 1960 the population of Ethiopia was about 23 millions. Currently, it is over 100 million. To improve the safety of these dams, non-structural measures such as emergency action plans and reservoir rule curves for normal operation and unusual events like floods and strong earthquakes etc. should be in place.

Figure 5.4: The oldest hydropower dams grouped under high seismic risk class: (a) Aba Samuel dam, (b) Koka dam

5.5 Conclusions

The risk classification of 30 major Ethiopian dams was carried out using the method proposed by Bureau (2003). The method takes into account factors such as dam type, reservoir volume, dam height, age rating, downstream hazard, predicted damage and seismic vulnerability of a dam. Based on the results of the simplified risk analysis, the following conclusions may be drawn:

(1) All large dams considered in the present seismic risk analysis are classified in risk class II and III, a moderate and high-risk rating and there is no dam having risk classes I or IV, low or extreme risk rating;

(2) The TRF values for the dams range from 64.0 to 219;

(3) In risk classes II and III there are 19 dams (64%) and 11 dams (36%), respectively;

(4) Among the 11 dams categorized under high risk, Tendaho dam in the Afar region has the highest seismic risk with a TRF-value of 219 followed by Kesem, Gidabo, Dire and Koka dams in decreasing order of TRF-value;

(5) The risks are likely to increase with time, mainly due to aging of the dams and due to the increase in population on the downstream part, therefore, risk analyses must be reviewed and updated periodically;

(6) The results of the present risk analysis are important for planning of dam safety rehabilitation measures, and the development and implementation of emergency preparedness plans;

(7) Five dams of the high risk category (Gibe III, GERD, Gidabo, Tendaho and Tekeze dams) are chosen for detailed seismic safety evaluation and dynamic stability analysis;

(8) A detailed seismic safety review is needed for the three Addis Ababa City Administration water supply dams (Dire, Legadadi, and Gefersa) and the oldest hydropower dams (Koka and Aba Samuel), which are in the high seismic risk class. The increase in population, economic development and expansion of urbanization downstream of these dams call for higher seismic safety standards.

Chapter 6

6 Seismic Safety Analysis of Selected Dams for Multiple Earthquake Effects

6.1 General

Site-specific seismic hazard analysis is a crucial element for the seismic design of new dams and safety evaluation of the existing ones in a seismically active region like the East African Rift System. The primary requirement for the earthquake-resistant design of dams is to protect life and property. Thus, large dams must be capable of resisting severe earthquake ground motion or fault movement at the dam site without the uncontrolled release of the water impounded in the reservoir. It is also important that the spillway and bottom outlets are operational after a major earthquake. In the case of the SEE, damage to the dam, even extensive, may be acceptable as long as no catastrophic flooding occurs (ICOLD, 2016). The spillway must be operable in order to release moderate floods after an earthquake as repairs of the damaged hydropower plants and irrigation and water supply facilities may take months or years. In addition, the bottom outlets should allow for the lowering of the reservoir after an earthquake in case of major damage to the dam. Concerning the reservoir, possible mass movements into the reservoir triggered by earthquakes and their consequences in terms of generated impulse waves and overtopping of the dam have to be explored.

6.2 Multiple Earthquake Effects on Dams

The main tectonic phenomenon, which has been a major concern for dam designers and is addressed in all seismic codes and guidelines, is the ground shaking. It causes stresses, deformations, cracking, sliding, overturning, liquefaction, etc. However, recent observations have demonstrated that major earthquakes can cause multiple hazards on dam projects, which can affect the dams in many different ways (Wieland,

2008). Examples include failure of Shih-Kang weir during the 1999 Chi-Chi earthquake in Taiwan due to fault displacement (Figure 6.1a); slope failures in a number of reservoirs in China during the 2008 Wenchuan earthquake (Fig. 6.b); collapse of Fujinuma earthfill dam during the 2011 Tohoku earthquake in Japan (Fig. 6.1c). During the 2008 Iwate-Miyagi earthquake in Japan, a massive landslide with a slope length of 1.3 km, a width of 0.9 km and a total volume of 67 Mm^3 occurred in the reservoir area of Aratozawa Dam. A volume of 1.5 Mm^3 moved into the reservoir and raised the water level by about 1.5 m. The embankment dam suffered only minor damage during the ground shaking with a recorded PGA of 1.0 g at the dam base (Matsumoto, 2010).

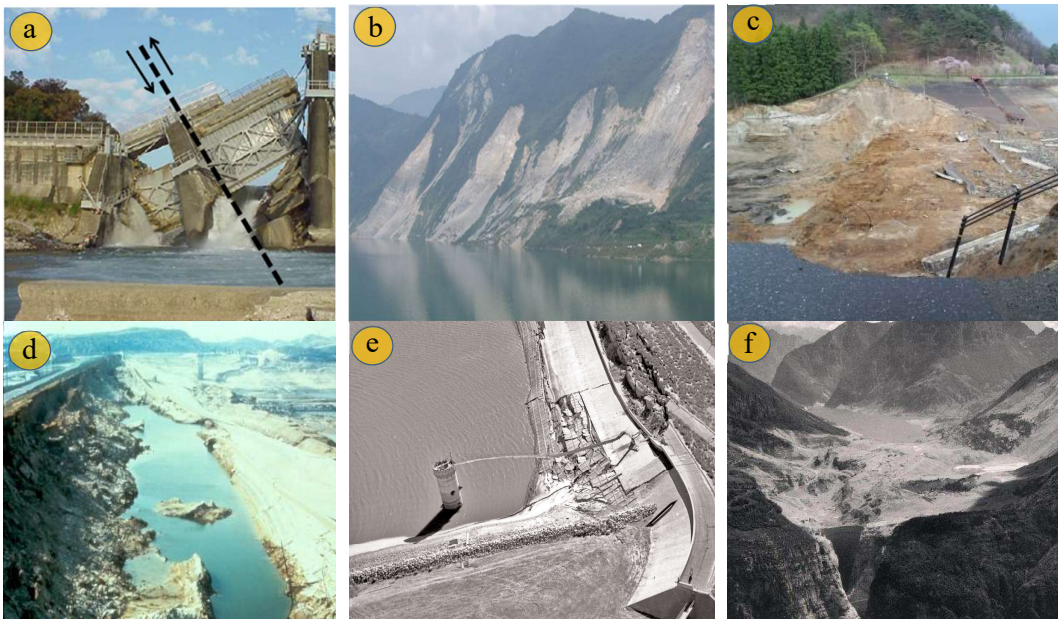

Figure 6.1: Geohazards affecting dam projects: (a) Shih-Kang dam failure during the 1999 Chi-Chi, Taiwan earthquake (Mw 7.6) due to fault movement, (b) Slope failures in the reservoir of Zipingpu CFRD dam in China during 2008 Wenchuan earthquake, (c) Fujinuma dam failure due to 2011 Tohoku earthquake, (d) and (e) Lower San Fernando dam failure due to liquefaction during 1971 San Fernando earthquake, (f) Vajont arch dam catastrophe due to rockslide into reservoir (1963).

These examples show that earthquakes can cause multiple hazards such as (i) ground shaking causing vibrations in dams, appurtenant structures and their foundations; (ii) fault movement in the dam foundation or discontinuities in dam foundation near major faults which can be activated during strong nearby earthquakes causing structural distortions; (iii) rockfalls from slopes causing damage to appurtenant structures (surface powerhouses, electro-mechanical equipment, penstocks,

switchyards and transmission lines); (iv) mass movements into the reservoir causing impulse waves and overtopping of dams; (v) mass movements that block access roads to dam sites and appurtenant structures, and (vi) settlements due to liquefaction or dynamic compaction of soil, causing distortions in dams and appurtenant structures, etc. According to Wieland (2012), most of these hazards were observed during the May 12, 2008, Wenchuan earthquake in China. However, focusing on the ground shaking other earthquake effects are often neglected in seismic hazard evaluation. The consequences of these hazards may be even worse than ground shaking.

Thus, the conventional seismic hazard evaluation technique, which is based on ground vibration hazard and practiced in many developing countries, may not be sufficient for large dam projects. Therefore, the assessment of multiple earthquake effects on dams is mandatory.

Five dams are selected in the present study for detailed seismic hazard analyses and safety evaluation with the main objective to address multiple earthquake effects. The selection criteria of these dams include the following: (i) multiple earthquake effects expected at the dam site, (ii) dam type and size, (iii) the level of earthquake ground motion (PGA) estimated at the dam site, (iv) the seismic risk classification, and (v) dam safety issue previously reported at the project site that can be expected to worsen during strong seismic events.

6.3 Methodology

To achieve the objectives of the present study, the following methodology is followed for the seismic safety evaluation of GERD, Gibe III, Gidabo, Tendaho and Tekeze dams:

- Identification of the geological and seismotectonic setup at the dam sites,
- Review the seismic hazard reports used for the dam design and identification of gaps,
- Site-specific seismic hazard analysis and determination of PGA,

- Development of uniform hazard spectra and disaggregation of the results to identify magnitude and distance of reference earthquakes for the sites,
- Selection of acceleration time histories and spectral matching with UHS, and
- 2D seismic stability analysis of dams (SEE ground motion).

For Tekeze arch dam, the seismic safety of the steep abutments and reservoir slopes is of main concern.

6.3.1 Uniform Hazard Spectra

For the site-specific seismic hazard analysis of the selected dam sites, the spectral accelerations are plotted versus the natural periods at various return periods. The resulting envelope curve is called uniform hazard spectrum (UHS) since each spectral ordinate has an equal rate of being exceeded. UHS is one of the final results of a probabilistic seismic hazard analysis (PSHA). The Crisis Program allows the calculation of the spectral accelerations for a given range of periods and exceedance probability. Hence, this spectrum may be the result of different earthquake events with different magnitudes and distances and should not be interpreted as the response spectrum from a single ground motion excitation. The UHS that were used as an input for spectral matching in time history analyses are given in respective sections.

6.3.2 Deaggregation of the Results

A seismic hazard curve or map combines magnitudes and distances to define the probability of exceedance of a given ground motion level and make it difficult to develop the sources that control the seismic hazard based on just the hazard curve or map. To overcome this limitation, deaggregation plots are provided for annual exceedence probabilities (AEP) of 1:475 and 1:10,000. Bin sizes of 5 km and 0.25 magnitude units were used in the deaggregation analysis. The deaggregation results clearly show the magnitude and distance that contribute mostly to the seismic hazard.

At a return period of 10,000 years, the primary hazard contributor for the two dams (Tendaho and Gidabo) within the MER is the large-magnitude earthquakes at a close distance from the sites. At a lower return period of 475 years, representing the design basis earthquake in seismic building codes, the major contributor of the hazard is a moderate-magnitude earthquake from a closer distance or large magnitude earthquakes at greater epicentral distance.

6.3.3 Selection of Acceleration Time Histories

Acceleration time histories that are appropriate input motions at bedrock level for the seismic analysis were developed for their compatibility with the UHS. Due to the limited number of representative time histories, it is necessary to scale available time histories to achieve a match to the UHS (target spectrum). The candidate time history should be appropriate for the structure to be analyzed, applicable to the specific site where the structure is located and consistent with earthquake scenario(s) that corresponds to the design load. Thus, the selection of acceleration time histories in the present study is guided by the following selection criteria and assumptions discussed below:

- Similarity in tectonic and geologic settings;
- Similarity in local site or subsurface conditions;
- Matching with the design earthquake in magnitude and epicentral distance;
- Compatible with the design response spectrum or UHS particularly in fundamental period range of interest; and
- Comparable duration of strong shaking.

Accordingly, the candidate time histories recorded in active shallow crustal tectonic environment, similar to earthquakes in the East African Rift System, are chosen. The magnitude of the earthquakes that generated the selected time histories is within the range of ± 0.5 of the design earthquakes. Normal and strike-slip type of faulting have been selected. The source-to-site distance is within a range of ± 50 % the design earthquake distance with similar subsurface or site conditions (rock or soil site).

Based on these preliminary screening criteria, 191 time history records are then selected from PEER, COSMO and European Strong Motion Database for further refining. Although the time histories are initially selected to be reasonably consistent with the seismic setting and design earthquake, these time histories and their response spectra may still differ substantially from the site-specific UHS. Spectrum matching of the recorded acceleration time histories is done according to the flowchart shown in Fig. 6.2.

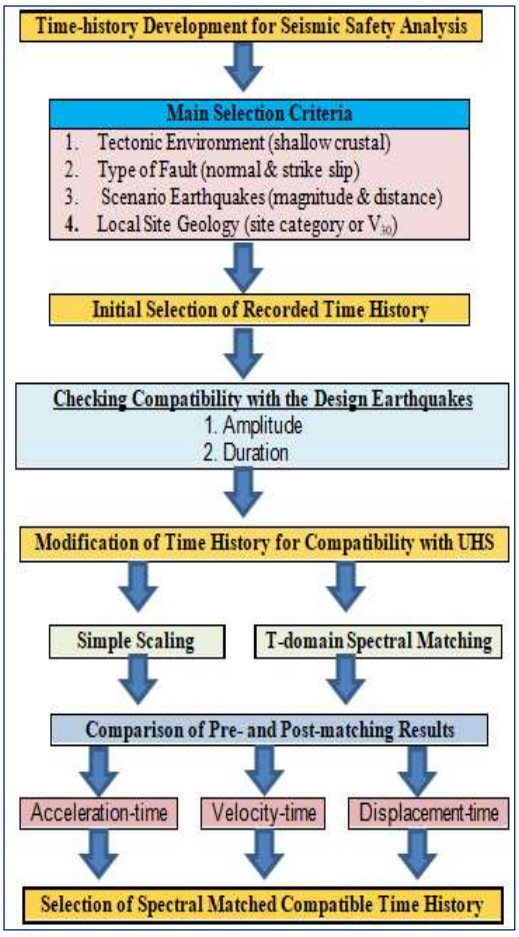

Spectrum matching is carried out using SeismoMatch (2018) computer program. The time-domain spectral matching approach proposed by Lilhanand and Tseng (1988) and Abrahamson (1992) were followed in the analysis. This approach normally provides a close fit to the target spectrum than Frequency Domain Approach (Gasparini and Vanmarcke 1976; Silva and Lee 1987).

After spectrum matching, the acceleration, velocity, and displacement time histories were examined to ensure that they are reasonably close to the original (recorded) time histories and the target response spectrum in terms of peak values, waveform and strong shaking duration.

Figure 6.2: Schematic diagram showing steps followed in developing time history used for seismic safety analysis

6.4 Seismic Safety Analysis of Gibe III Dam

6.4.1 Introduction

The Gibe III hydropower Project consists of an RCC gravity dam with a height of 243 m, a gated crest spillway with 7 bays, 2 headrace tunnels, 3 river diversion tunnels, and a powerhouse with 10 Francis units with a total installed capacity of 1870 MW (Fig. 6.3). The storage capacity of the reservoir is 15 km^3 and it is 155 km long. The dam is located in a narrow gorge of the Omo River. The project was commissioned in 2016 and currently, it is in full operation. It is the world's highest RCC dam. With respect to the seismicity, the dam site is located at the border of seismically active MER.

Figure 6.3: Gibe III project site model showing dam and appurtenant structures (EEPCO, 2009)

Large concrete dams were among the first structures for which seismic analysis and design had been conducted (Wieland, 2008). The pseudostatic method of seismic analysis first developed by Westergard in the 1930s for the Hoover dam has found worldwide acceptance among designers of concrete dams until the late 1970s

(Wieland, 2008). Currently, various performance levels are considered for evaluating the response of concrete dams to earthquake ground motion. USACE (2007) presented four procedures for the seismic safety evaluation of concrete hydraulic structures. These include linear static, linear dynamic, nonlinear static and nonlinear dynamic analyses.

In this section, the site-specific seismic hazard evaluations carried out for the Gibe III dam site are reviewed at the beginning, followed by the seismic stability analysis of the dam. A probabilistic seismic hazard analysis was conducted. Seismic stability analyses are carried out to check the response of the dam for the increased level of safety evaluation earthquake (SEE) ground motion obtained from an updated seismic hazard analysis. The static and dynamic analyses are performed using two-dimensional (2D) plane stress finite element models of the highest overflow and non-overflow cross-sections of the dam. First, a linear-elastic dynamic analysis is carried out followed by the dynamic sliding stability analysis of different detached concrete blocks. All dynamic analyses are done by direct time integration of the equations of motion.

For this purpose, the following tasks were carried out:

- Identification of the geological and tectonic setup;
- Site-specific seismic hazard assessment;
- Selection of acceleration time histories and spectral matching with response spectra obtained from the site-specific seismic hazard analysis;
- Defining 2D plane stress models of critical sections of the RCC gravity dam and eigenfrequency analysis for full and empty reservoir;
- Linear Time History Analysis (LTHA);
- Evaluation of the LTHA results;
- Defining critical concrete blocks based on LTHA results;
- Sliding block analysis using acceleration time histories from the LTHA as the base input; and
- Evaluation of the overall stability of the dam for the increased level of SEE ground motion.

6.4.2 Geology and Tectonics Background

The Gibe III project is situated in the margin of the Main Ethiopian Rift (MER) in the South-West direction. The geology at the project site exposes dominantly Tertiary and Quaternary deposits which are both active in terms of seismicity as discussed in Chapter 3. The dam site is placed on thick massive Miocene-Pliocene basalts of the Trap Series overlying the older volcanic sequences with a variable degree of weathering (EEPCO, 2007). The geology of the project area is divided into three major groups of rocks units, based on age: (i) the early flood basalts, Eocene to Miocene pre-rift volcanic rocks, (ii) a transitional series of intercalated basaltic and felsic volcanics (Oligocene-Miocene), and (iii) late Miocene to Holocene and post-rift deposits.

In terms of the structural geological setup, the orientations of the faults in the region can be grouped into the predominant NE/NNE-trending and the subordinate NW-trending fault systems, reflecting the main stress fields affecting the region. The older ones with NW–trending fault traces origin in the Precambrian with repeated reactivations in the Mesozoic (EEPCO, 2007). The younger NE/NNE-trending faults are the result of the NW-SE directed extension related to the Main Ethiopian Rift.

6.4.3 Seismic Activity

The seismicity of the project site is mainly controlled by the southern part of MER. According to the short period of instrumentally recorded earthquake data compiled for the region, there are six earthquakes with magnitude above 6 recorded within a distance of 150 km from the project site (Fig. 6.4). These include Mw 6.5 1919 earthquake (about 145 km south), Ms 6 1928 earthquake in Bako-Bulki region (about 40 km west), Ms 6 1944 earthquake (about 110 km southeast), Ms 6.1 1954 earthquake (about 120 south), Ms 6.3 1960 earthquake (about 140 km east), and Mw 6.2 1987 earthquake (about 150 km south). In addition, as per ISC catalogue and the paper by Ayele (2016), the 1913 earthquake (Ms 6.2) in southern Ethiopia is reported at coordinates (6^{o}N, 36.5^{o}E), which is closer to Koysha and Gibe III dam site, i.e. about 50 km southeast of Koysha dam and about 110 km southwest of Gibe III dam.

However, this earthquake is relocated close to the Ethiopia-Kenya border (Gouin, 1979), which is at greater distance from both dam sites.

Mb 4.2 2013 earthquake is the lowest magnitude earthquake listed by ISC close to the Gibe III dam site, which occurred during dam construction at about 20 km upstream of the dam in the reservoir margin (Fig. 6.4). The highest magnitude earthquake recorded close to the dam site is the 1928 earthquake west of the dam site. Originally, the epicenter of this earthquake was located east of the dam site by Gutenberg and Richter (1949) and ISC. However, it is relocated to about 40 km West of Gibe III dam site around the Bako-Bulki region (coordinates: 6.9°N, 36.9°E) and adapted for the computation of the seismicity of Ethiopia in the past (Gouin, 1979).

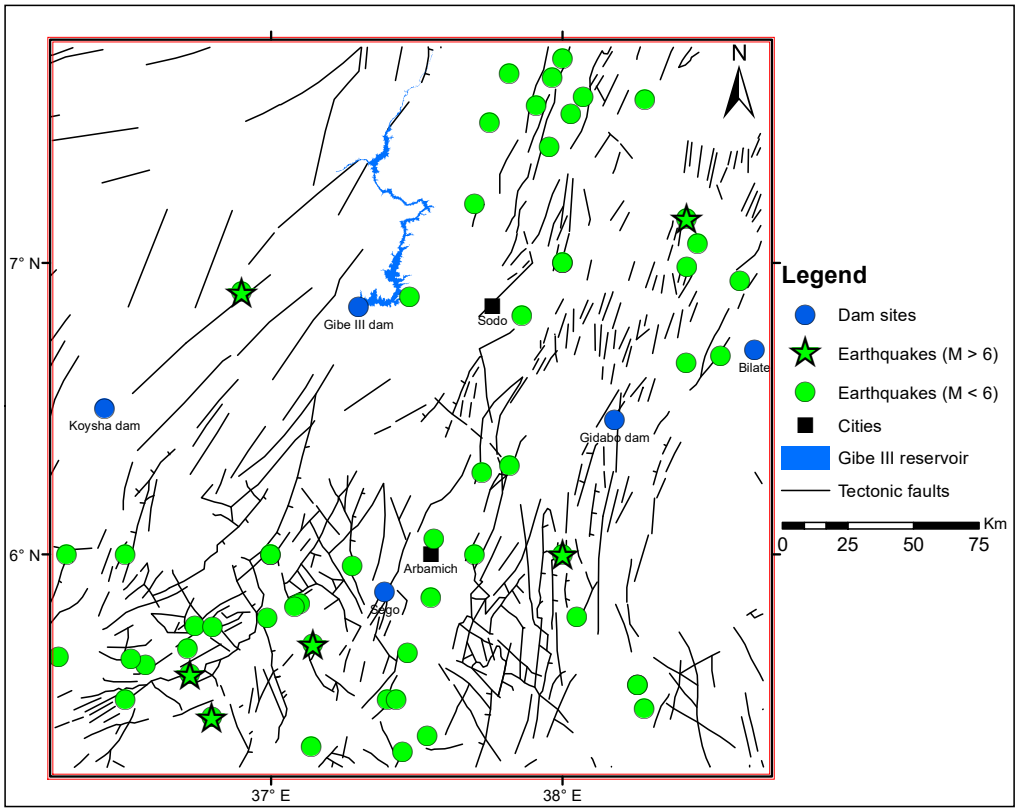

Figure 6.4: Seismotectonic map of southern part of Ethiopia showing epicenters of the instrumentally recorded earthquakes and major tectonic faults found at proximal distance to Gibe III dam site.

In addition, the Bako-Bulki region is considered by Mohr (1974) as a zone of recent horst-graben development to be an expression of major active crustal extension is ongoing outside the Ethiopian Rift (Gouin, 1979). The above-discussed earthquake

events together with tectonic and geothermal activities show that the dam site is located in a seismically active zone.

During the design stage, a seismic hazard analysis was conducted for the dam site using a deterministic approach. The peak ground accelerations (PGA) estimated for different return periods are given in Table 6.1 (EEPCO, 2007). The horizontal PGA-value obtained from the deterministic seismic hazard analysis was 0.15 g. This value is rather small in view of the seismotectonic setup and the historical seismicity of the region. A PGA-value of 0.15 g corresponds roughly to a seismic coefficient of 0.1 commonly used in the past, irrespective of the seismicity at the dam site. In addition, the deterministic approach alone may not be enough to estimate the worst ground motion at dam sites in the East African Rift where the seismic activity and slip rates of active faults are not well known.

Table 6.1: Ground motion parameters and earthquake scenarios for different design earthquakes used for the seismic design of Gibe III (EEPCO, 2007)

Design Earthquake	PGA (g)	M	R (km)	Earthquake Duration (s)
MCE	0.15	7	29	16
MDE	0.11	6	29	11
OBE	0.06	5	29	7

PGA: horizontal peak ground acceleration on rock surface, M: magnitude, R: epicentral distance, MCE: maximum credible earthquake, MDE: maximum design earthquake (return period: 950 years), OBE: operating basis earthquake (return period: 145 years) (Note: The return period of the MDE ground motion parameters should be 10,000 years and not 950 years)

6.4.4 Results of updated Seismic Hazard Analysis

The present (updated) site-specific seismic hazard analysis is conducted based on the probabilistic approach following the procedures discussed in Chapter 4. Accordingly, the PGA-value for the SEE (10,000 years return period) is 0.34 g for the horizontal earthquake component on the outcropping rock.

The PGA-value of 0.15 g obtained during the design stage differs greatly from the results of the current study and does not comply with the seismicity of the dam site. The difference in the two results is due to (i) additional seismic information and the

source zone model, (ii) the attenuation relationships used, and (iii) the method of seismic hazard analysis, which is deterministic in the original study (EEPCO, 2007) and probabilistic in the current study. Therefore, the dynamic response of the dam must be checked for the ground motion parametersobtained from the current study.

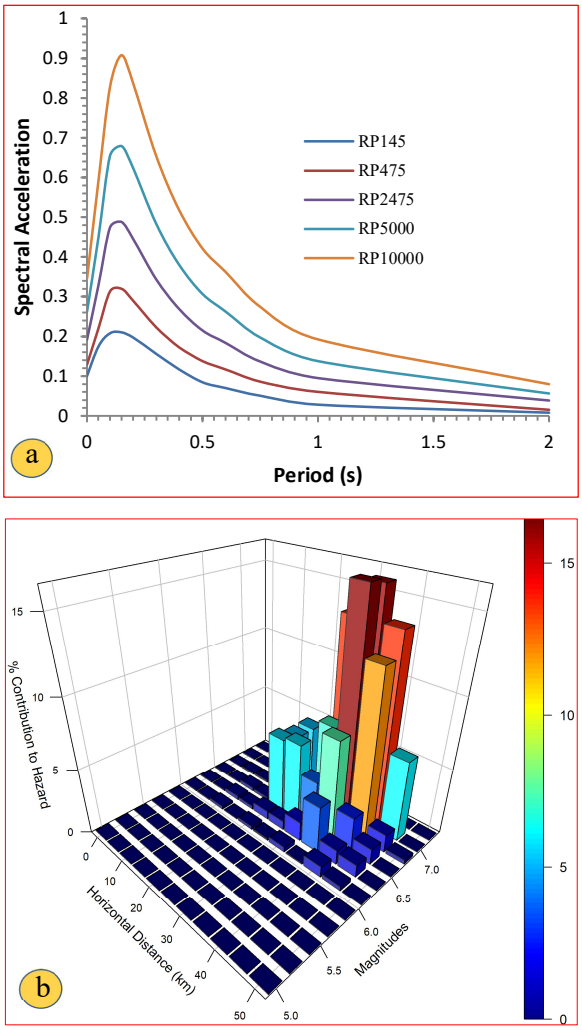

Figure 6.5: a. Uniform hazard spectra for various return periods for the Gibe III dam site for horizontal earthquake component on outcropping rock and 5% damping (RP- return period) b. Deaggregation of the result for 10,000 years return period earthquake ground motion showing the dominance of magnitude 7 earthquakes at epicentral distance of 25 km to 40 km.

The main results of the probabilistic seismic hazard analysis (PSHA) are uniform hazard spectra for 5% damping for various return periods (Fig. 6.5a). In addition, a deaggregation analysis was done to identify the magnitude and distance of seismic

events with the greatest contribution to the seismic hazard at the dam site (Fig. 6.5b). Based on the magnitude and distance of the deaggregation analysis, three recorded acceleration time histories were selected (Table 6.2). These time histories were spectrally matched with the site-specific uniform hazard spectra for a return period of 10,000 years (Fig. 6.5a).

Table 6.2: Details of earthquakes selected for time history analysis

No.	**Earthquake**	**Station**	**Year**	**M**	**Type of Faulting**	**Epicentral Distance (km)**
TH1	Central Italy	Accumoli	2016	6.5	Normal	19
TH2	Imperial Valley 06	Cerro Prieto	1979	6.53	Strike Slip	15
TH3	Landers	Big Bear Lake	1992	7.28	Strike Slip	45

6.4.5 Seismic Performance of RCC Dam

The seismic analysis of RCC dams is identical to that of conventional concrete dams. RCC dams are built by the placement of concrete in 30-40 cm thick layers that produce horizontal joints whose tensile strength is less than that of the parent concrete (USACE, 2003). During a major earthquake, it is likely that cracks develop along the horizontal lift joints in the upper portion of the dam, along the dam-foundation contact, and at locations where stress concentrations occur, i.e. at kinks on the upstream and downstream dam faces (Fig. 6.6). As a result, the failure mechanisms may involve sliding and rocking along the cracked sections (Fig. 6.7). The sliding displacement and rotation demands must be sufficiently small not to jeopardize the safety of the dam during and after the earthquake.

The seismic performance of the RCC dam can be evaluated on the basis of stress results obtained from the linear-elastic time history analysis. In general, the maximum compressive stress should be less than the compressive strength of mass concrete or RCC, and the maximum tensile stresses should not exceed the tensile strength of the RCC layers (lift joint tensile strength). These criteria might be satisfied for the OBE ground motion, however, for strong ground shaking, the dynamic tensile strength of the RCC at the lift joints and locations of stress concentrations will be exceeded.

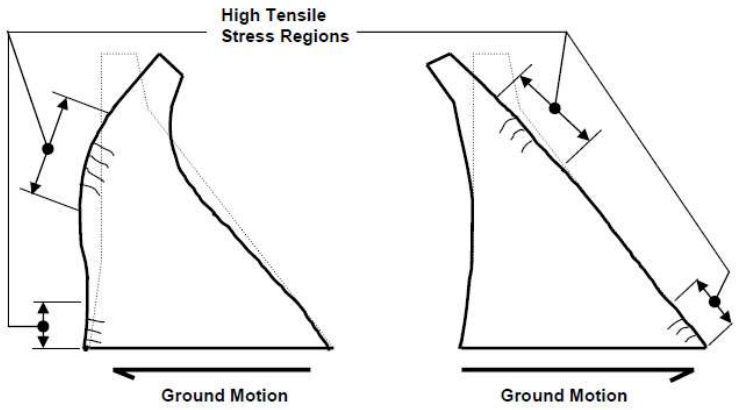

Figure 6.6: Gravity dam subjected to earthquake ground motions (USACE, 2003)

Therefore, a dynamic stability analysis of detached concrete blocks will be required using the acceleration at the base, obtained from the LTHA, as input. This is a simplified approach. A more realistic analysis is a nonlinear time history analysis of the post-cracking state of the dam in which the expected sliding surfaces are modelled by interface elements (Fig. 6.7).

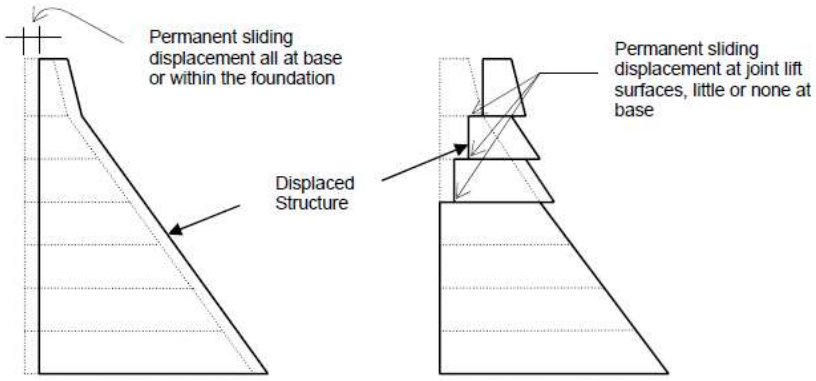

Figure 6.7: Dam permanent sliding displacements obtained from a nonlinear time history analysis (USACE 2003)

The nonlinear dynamic stability analyses must be done in the time domain, requiring the seismic input in the form of acceleration time histories. The main results required for the safety checks are the inelastic sliding deformations of the dam after the earthquake as shown in Fig. 6.7.

6.4.6 Finite Element Model and Assumptions

The 2D finite element model of the dam-reservoir-foundation system is modeled with plane stress elements in the dam body and plane strain elements in the foundation. The analyzed dam-foundation systems of the overflow and non-overflow dam sections are shown in Fig. 6.8. For simplicity, the spillway bucket of the overflow section is not included in the model for the overflow section (Fig. 6.9). The horizontal foundation boundary is assumed fixed both in the horizontal and vertical directions and along the vertical foundation boundaries the nodal points are fixed only in the horizontal direction.

The foundation rock is assumed massless, which implies that only the kinematic interaction effects are considered. The RCC and the foundation rock are assumed to be homogeneous, isotropic, linear-elastic materials. The material properties used for the dynamic analysis in the original design are given in Table 6.3 and Fig. 6.10 (EEPCO, 2009).

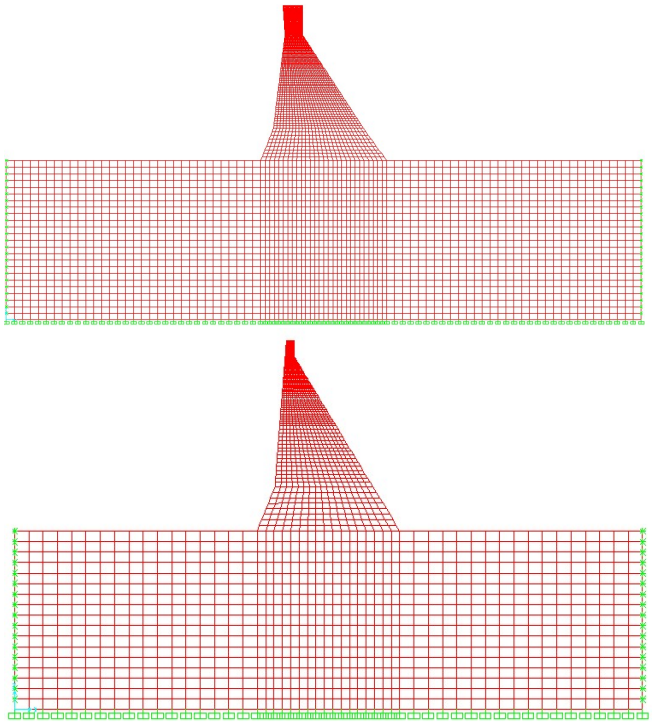

Figure 6.8: Finite element models of overflow (top) and non-overflow sections (bottom).

Figure 6.9: View of Gibe III dam showing overflow and non-overflow dam sections: the two MLO are spilling

The dynamic tensile strength of RCC is taken as 1.5 times the static tensile strength. The dynamic modulus of elasticity is taken as 12 GPa for the foundation rock and 13.15-28.15 GPa for the RCC. No increase in uplift pressures is assumed along the dam-foundation contact during earthquake action. Rayleigh damping with damping ratio of 7% is assumed.

Table 6.3: RCC properties in different zones of Gibe III dam

RCC Zone	Unit weight (kN/m3)	E (MPa)	Poisson's ratio	Compressive strength (MPa)	Friction angle (degrees)	Cohesion (kPa)
1	23.5	22500	0.2	>15	45	1000
2	23.5	18000	0.2	>12	45	800
3	23.5	15000	0.2	>10	45	600
4	23.5	10500	0.2	>7	45	400

For the earthquake analysis, the direct time integration method is used. The hydrodynamic pressure acting on the upstream face of the dam was represented by an added mass in accordance with the Westergard method (1933), assuming incompressible behavior of the infinite reservoir. The spectrum-matched acceleration time histories discussed in the previous section were used as input in the dynamic analysis, the earthquake loads are applied simultaneously in horizontal and vertical directions.

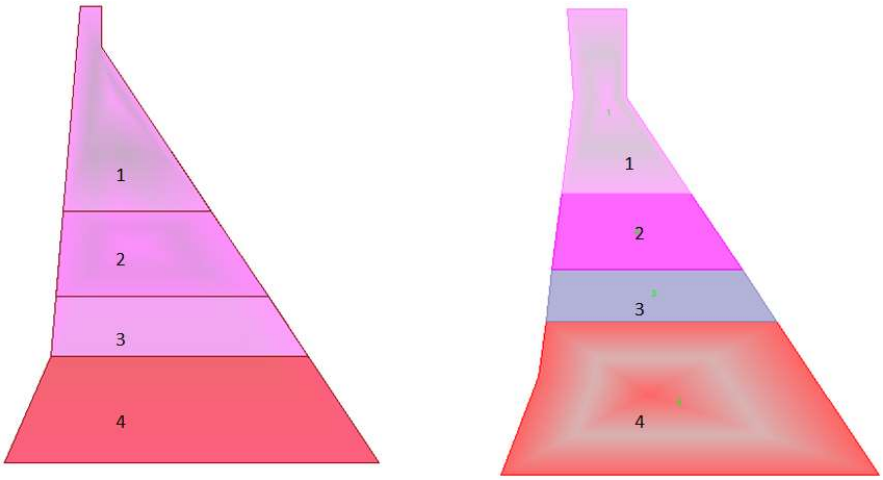

Figure 6.10: RCC zoning of materials for Gibe III dam the non-overflow section (left) and overflow section (right)

6.4.7 Eigenfrequency Analysis

In the first step of a dynamic analysis an eigenfrequency analysis is carried out in which the eigenfrequencies and mode shapes of the dam-reservoir-foundation system are calculated. This information is valuable for understanding the dynamic behavior of the dam. The eigenfrequency analysis of the dam is conducted for full reservoir conditions. The results of the analysis show that the dynamic response of the dam can be represented by the first three modes of vibration with mass participation of over 90%. The 1st and the 2nd modes are dominated by the horizontal earthquake component and the third mode is excited by the vertical component (Fig. 6.11).

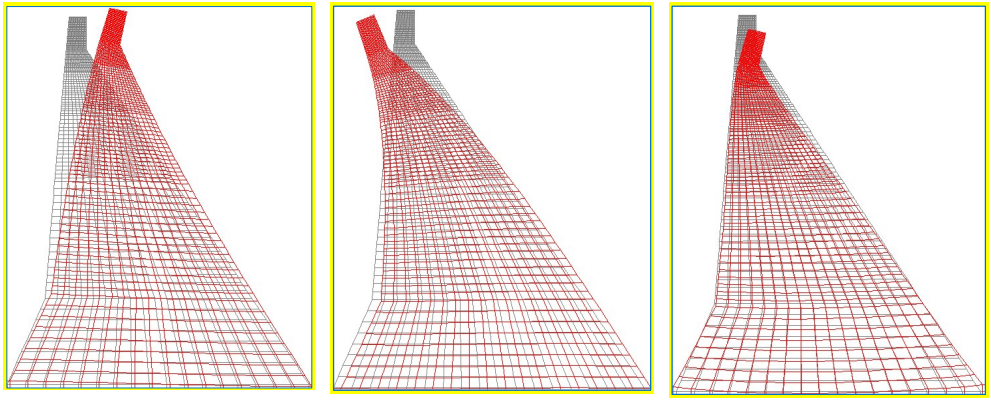

Figure 6.11: The first three modes of vibration of the non-overflow section of Gibe III dam

6.4.8 Dynamic Loads and Seismic Load Combinations

For the seismic safety evaluation of the dam, a load combination comprising the usual static loads and the earthquake loads is analyzed. The static loads include dead load, hydrostatic pressure at the upstream face, tail water pressure at the downstream face, and uplift pressure. The dynamic loads are the inertia forces due to the horizontal and vertical earthquake components and the hydrodynamic pressure of the reservoir, which is represented by an added mass (incompressible behavior of water). The seismic analysis is done for the SEE. The horizontal PGA-value of the SEE for Gibe III is 0.34 g. The direct time integration method is used to calculate displacements, absolute accelerations and stresses. The analysis was done for the following four seismic load combinations (H+ V+, H+ V-, H- V+ and H- V-) that take into account the vertical (V) and horizontal (H) earthquake components. The + and – signs indicate that the seismic loads are multiplied by +1 and -1 to take into account the most unfavorable earthquake directions.

6.4.9 Linear-Elastic Time History Analysis

The linear-elastic time history analysis of the dam-foundation system was carried out using the direct time integration method in the SAP2000 program. The seismic performance of the dam was evaluated on the basis of stress checks. The performance evaluation and the assessment of damage level is formulated based on magnitudes of demand-capacity ratios (DCR), cumulative duration of stress excursions beyond the tensile strength of the concrete and spatial extent of overstressed regions. According to USACE, the maximum allowable DCR for linear transient dynamic analysis of dams is 2. This corresponds to a stress demand twice the tensile strength of the concrete. The dam response to an earthquake is considered to be within the linear-elastic range of behavior with little or no possibility of damage if the computed stress demand-capacity ratios are less than or equal to 1.0. The dam would exhibit nonlinear response in the form of cracking of the concrete and/or opening of construction joints if the estimated stress demand-capacity ratios exceed 1.0. The level of nonlinear response or cracking considered produce low or moderate damage if the demand capacity ratios are less than 2.0 and limited to 15 percent of the dam cross-sectional

surface area, and the cumulative duration of stress excursions beyond the tensile strength of the concrete falls below the performance curve.

Accordingly, the envelopes of minimum principal stresses were checked for the maximum value of compression achieved in the dam body during the seismic event for the three SEE earthquakes and the four load combinations. The lower parts of the downstream face near the dam toe are the most stressed areas under compression for both sections. In most parts of the cross-section compression is within the acceptable range. Similarly, the envelopes of maximum total vertical stresses are checked for the maximum value of tension achieved in the dam body during the seismic event for the three SEE earthquakes and the four load combinations. The stress contour plots show that at the upstream face near the dam heel, area of change in slope geometry and the upper part of the upstream and downstream face (Fig. 6.12), shown in blue, undergo tension values exceeding the acceptance limits which require checking of stress excursions over the tensile strength according to USACE recommendation.

The indicative demand capacity ratio (DCR) in high tension zones at the base and crest region are shown in Fig. 6.13a-d. The DCR for those elements exceeds two. The cumulative inelastic duration (CID) for elements is also greater than the performance curve (Fig. 6.13 e). This indicates, the acceptable levels of damage on the basis of linear-elastic analysis are exceeded indicating the need of non-linear analysis. For the subsequent dynamic stability analyses, the stress response has no significance as the dynamic tensile strength of mass concrete is exceeded during the SEE ground motion. Based on this result, it can be assumed that horizontal cracks will develop along selected lift elevations at the crest of the dam and dam foundation contacts. According to the DCR and CID, the extent of cracks expected to be fully developed in the crest region and limited to the dam heel area at the base which is less than 15 % of the base of the dam. However, for conservative assumption, the crack is assumed fully developed at the base.

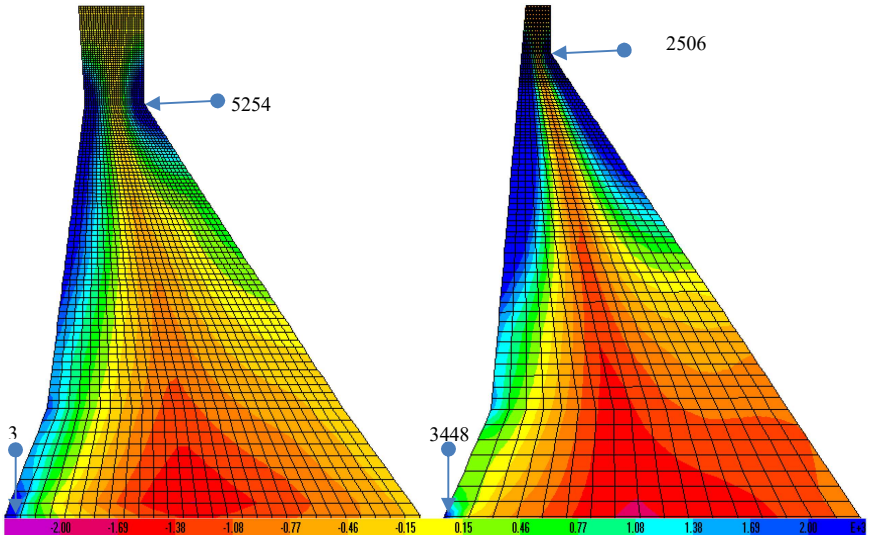

Figure 6.12: Envelopes of maximum vertical stresses in dam for SEE (time-history - TH2) showing tensile region of overflow section (left) and non-overflow section (right).

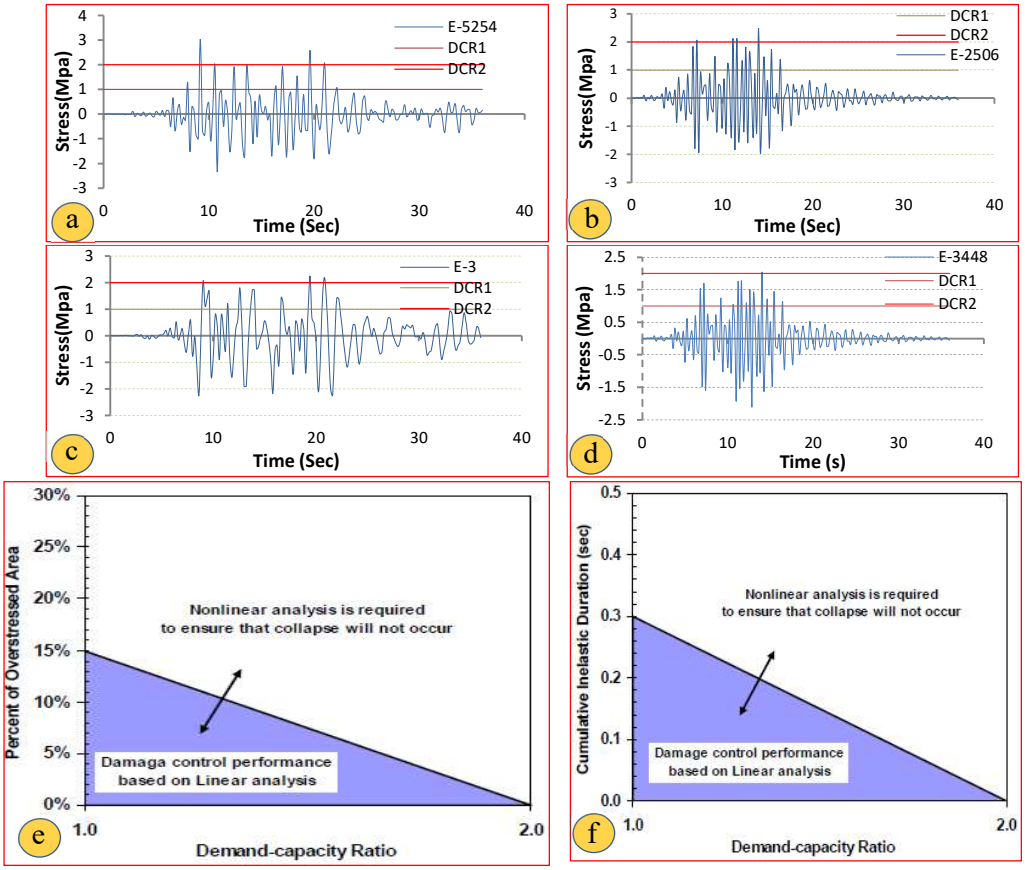

Figure 6.13: Effective vertical stress time histories: a and c - Element Overflow section and b and d - Non-overflow section, e and f - Performance curve for concrete gravity dams according to USACE (2007).

The horizontal absolute acceleration time histories at dam foundation (right) and crest of the dam (left) are given in Fig. 6.14 for one of the three ground motions time history (TH2). The peak acceleration at the crest is about five times as large as that at the dam base for the non-overflow section.

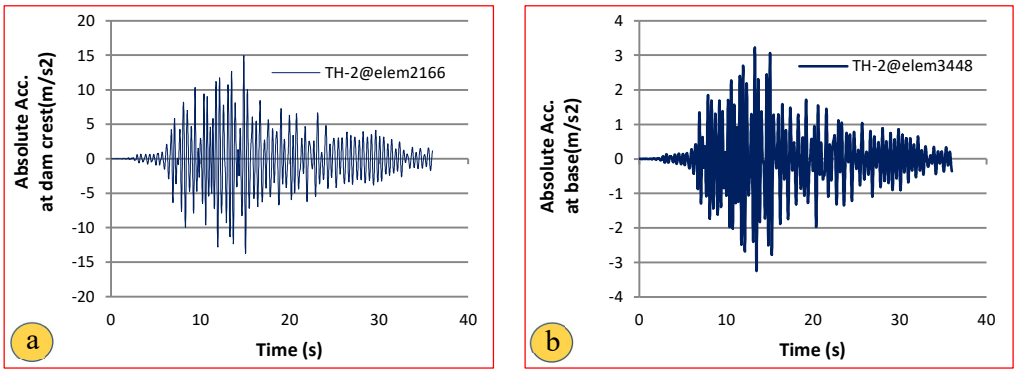

Figure 6.14: Horizontal absolute acceleration time histories at dam crest (a) and foundation of the dam (b) of non-overflow section.

6.4.10 Non-Linear Dynamic Stability Analysis

The seismic performance evaluation of the dam started with a linear-elastic time history analysis to identify overstressed regions and the most critical load combinations that would experience cracking, followed by dynamic sliding block analyses. The maximum sliding displacement of the dam and critical blocks (Fig. 6.15) are worked out under this section. The analysis is carried out with the computer program RSDAM (Leclerc et al., 2002). The dynamic uplift pressure at the lift joints is assumed to follow a triangular distribution for the two blocks in the crest region. At the base, the grout curtain and functioning of drainage system are taken into account in the uplift pressure distribution. The crest blocks have been selected based on the large amplification of the acceleration in the top part of the dam and the large dynamic tensile stresses obtained from the dynamic analysis. There are three load combinations analyzed for non-linear dynamic analysis, which include the dead load of the dam, the hydrostatic pressure at full reservoir level and the acceleration time histories at the base of the dam and the blocks which are obtained from the linear dynamic analysis.

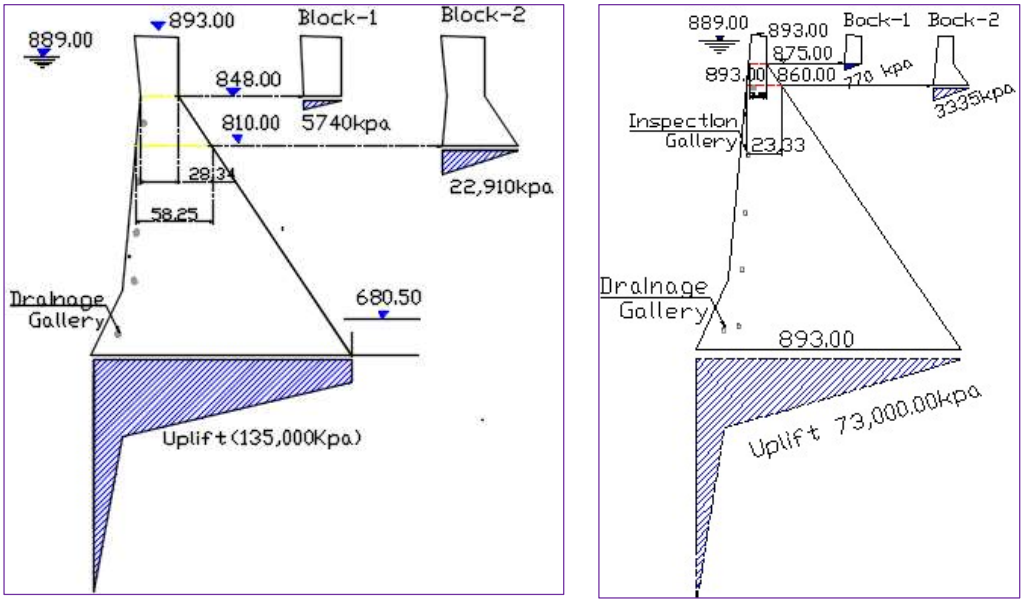

Figure 6.15: Sliding blocks and uplift pressure distribution at base and at critical blocks in crest region used for the dynamic stability analysis of the overflow section (left) and non-overflow section (right).

6.4.10.1 Sliding of Dam Body along Dam-foundation Contact

The dam-foundation contact is one of the zones where sliding may occur as the bond between the concrete and rock may be damaged. In addition, there are high tensile stresses at the upstream heel of the dam, where cracks will occur. High tensile stresses cause cracking of the dam at its contact with the foundation which may cause sliding movement during strong earthquakes. For the dynamic stability analysis, it is assumed that the crack at the base has developed over the whole length from upstream to downstream. The time histories of the sliding movement of the dam along the contact with the foundation are shown in Fig. 6.16. The maximum downstream sliding displacement for the overflow and non-overflow dam sections varies from 3 to 14 cm for the three earthquakes considered.

The maximum sliding displacement is due to the scaled Imperial Valley earthquake (TH2) and the lowest for the Central Italy earthquake. Similarly, the overflow section (4.8 to 14 cm) will experience larger sliding displacement than the non-overflow section (2.6 to 7.8 cm). In Fig. 6.17, the effect of the friction angle on the sliding

movement is shown, which will increase from 14 cm to about 36 cm when the friction angle reduces from 45° to 41°.

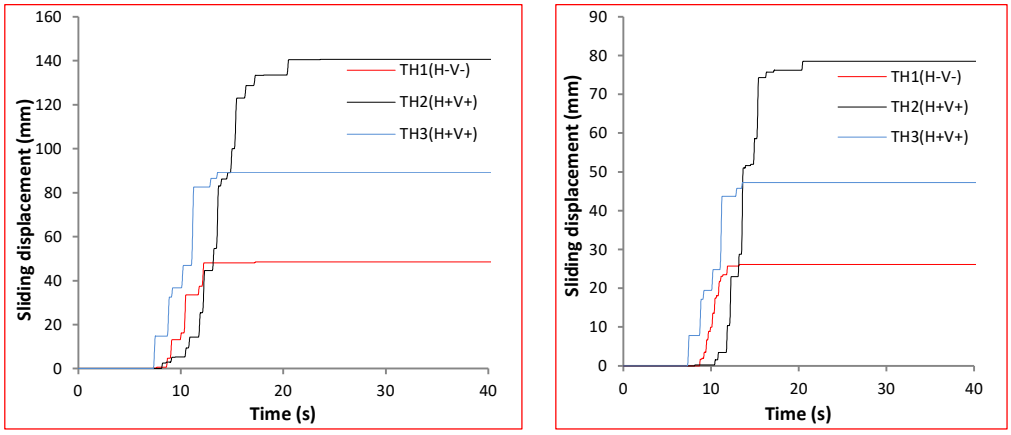

Figure 6.16: Horizontal sliding displacement of dam along the contact with the foundation rock (downstream movement with full uplift) for three different earthquakes. Overflow section (left) and non-over flow section (right) (Φ 45°).

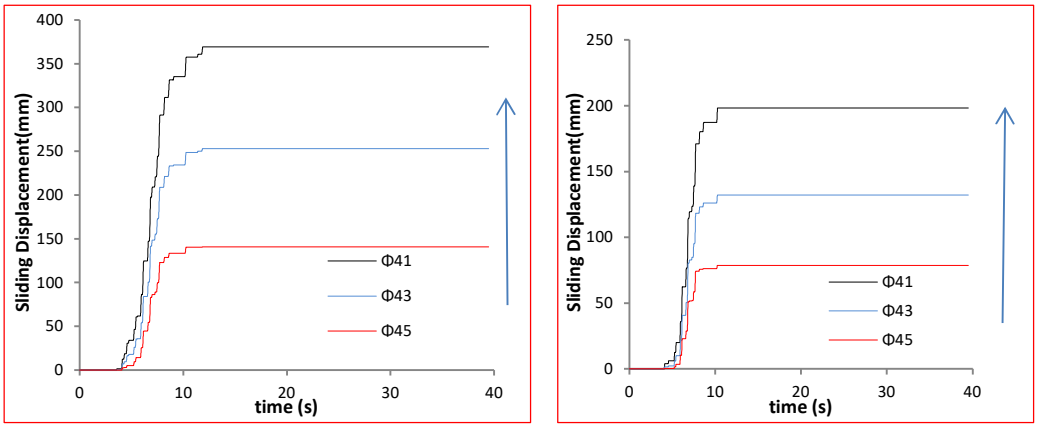

Figure 6.17: Effect of friction angle on horizontal sliding displacement of dam along the contact with the foundation rock for the most severe earthquake time history (TH2) (downstream movement with full uplift); overflow section (left) and non-overflow section (right).

Similarly, by reducing the uplift pressure by 25%, the sliding displacement is reduced by about half. The sliding displacements obtained in the present analysis are due to conservative assumptions regarding shear strength, crack development, simplified dynamic analysis of dam-foundation system, neglect of shear keys or friction in block joints and others.

6.4.10.2 Sliding Movement of Block-1 at Crest

The time histories of the sliding movement of Block-1 of the two sections for three different earthquakes are shown in Figs. 6.18 and 6.19. The sliding displacement varies from 147 to 245 cm for the non-overflow section and 34 to 62 cm for the overflow section with full triangular uplift water pressure in the crack as shown in Fig. 6.15.

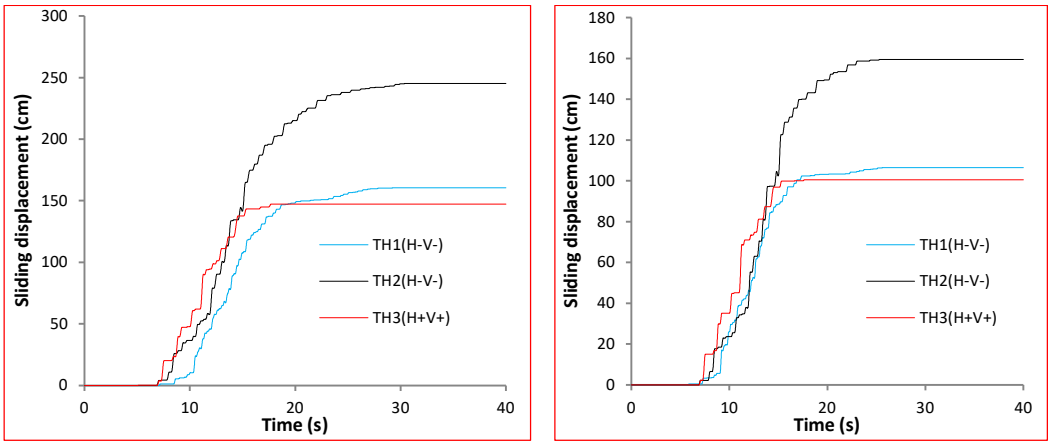

Figure 6.18: Sliding displacement of Block-1 (non-overflow, section downstream movement) with uplift (left) and without uplift (right) (Φ 45°).

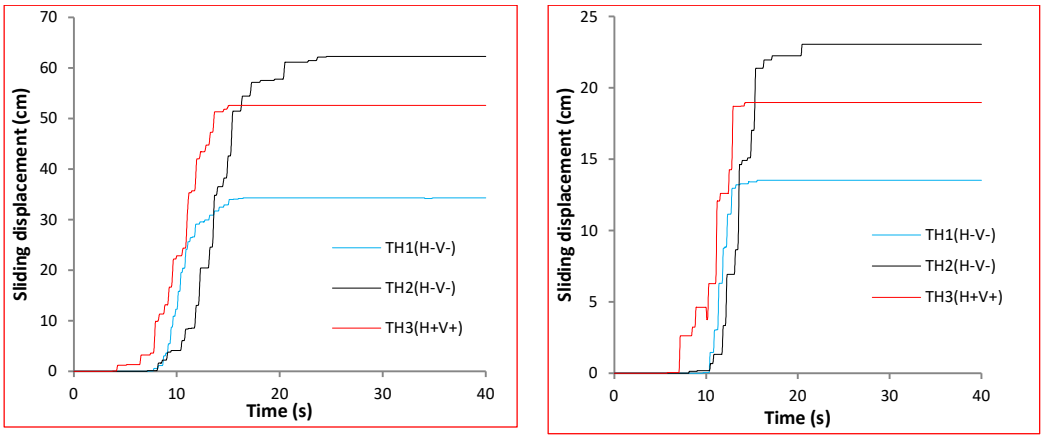

Figure 6.19: Horizontal sliding displacement of Block-1 (overflow section - downstream movement); with uplift (left) and without uplift (right) (Φ 45°).

When the uplift pressure is omitted the sliding displacement is reduced to 106 to 159 cm for the non-overflow section and 16 to 23 cm for the overflow section.

6.4.10.3 *Sliding Movement of Block-2 at Crest*

The time histories of the sliding movement of Block-2 of the two cross-sections for the three earthquakes are depicted in Figs. 6.20 and 6.21. The sliding displacement varies from 178 to 322 cm for the non-overflow section and 52 to 111 cm for the overflow section with full uplift in the crack. When the uplift pressure is omitted, the sliding displacement is reduced to 62 to 136 cm for the non-overflow section and 9 to 16 cm for the overflow section.

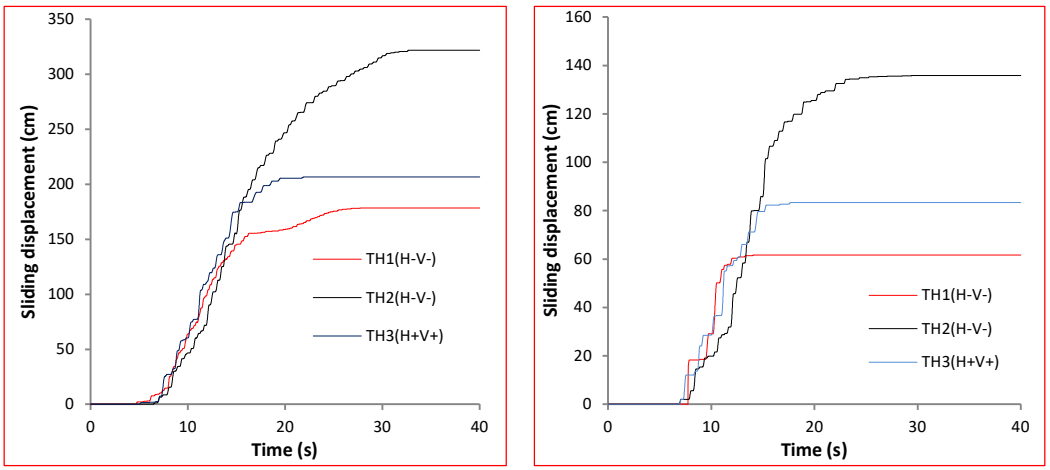

Figure 6.20: Horizontal sliding displacement of block-2 (non-overflow section downstream movement) with the uplift force (left) and without uplift force (right) (Φ 45°).

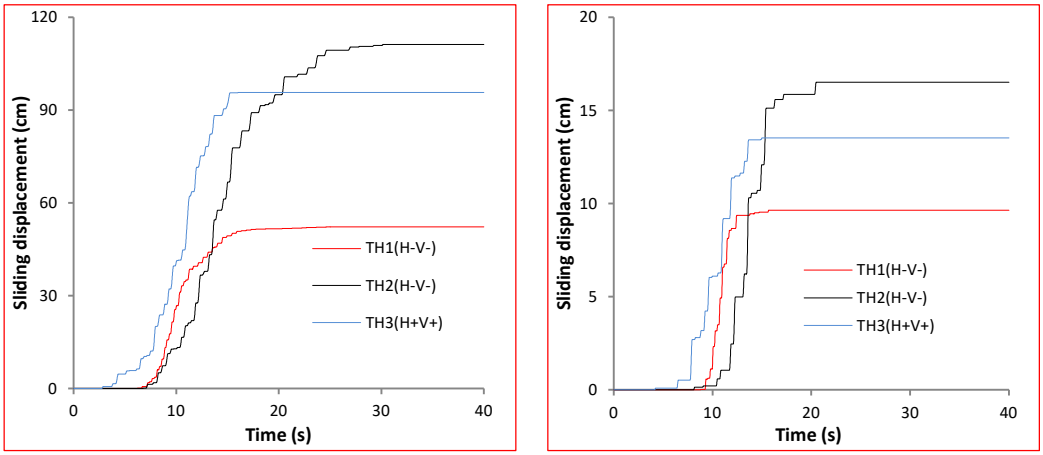

Figure 6.21: Horizontal sliding displacement of block-2 (non-overflow section downstream movement) with the uplift (left) and without uplift (right) (Φ 45°).

The comparison of the sliding movements of the two blocks for both sections shows high sliding movement of the upper two blocks (Block-1) without uplift case and for the lower block (Block-2) with uplift case. The larger movement of the Block-1 of the cross-sections relative to the corresponding Block-2 without uplift case is due to the higher horizontal acceleration at the base of the upper block in the crest region. Whereas the higher movement of the Block-2 as compared to Block 1 with the uplift cases for each section is due to the higher uplift acting at the base of Block 2. A summary of the main results of the dynamic sliding stability analysis results of the two blocks for the non-overflow and overflow sections is given in Table 6.4.

Table 6.4: Summary of sliding stability analysis of detached concrete blocks

Horizontal Displacement of Non-overflow Section (cm)				
History	With uplift		Without uplift	
	Block-1	Block-2	Block-1	Block-2
TH-1 (H+V+)	160	178	106	62
TH-2 (H+V+)	245	322	159	136
TH-3 (H-V-)	147	206	100	83
Horizontal displacement of Overflow Section (cm)				
History	With uplift		Without uplift	
	Block-1	Block-2	Block-1	Block-2
TH-1 (H+V+)	34	52	14	9
TH-2 (H+V+)	62	111	23	16
TH-3 (H-V-)	53	96	19	13

6.4.11 Discussion of Results

Gibe III dam must be able to withstand the effects of the ground motion of the safety evaluation earthquake (SEE), which has a return period of 10,000 years according to ICOLD (2016). The safety-critical elements such as bottom outlets, spillway gates, power supply and related control units must also be able to withstand the ground shaking of the SEE. According to the results of the present hazard analysis, the PGA-values of the horizontal earthquake component on the outcropping rock for 10,000 years return period is 0.34 g. The horizontal PGA-value of 0.15 g obtained for MCE in the previous seismic hazard assessment report underestimates the seismic hazard at

the dam site. Therefore, the dynamic response of the dam was checked for the increased level of SEE ground motion in the present study.

The results of the dynamic analyses carried out for the two highest overflow and non-overflow cross-sections of the dam show that the dam will undergo inelastic deformations when it is subjected to the SEE ground motions as the maximum dynamic tensile stresses exceed the dynamic tensile strength of RCC. Due to this, cracks may develop along the dam and foundation contact and along the horizontal lift joints in the crest region. To check the seismic safety of the dam, the sliding movements of critical concrete blocks are evaluated. The maximum downstream movement of the dam along the contact with the foundation is 16 cm taking into account the angle of friction of 45º considered in the design and neglecting downstream key block as well as friction effects along the vertical block joints. In general, such movements are acceptable as long as the relative movements between adjacent blocks of the spillway in the crest region will not affect the operability of the gated spillway. When a residual friction angle of 41° or less is assumed, the downstream sliding movement increases substantially.

The maximum horizontal displacement of the critical block separated by cracks along horizontal lift joints near the crest is about 3.2 m for Block-2 (non-overflow section). The width at the base of this block is 23 m. Thus, a downstream movement of 3.2 m can be accepted as long as the allowable overturning safety factor of this block after the earthquake is satisfied and the reservoir can be retained after the SEE. However, water leakage will occur at the crack along the lift joint which may need lowering of the reservoir. For this, the operability of spillway gates is important and problems have to be anticipated with the gates of a crest spillway.

In the analysis of the sliding movement of the critical blocks, several conservative assumptions were made such as neglect of friction at block joints, full uplift in the cracked lift joint, and conservative simplified dynamic analyses and others, it can be assumed that the block movements will be considerably less than 3.2 m. Moreover, the dynamic stability analysis of Block-2 shows that by eliminating the uplift forces, the downstream sliding movement can be reduced from 3.2 m to 1.36 m.

The present simplified dynamic stability analyses of the Gibe III RCC dam show that significant movements are possible, which have an inacceptable effect on the operation of spillway gates after a strong earthquake.

6.4.12 Conclusions

Gibe III dam site is located in the margin of MER, which is a region that is significantly affected by tectonic faults and major seismic activity in the past. The dam is the highest RCC dam in the world at present. The dam must be able to withstand the effects of the ground motion of the safety evaluation earthquake, which has a return period of 10,000 years according to ICOLD (2016). A probabilistic site-specific seismic hazard analysis is conducted for the dam. The present study shows that the dam can be subjected to significantly stronger ground shaking than assumed in the seismic hazard analysis report at the design stage.

The dynamic response of the dam has been checked for the revised level of SEE ground motion for two maximum cross-sections of the dam. The analysis is carried out using a simplified liner-elastic dynamic analysis followed by a dynamic stability analysis of three different detached concrete blocks formed by cracks along horizontal lift joints.

The results of the dynamic analyses carried out for the two cross-sections of the dam show that the dam will experience sliding movements when it is subjected to the SEE ground motion. As the maximum dynamic tensile stresses exceed the dynamic tensile strength of the RCC, cracks may develop along the dam and foundation contact and along horizontal lift joints in the crest region. To check the seismic safety of the dam, the sliding movements of critical concrete blocks are evaluated.

Due to the SEE the maximum sliding movement along the dam-foundation contact is about 16 cm for the overflow section. The maximum downstream movement of the detached concrete blocks near the crest (Block-2) is 3.22 m for the non-overflow section. These values are obtained for a friction angle of 45°, which is higher than the residual friction angle. The results of sliding movement of the critical blocks show

that the overflow section experiences larger sliding displacements at the base than the non-overflow section.

The present simplified dynamic stability analyses of the Gibe III RCC dam show that significant movements are possible, which may have an inacceptable effect on the operation of the gates of the crest spillway after a strong earthquake. However, due to narrow valley of the gorge of Gibe III dam and also in view of the different conservative assumptions made in the analysis, a refined dynamic analysis of the dam is required to confirm the present results.

6.5 Seismic Safety Analysis of GERD CFRD Saddle Dam

6.5.1 Introduction

Grand Ethiopian Renaissance Dam (GERD) is the largest hydropower station currently under construction in Africa. The main dam is 145 m high and has a crest length of 1780 m. It is an RCC gravity dam with an RCC volume of 10.1 Mm^3. The dam is presently under construction and will create a reservoir with a volume of about 74 km^3 and a surface area of 1874 km^2. The generating capacity is 5150 MW with 13 Francis turbine units. The project is located at the Blue Nile about 20 km away from the border with Sudan. The seismicity in the project area is assumed to be very low. However, the information on historical seismicity is very scarce in the region.

Besides the RCC dam, there is a 5.2 km long saddle dam with a maximum height of 65 m. It is a concrete faced rockfill dam (CFRD) with an embankment volume of 17 Mm^3. The saddle dam is found in the right bank of the main dam (Fig.6.22). It is one of the longest CFRD dams in Africa. The original design was an asphalt face rockfill dam before it was changed to a CFRD. The safety requirements for the saddle dam must be the same as those of the main dam.

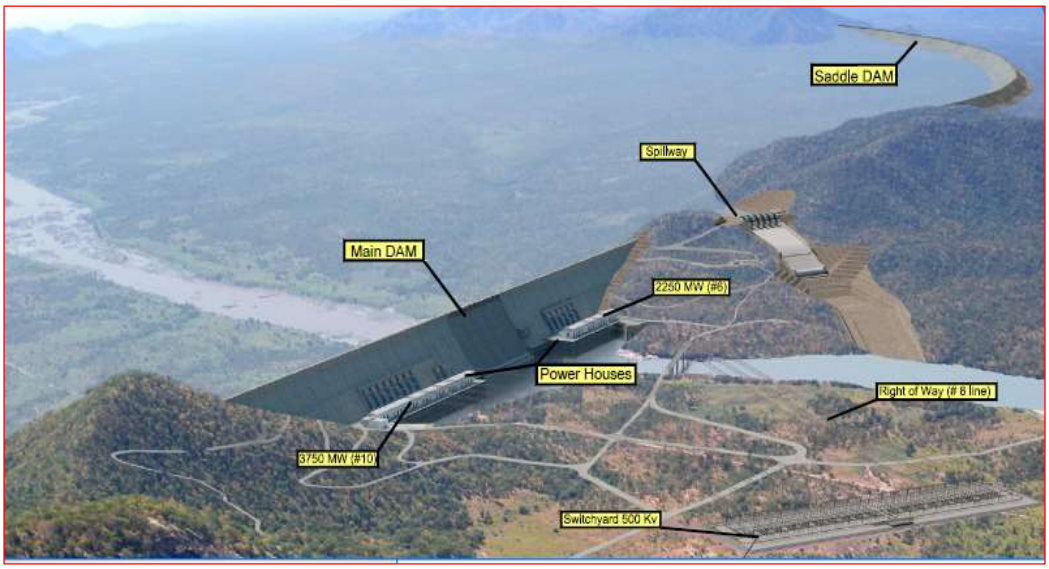

Figure 6.22: GERD project site model showing dam and appurtenant structures: main dam with two surface powerhouses, spillway in the center and the saddle dam (EEP, 2013).

In this section, the site-specific seismic hazard evaluations conducted for the GERDproject are reviewed, followed by the seismic stability analysis of the saddle dam. The seismic stability of the saddle dam is checked for the ground motion with a return period of 30,000 years determined by a probabilistic seismic hazard analysis. The dynamic analysis of the saddle dam is carried out by the equivalent linear method using a two-dimensional (2D) dam model of the highest cross-section founded on rock. The scope of work of the seismic safety analysis for GERD saddle includes the following:

- Identification of the geological and tectonic setup;
- Site-specific seismic hazard assessment;
- Selection of appropriate acceleration time histories and spectral matching with response spectra obtained from the site-specific seismic hazard analysis;
- 2D seismic response analysis using the equivalent linear method;
- Selection of potential sliding masses and calculation of yield accelerations;
- Calculation of permanent earthquake-induced displacements of potential sliding masses;
- Estimation of seismic settlement due to vibration-induced densification of dam materials; and
- Determination of total reduction of freeboard and seismic safety of the dam.

6.5.2 Geology and Tectonics Background

The GERD project is situated in the western margin of the Ethiopian plateau, near the Sudanese border, within Precambrian intrusive and metamorphic rocks, as well as meta-sedimentary and meta-volcanic rock. The Ethiopian-Sudanese border in the west is underlain by gneiss and migmatite known as the Baro Group. It is flanked on the east by a large tract of land underlain by the relatively low-grade volcano-sedimentary succession known as the Birbir group (EEP report, 2012). The main dam site lies entirely on the Precambrian metamorphic and intrusive rocks of the western Ethiopia basement. Based on the structural and lithological criteria, the rock types outcropping in the main dam site consist of seven main units: gneisses, meta-granitoids, schist,

meta-sediments, volcanic (basalt and meta-basalt), tectonic intrusives (pegmatites and quartz veins) and recent alluvial and colluvial deposits.

The region was involved by a complex tectonic history that can be characterized by two broad phases: (i) compression stress regimes - orogenic cycle (Pre-Cambrian time) and (ii) tensional stress regimes - rifting (Triassic-Cretaceous and Neogene-Quaternary time). During the compressional stage (870 to 550 Ma), the rocks at the GERD project site were affected by the Pan-African event, a tectono-thermal event. Tensional stages developed after the compressive stage in the following main phases:

1. Triassic–Cretaceous NE–SW-directed tensile stress associated with Gondwana break-up leading to NW-trending Mesozoic rift including the Blue Nile rift basin.
2. In the Cenozoic, the last dilatational stage is represented by approximately E-W faults reaching a length of 30 to 40 km.
3. Late Miocene to Quaternary tensile stresses associated with the opening of the Main Ethiopian Rift and Afar depression (NW–SE and E–W directed tensile stress) and Quaternary E-trending Ambo Lineament (NNE–SSW tensile stress).

6.5.3 Seismic Activity and Dam Seismic Design Criteria

GERD dam site is located between the Nubian (West Africa) and Somalian (East Africa) plates, whose boundary is marked by the East African Rift, which is the locus of east-west stretching due to the separation of these plates. Based on instrumentally recorded earthquakes, the seismicity is mainly concentrated eastward of the site. A smaller number of foci are observed west-ward and south-ward of the site, well within the Nubian plate, as rift associated intraplate earthquakes with normal or strike-slip faulting mechanisms (EEP, 2012). During the design stage, a seismic hazard analysis was carried out for the GERD dam site using a deterministic and probabilistic approach. The estimated peak ground accelerations for different return periods are given in Table 6.5.

Table 6.5: Ground motion parameters and earthquake scenarios for different design earthquakes used for the seismic design of GERD dam (EEP, 2013)

Ref. Earthquake	RP (year)	M	R (km)	PGA (g)
SEE	10,000	7	100	0.113
OBE	145	5-	80	0.012
RTE	-	5-	33	0.113

PGA: horizontal peak ground acceleration on rock surface, M: magnitude, RP: return period, R: epicentral distance, SEE: safety evaluation earthquake, OBE: operating basis earthquake, RTE: reservoir triggered earthquake.

6.5.4 Results of the Present Seismic Hazard Analysis

Based on the current seismic hazard analysis result, the GERD dam site is located in a low seismic hazard zone. The PGA-values of the horizontal earthquake component on the outcropping rock for different return periods are as follows: 0.011 g (145 years), 0.021 g (475 years), 0.032 g (1000 years), 0.048 g (2500 years), 0.067g (5000 years) and 0.1 g (10,000 years).

The PGA-values of 0.113 g obtained for 10,000 years return period hazard in the previous seismic hazard analysis is reasonable compared to the results from the current study. However, taking into account the importance of the project, the scarcity of historical earthquakes, uncertainties in the hazard analysis and attenuation models and reservoir triggered seismicity close to the dam site, a higher level of earthquake ground motion was used to check the seismic stability of the dam i.e. 30,000 years return period. Such a high return period is not mentioned by ICOLD (2016). However, longer return periods have been specified for very large reservoirs in the UK. For probabilistic safety assessments of nuclear facilities much longer return periods are used. Similarly, for large storage dams with very high consequences located in areas of low to moderate seismicity where the maximum possible ground motion levels are still increasing with increasing return period, higher return periods should be considered. Likewise, one could state that every large reservoir, where there is hardly any information available on the seismic safety, should be able to withstand a ground motion with a horizontal PGA of say 0.3 g. Such an argumentation would be in line with the old concept of the seismic coefficient, in which a value of 0.1 was

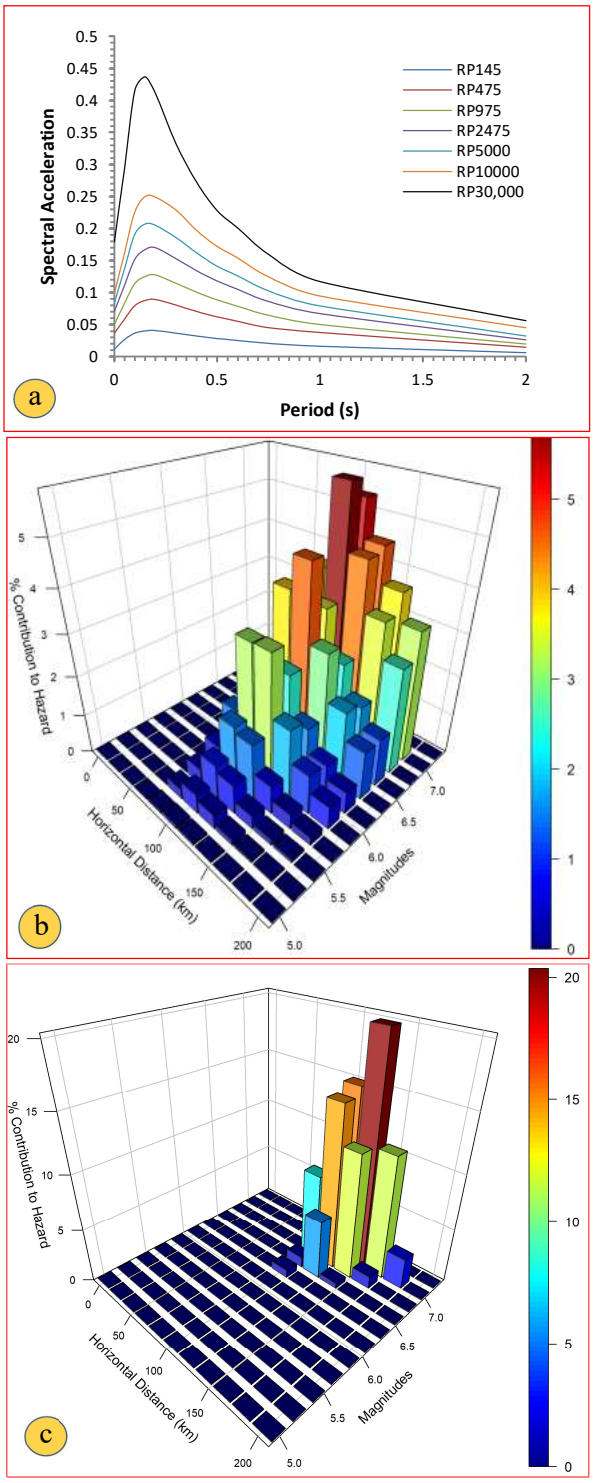

Figure 6.23: a. Uniform hazard spectra for various return periods for the GERD dam site for horizontal earthquake component on outcropping rock and 5% damping (RP- return period) b. Deaggregation result for 475 years return period earthquake ground motion. C. Deaggregation result for 30,000 years return period earthquake ground motion showing the dominance of magnitude 7 and above earthquakes at epicentral distances of 100 to 150 km.

used almost universally when no information was available on the historical seismicity. Moreover, a seismic coefficient 0.1 corresponds to a PGA-value of about 0.15 g, i.e. in the past GERD would have been designed for 0.15 g, which is higher than the present value of 0.1 g for a return period of 10,000 years.

Therefore, the dynamic response of the saddle dam was checked for the increased level of earthquake ground motion for a return period of 30,000 years. The main results of the probabilistic seismic hazard analysis (PSHA) are uniform hazard spectra for 5% damping ratio for various return periods (Fig. 6.23a).

Table 6.6: Details of earthquakes selected for time history analysis

No.	Earthquake	Station	Year	M	Faulting	Epi. S (km)	Site class Vs30(m/s)
1	Centeral Italy	Amatrice A. - MZ28	2016	5.9	Normal	35	B
2	Sitka- Alaska	Sitka Observatory	1972	7.68	Strike Slip	35	650
3	Gulf of Aqaba	Eilat	1995	7.2	Strike Slip	44	382
4	Izmit Turkey	Heybeliada-Senatoryum	1999	7.6	Strike Slip	78	Rock
5	Hector Mine	Joshua Tree N.M.	1999	7.13	Strike Slip	50	686

Based on the magnitude and distance of the deaggregation analysis, representative acceleration time histories were selected. These time histories are spectrally matched with the site-specific uniform hazard spectra for a return period of 30,000 years (Fig. 6.24).

After spectrum matching, the acceleration, velocity, and displacement time-histories of the SEE were examined to ensure that they are reasonably close to the original time histories and target spectrum values in terms of peak values and waveform (Fig. 6.25). By checking the significant peaks and desired aspects of the ground motion were not altered too much, the acceleration time histories of three recoded earthquakes were selected and used for dam stability analysis (Table 6.6).

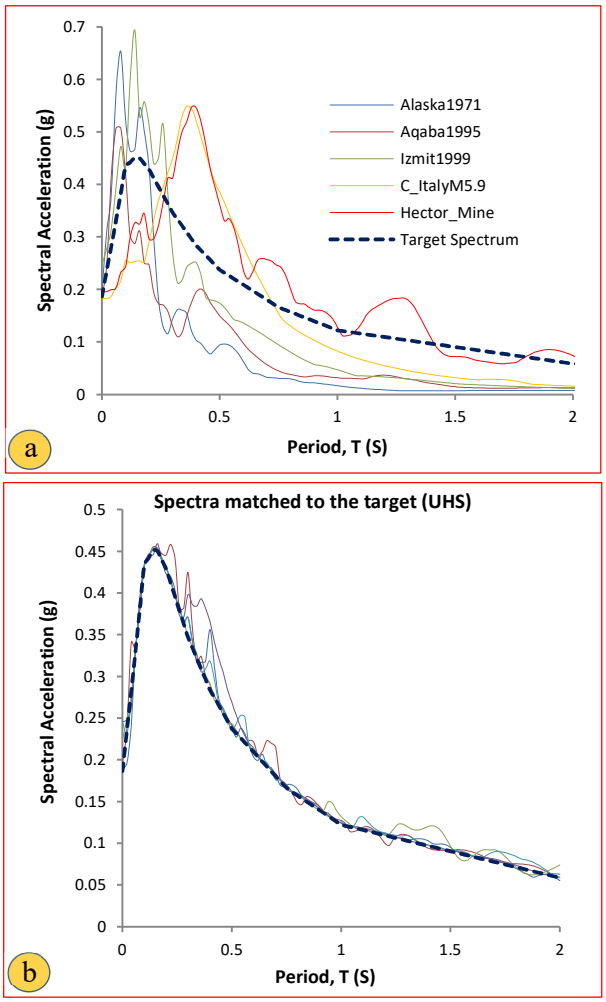

Figure 6.24: Acceleration response spectra of various earthquakes selected for time history analysis with UHS of GERD dam site for 30,000 years return period: a) response spectra of acceleration records, b) response spectra after matching with the target (UHS).

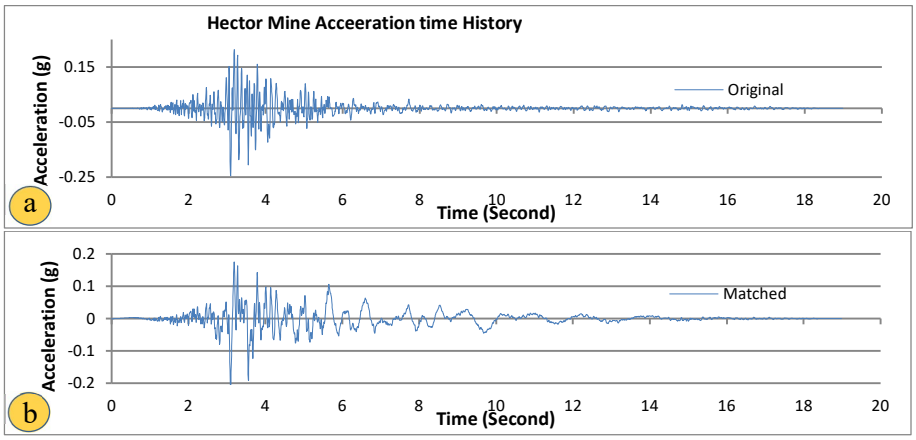

Figure 6.25: Pre and post spectral matching results for Mw 7.13 1999 Hector Mine EQ with GERD dam site UHS; a) Original acc. time history b) acc. time history after spectral matching

6.5.5 Seismic Analysis of Dam Body with Equivalent Linear Method

The two-dimensional (2D) dynamic analysis of GERD saddle dam was conducted for the maximum cross-section of the dam assuming plane strain conditions and using the equivalent linear analysis concept with shear strain-dependent material properties to estimate deformations of the dam subjected to the ground motions of the SEE with 30,000 year return period.

6.5.5.1 Dam Zoning used for Saddle Dam Stability Analysis

The material used in different zones CFRD saddle dam and the main features of the dam are given under Fig. 6.26.

Dam height	50 m
Crest length	5 200 m
Dam volume	4.1Mm^3
Crest width	8 m
Full supply level	640.0 m
Max. flood (10,000)	642.5 m
Extreme flood (PMF)	643.3
Upstream slope	1.3:1
Downstream slope	1.3:1

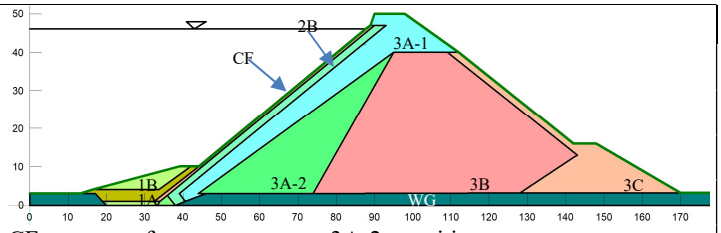

CF- concrete face
1A- fine backfill
1B- coarse backfill
2B- cushion
3A-1 transition
3A-2 transition
3B - main rock fill
3C - large rock
WG - weathered granite

Figure 6.26: Maximum cross-section of GERD Saddle Dam at Ch. 4 000 m showing main features and material zoning.

6.5.5.2 Static Deformation and Stress Analyses

The deformation analysis under static loading for GERD saddle dam was carried out by the computer program SIGMA/W (GEO-SLOPE International Ltd., 2019) using the Mohr-Coulomb elasto-plastic model. Material properties in different zones were obtained from the design report (Table 6.7).

Table 6.7: Material properties for static deformation and stress analyses (EEP, 2014) (v: Poisson‘s ratio, $; modulus of elasticity, γ: unit weight, C: cohesion, Φ’: friction angle, and K: permeability)

Material Description	v	E (MPa)	γ (kN/m3)	C' (kPa)	Φ' (degrees)	K (m/s)
Fine Backfill - 1A	0.26	100	18	0	25	10^{-5}
Course backfill - 1B	0.3	100	18	0	25	10^{-5}
Peripheral Joint Filter – 2A	0.3	150	23	0	46	10^{-3}
Cushion – 2B	0.26	150	23	0	46	10^{-3}
Transition – 3A_1	0.26	120	22	0	46	10^{-2}
Transition – 3A_2	0.26	90	21	0	44	10^{-2}
Main Rockfill – 3C	0.25	60	20	0	50	10^{-2}
Large Rock – 3C	0.24	60	17	0	50	10^{-1}
Concrete Face – CF	0.20	5000	23	0	46	10^{-10}
Plinth and Gallery	0.20	31200	23	-	-	10^{-10}
Weathered granite	0.25	2640	26	260	54	10^{-6}
Slightly weathered granite	0.2	30648	26	2040	64	10^{-6}

The static loads considered in the analysis are gravity load and water load. The water load was applied as hydrostatic pressure acting on the concrete face. The contour plots of the vertical stress for the gravity load are given in Fig. 6.27.

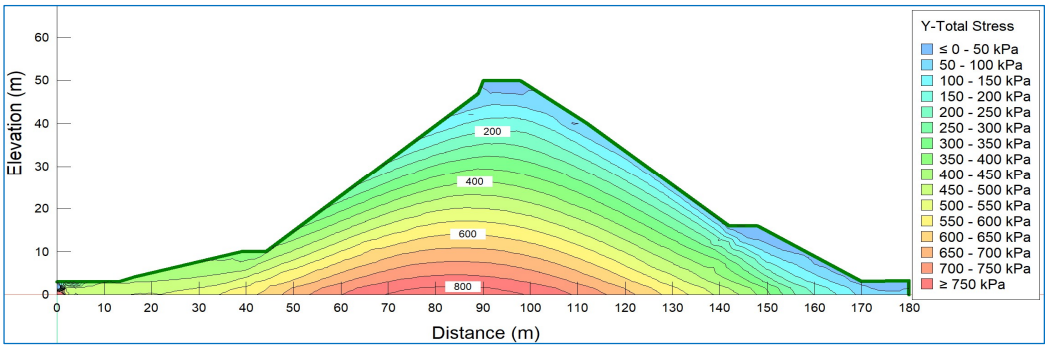

Figure 6.27: Contour plot of vertical stress from gravity load (dam body); maximum vertical stress 820 kPa

6.5.5.3 Dynamic Material Properties

The dynamic material properties required for the earthquake response analysis are the dynamic shear modulus (G) and the damping ratio; both are given as functions of the dynamic shear strain. The dynamic shear modulus G is commonly determined as the ratio G/Gmax (reduction function) as a function of the cyclic shear strain and the maximum dynamic shear modulus Gmax. The material parameters used for the

earthquake analysis of the dam by the equivalent linear method are obtained from design report, literature review, other dam projects and in situ geophysical tests and are given in Table 6.8.

Table 6.8: Dynamic material properties in different zones of CFRD

Material	K_{2max}/Vs	v	Modulus Reduction	Damping Ratio	Material Model
Fine Backfill - 1A	60	0.35	1*	1*	Non-linear
Course backfill - 1B	70	0.35	1*	1*	Non-linear
Filter–2A	80	0.30	2*	2*	Non-linear
Cushion – 2B	80	0.30	2*	2*	Non-linear
Transition – 3A_1	90	0.30	2*	2*	Non-linear
Transition – 3A_2	90	0.30	2*	2*	Non-linear
Main Rockfill – 3B	130	0.30	3*	3*	Non-linear
Large Rock – 3C	130	0.30	3*	3*	Non-linear
Concrete Face – CF	-	0.20	Elastic	5%	Linear
Plinth/Insp. gallery	-	0.20	Elastic	2%	Linear

1*- Average relationship for sands by Seed and Idriss 1970 (Figs. 6.28 c and 6.28d), 2* Seed et al. 1984 gravels (Figs. 6.28c and 6.28d) 3* Siah Bishe rockfill material used in CRFD dam project, Iran (Figs. 6.28e and 6.28f), Vs- average shear wave velocity used for G_{max} calculation

The maximum dynamic shear modulus (G_{max}) for coarse grain materials can be obtained from the following equation:

$$G_{max} = 220\, k_{2max}\, \sigma'_m{}^{0.5} \quad \ldots\ldots\ldots\ldots\ldots (6.1)$$

Where k_{2max} is a material coefficient that depends primarily on the void ratio and the relative density and σ'_m is the mean effective static stress. Usually, the shear modulus for cyclic shear strain amplitude of 0.0001 % is chosen as G_{max}, since the dynamic shear modulus is practically constant for strain amplitudes below this level. The values of k_{2max} for various gravel soils are illustrated in Fig. 6.28.

Alternatively, G_{max} may be derived from the shear wave velocity as follows:

$$G_{max} = \rho V_s^2 \quad \ldots\ldots\ldots\ldots\ldots\ldots (6.2)$$

The dynamic material properties used for the earthquake response analysis are given in Table 6.8. The plinth, gallery block, foundation rock and the concrete face slab were assumed to be linear-elastic materials. The dynamic shear modulus and the damping ratio of the embankment material were assumed to vary with the cyclic shear strain amplitude as depicted in Fig. 6.28. In these figures upper bound, lower bound and average shear strain-dependent material properties are shown.

6.5.6 Earthquake Response Analysis

The dynamic response of the maximum saddle dam cross-section (on rock foundation) subjected to the SEE ground motion was carried out using the equivalent linear method (Seed and Idriss, 1970). The method consists of an iterative computational process to adjust the damping ratio and the dynamic shear stiffness of each finite element until the dynamic properties are compatible with the dynamic shear strains. This method is extensively used in practice for the dynamic analysis of embankment dams.

The 2D earthquake response analysis was carried out for the SEE ground motion only. The horizontal and vertical input acceleration time histories were applied at the base of the model. The vertical component is taken as 2/3 of the horizontal component. The boundary condition is fixed in the vertical and horizontal direction at the base and the vertical direction is fixed in the two sides. The dynamic analysis was carried out by QUAKE/W computer program, (GEO-SLOPE International Ltd., 2019). The main characteristics of these earthquakes are presented under table 6.7. The contour map of absolute maximum horizontal and vertical acceleration in the dam body is given under Fig. 6.29. The peak absolute horizontal crest acceleration due to the SEE excitation is about 0.36 g (Fig 6.30).

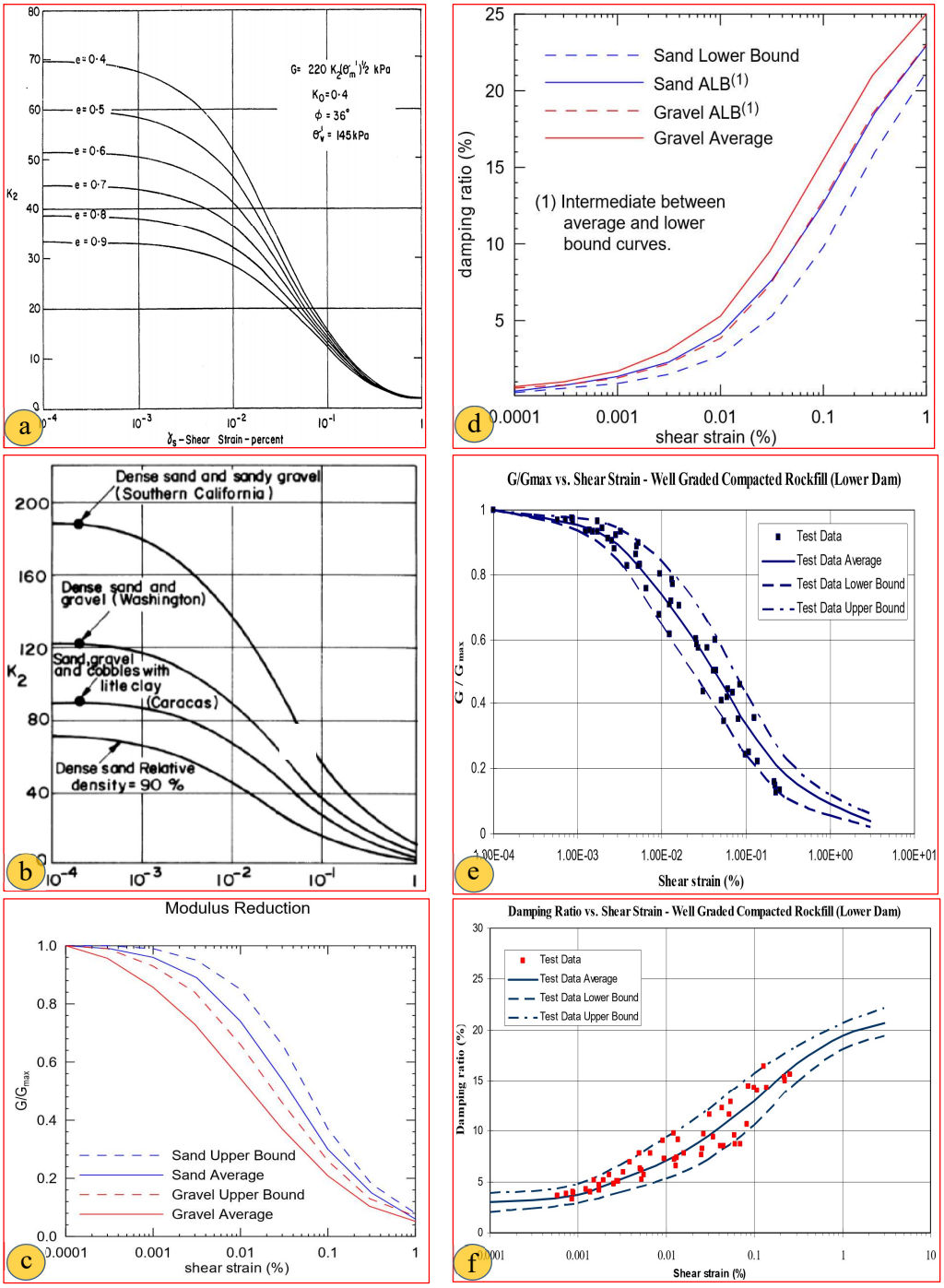

Figure 6.28: K_{2max}, G/G_{max} and damping ratio variation curves with shear strain used for different embankment layers in dynamic analysis: (a) and (b) - K_{2max} relationship for sandy and gravelly soil respectively (Seed and Idriss 1970); (c) G/G_{max} relationship for gravel (Seed et al., 1996) and sand (Seed and Idriss, 1970), (d) damping ratio relationship for gravel (Seed et al., 1996) and sand (Seed and Idriss, 1970), (e) and (f) - G/G_{max} and damping ratio relationship for compacted rockfill dam (Siah Bishe dam project).

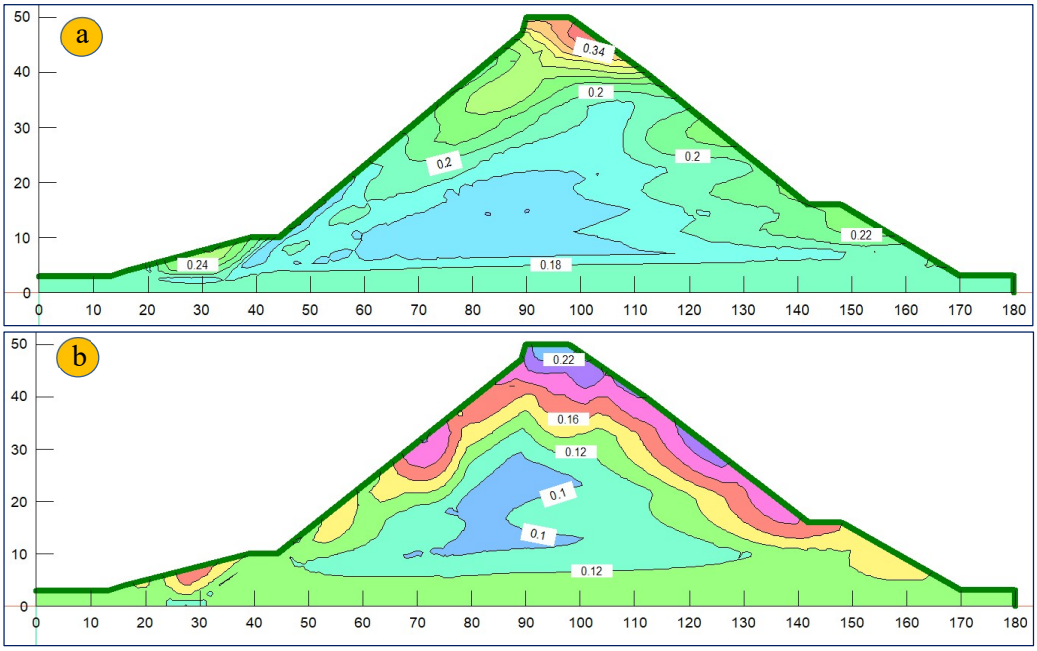

Figure 6.29: Contour plots of absolute maximum horizontal (a) and vertical (b) accelerations in dam body (SEE of 30,000 years return period): horizontal peak acceleration: 0.36 g, and vertical peak acceleration: 0.23 g.

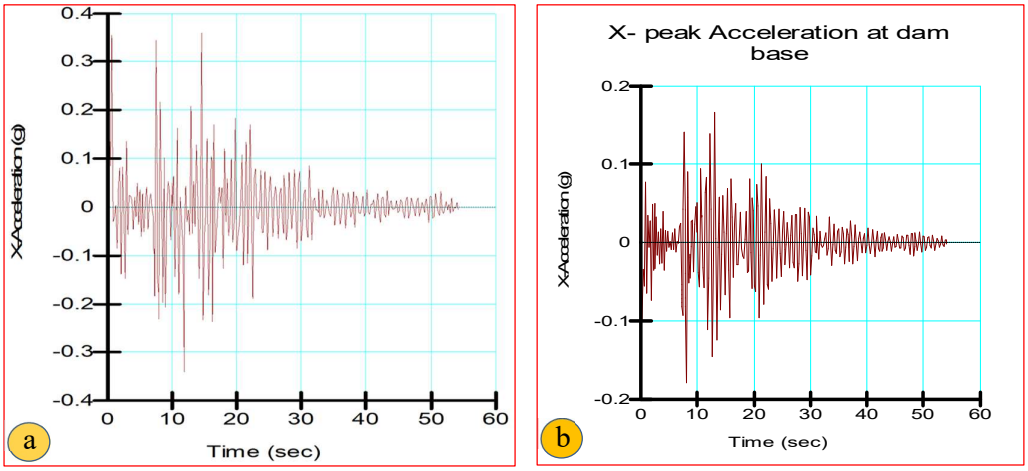

Figure 6.30: Acceleration time histories in the dam body for SEE of 30,000 RP: horizontal acceleration at crest (a), horizontal acceleration at the base (b).

6.5.7 Dynamic Slope Stability Analysis

For the dynamic stability analysis of a potential sliding mass, the acceleration in the center of gravity must be determined based on the results of the linear equivalent

analysis of the dam. The shear strength parameters used for the dynamic slope stability analysis are given in Table 6.9. For the dynamic stability analysis of a potential sliding mass, its yield acceleration has to be determined first (0.18 g downstream critical slope and 0.1 g upstream critical slope). The inelastic slope displacements are calculated using Newmark's sliding block method.

Table 6.9: Material properties for dynamic slope stability analysis

Description	γ (kN/m3)	C' (kPa)	Φ′$_o$ (°)	Δ Φ′ (°)
Fine Backfill - 1A	18	0	25	0
Course Backfill - 1B	18	0	25	0
Peripheral Joint Filter – 2A	23	0	46	7
Cushion – 2B	23	0	46	7
Transition – 3A_1	22	0	46	7
Transition – 3A_2	21	0	44	7
Main Rockfill – 3C	20	0	50	8
Large Rock – 3C	17	0	50	8
Concrete Face – CF	23	0	46	7
Plinth and Gallery	23	-	-	-
Weathered Granite	26	260	54	8

The maximum sliding displacements of the critical blocks passing through the crest are 2.8 cm (downstream slope) and 0.6 cm (upstream slope). Typical results of Newmark's sliding block analysis for GERD saddle dam are shown in Fig. 6.31. The crest settlement is taken as the vertical component of the slope movement. Although the slopes of the CFRD are steep (1:1.3), the slope displacements are small for the worst ground motion at the dam site.

As the displacements are almost negligible, a sensitivity analysis is conducted by multiplying the accelerations of the moving mass by a factor of 1.5 and 2. Accordingly, the sliding displacement of the critical blocks passing the crest of the dam is still small and within the acceptable limit.

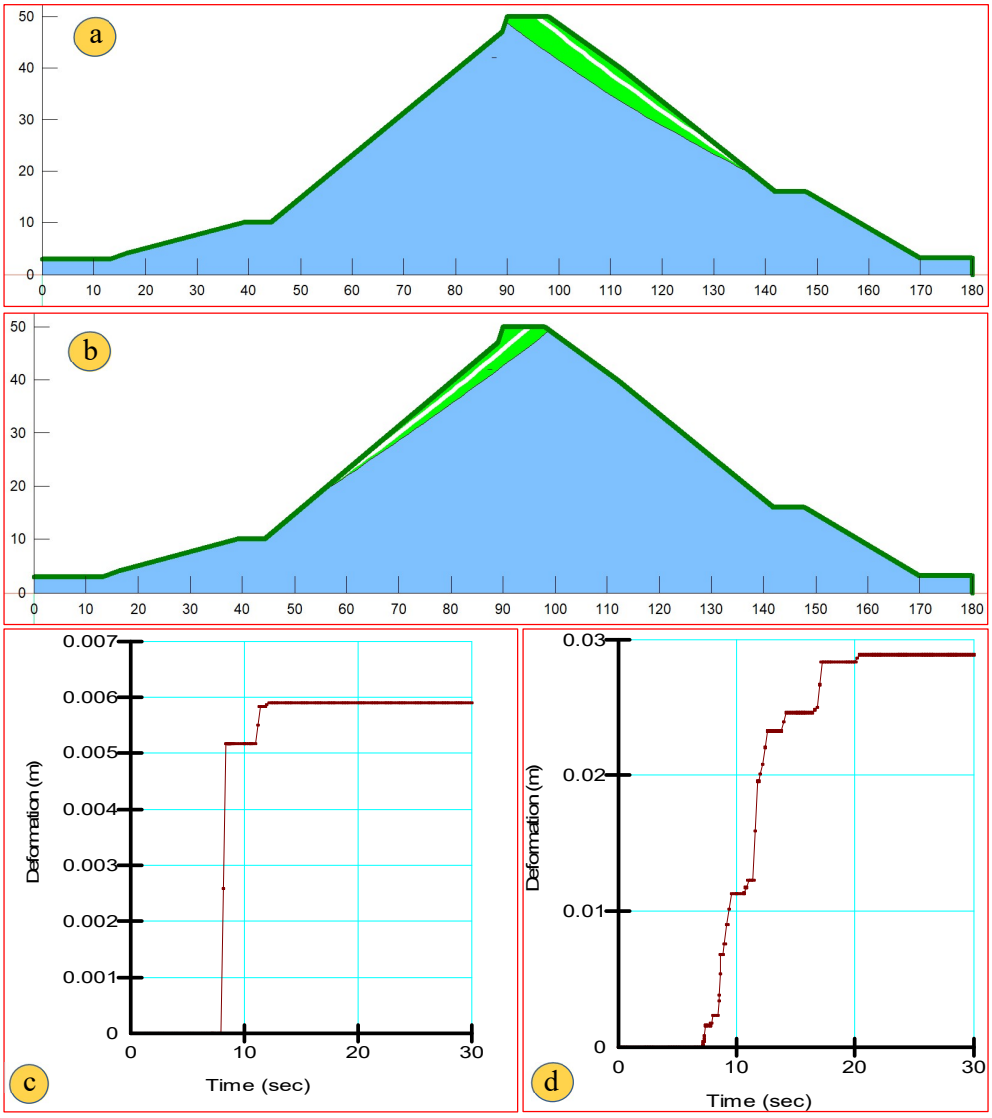

Figure 6.31: Newmark sliding block analysis results of GERD saddle dam for SEE (scaled Hector Mine accelerogram): (a) critical downstream slope (yield acceleration: 0.18 g), (b) critical upstream slope (yield acceleration: 0.1 g) (c) displacement time history of critical downstream slope, and (d) displacement time history of critical upstream slope.

6.5.8 Seismic Settlement and Loss of Freeboard

The estimate of loss of freeboard for GERD saddle dam due to seismic sliding displacements of the critical downstream and upstream slopes was evaluated. During the SEE the upstream and downstream movements occur at different times and are assumed to have a cumulative effect on the vertical displacement of the crest.

Therefore, the total reduction of the freeboard because of SEE induced sliding displacements is obtained as the sum of the vertical projections of the sliding movements of the two critical slopes.

The total vertical movement due to slope movements is 1.7 cm which is the sum of the two vertical components, i.e. 1.4 cm (downstream) and 0.3 cm (upstream) slopes (maximum values from three different earthquakes).

The crest settlement due to densification may be determined using the empirical method by Bureau (1997), which results in a settlement of less than 0.1% of the dam height, therefore, a seismic settlement of 5 cm has been estimated for the 50 m high dam.

6.5.9 Earthquake Safety

The main dynamic analyses results of GERD saddle dam are discussed as follows:

- The maximum absolute horizontal crest acceleration due to the SEE ground motion is 0.36 g.
- The total settlement due to densification of the dam body (5 cm) plus the vertical crest displacement due to upstream and downstream slope movements (1.7 cm) is about 6.7 cm.

The GERD saddle dam is safe against overtopping during the SEE, as the freeboard provided is 4 m.

6.5.10 Conclusions

GERD is the largest hydropower project currently under construction in Africa. The project consists of the main RCC dam and a 5.2 km long CFRD saddle dam. The safety criteria for the saddle dam should be the same as those of the main dam. The seismicity in the project area is low. However, the information on historical seismicity is very scarce in the region. Based on site-specific probabilistic seismic hazard

analysis, the horizontal PGA calculated at the project site is 0.19 g for a return period of 30,000 years. The seismic safety of the saddle dam is checked using the equivalent linear method. The results show that the dam is safe and the seismic deformation is insignificant compared to the available freeboard.

In this analysis only the overtopping failure mode due to inelastic deformations of the saddle dam have been checked. However, the concrete face could still be damaged by this earthquake if the modulus of elasticity of the rockfill is low or if the vertical joints between adjacent concrete slabs are closed. The resulting cracks in the concrete face will increase leakage losses but should not have any effect on the post-earthquake safety of the dam. It should also be mentioned that due to the size of the reservoir, it will not be possible to lower it after a strong earthquake, therefore, any repairs of the concrete face would have to be done with the help of divers.

6.6 Seismic Safety Analysis of Gidabo Dam

6.6.1 Introduction

Gidabo dam is a central core earthfill dam with a height of 27 m, a crest length of 335 m and a reservoir volume of 62.3 Mm^3 (Fig. 6.32). The reservoir is used for the irrigation of 13,000 ha in the downstream part of the dam. The construction of the dam commenced in 2011 and was completed in 2018. The project includes an intake tower supported by pile foundation in the upstream part of the dam and connected with a diversion conduit laid on weak compressible foundation passing through the dam body. The geotechnical investigation conducted at the design stage reveals that the dam foundation is filled with unconsolidated thick alluvial and lacustrine sediments consisting of gravel, sand, silt and organic rich clay sediments to a depth of 40 m at the central part of the valley. The SPT test results confirmed that the material has high variability in terms of firmness from loose to very dense. Due to this, the original design recommended pile foundation for the intake tower as well as the conduit. However, during the design modification for heightening of the dam, the proposed pile foundation for the conduit was eliminated and the conduit constructed on improperly treated backfill material. However, the intake tower was built on pile foundation according to the original design.

During dam construction (2016), the conduit that was laid on the soil foundation settled during the construction phase creating a vertical offset of more than 50 cm at the joint between the pile-supported intake tower and the conduit. The main purpose of the conduit was for river diversion during construction and in the final project as irrigation outlet. Following the settlement of the conduit, a review team was appointed and an assessment has been made. Various remedial measures were proposed. Among the measures proposed to compensate the expected settlements, heightening of the dam by 5 m, which was implemented.

Settlements and liquefaction are the major causes of embankment dam failures during an earthquake as observed, for example, during the 2001 Gujarat earthquake in India, discussed in Chapter 2, where over 240 earth dams were damaged and has to be strengthened after the earthquake. The settlement observed in the conduit through

Gidabo dam was due to static loads only. However, as the dam site is located in the seismically active Main Ethiopian Rift (MER) (Fig. 6.4), dam deformations are also expected during strong earthquakes. Several destructive earthquakes have occurred in the past in the MER region with magnitudes over 6.

Figure 6.32: Gidabo dam with spillway at left abutment and irrigation intake tower.

In this section, the site-specific seismic hazard evaluations conducted for the Gidabo dam project are summarized, followed by the seismic stability analysis of the dam. A probabilistic seismic hazard analysis was carried out. The main purpose of the seismic stability analysis is to determine the maximum settlement of the conduit when it is subjected to SEE ground motion with 10,000 years return period. The dynamic analysis of the dam is carried out by the equivalent linear method using a two-dimensional (2D) dam model of the highest cross-section founded on soil. The scope of work of the seismic safety analysis includes the following:

i. Identification of the geological and tectonic setup;
ii. site-specific seismic hazard assessment;
iii. Selection of appropriate acceleration time histories and spectral matching with response spectra obtained from the site-specific seismic hazard analysis;
iv. 2D seismic response analysis using the equivalent linear method;
v. Selection of potential sliding masses and calculation of yield accelerations;

vi. Calculation of permanent earthquake-induced displacements of potential sliding masses,
vii. Estimation of seismic settlement due to vibration-induced densification of dam materials; and
viii. Determination of total reduction of freeboard, offset of conduit and seismic safety of the dam.

This study is important to judge what kind of remedial measures are required to improve the seismic safety of the dam.

6.6.2 Geology and Tectonics Background

The Gidabo dam and reservoir area lay within the Southern Main Ethiopian Rift (SMER) which is characterized by active extensional tectonics that produced a series of horst and graben structures. The project area is covered by recent volcano-tectonic events and fluvial deposits, in which the former volcano-tectonic events with some water action are an essential part of the area. According to the engineering geological investigation carried out, the dam site has an overburden ranging in thickness up to 33 m at the left abutment and over 40 m at the right abutment (Fig. 6.33). The Standard Penetration Tests (SPT) results confirm the loose and compressible nature of the soil covering the dam foundation.

The orientation of faults in the project area is dominated by North-North-East trending swarms of en-echelon tensional faults that commonly produce horsts and grabens. Gidabo River is the main river in the southern Main Ethiopian Rift that flows from the western rift escarpment towards the rift floor and draining into Lake Abaya. A series of intense normal faulting and Quaternary volcanism observed in Gidabo river basin is believed to represent the southern sector of the Wonji Fault Belt (WFB). The dam site is located between two parallel faults trending NNE direction.

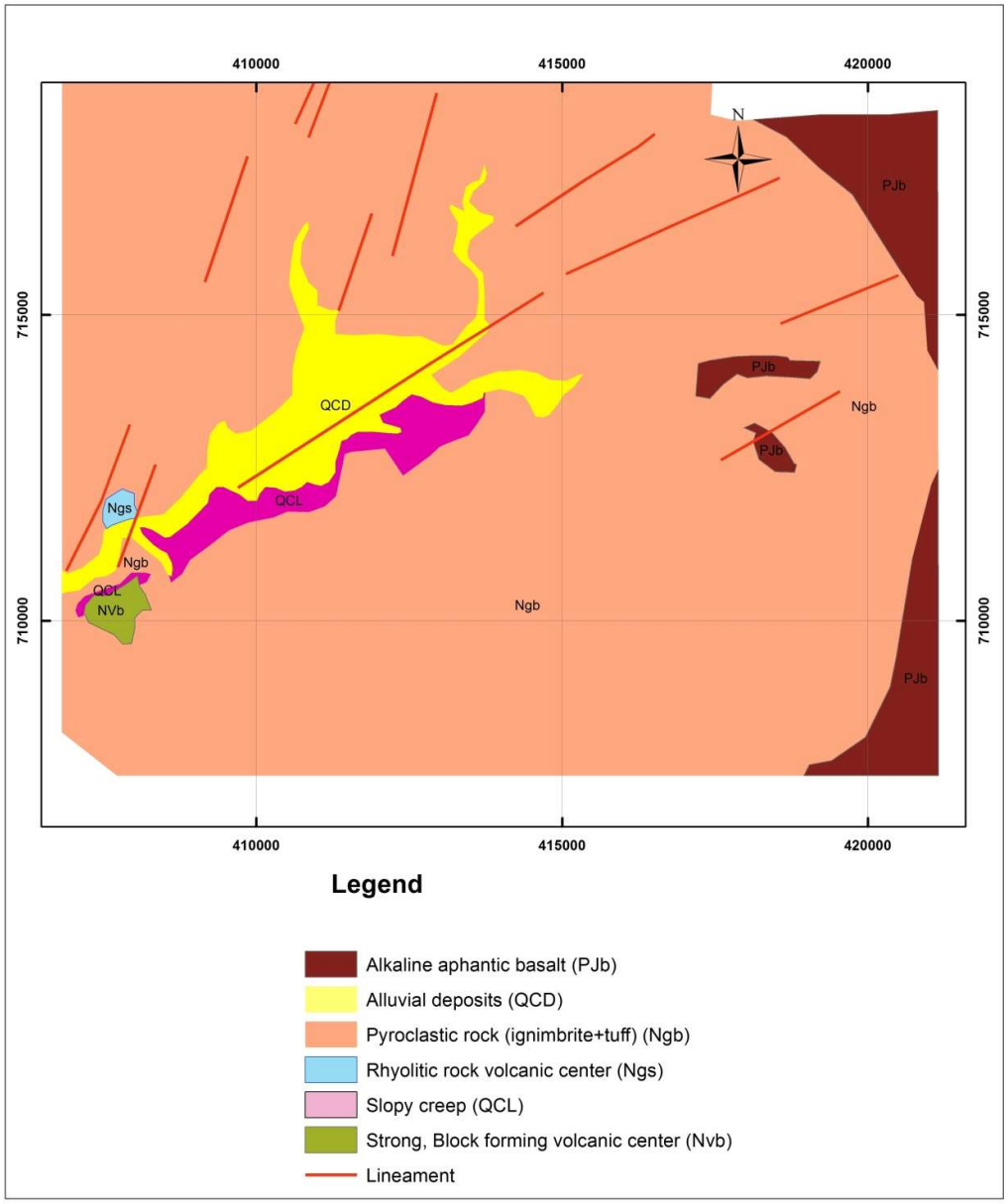

Figure 6.33: a) Geological map of Gidabo dam site showing the presence of alluvial deposit extensively covering the dam site and project area.

6.6.3 Seismic Activity and Dam Seismic Design Criteria

The seismicity at the dam site is mainly controlled by the southern Main Ethiopia Rift. The seismic activity is high and characterized by intermediate size earthquakes. Several earthquakes have occurred in the past in this zone with magnitude above Mw 6. Two events are recorded at a distance of less than 80 km from Gidabo dam site. At

the design stage, no site-specific seismic hazard study was carried out. The estimated horizontal peak ground acceleration (PGA) for different design earthquakes are given in Table 6.10 (WWDSE, 2008). The methodology followed for the estimation of the seismic hazard was not indicated in the site investigation report for Gidabo dam.

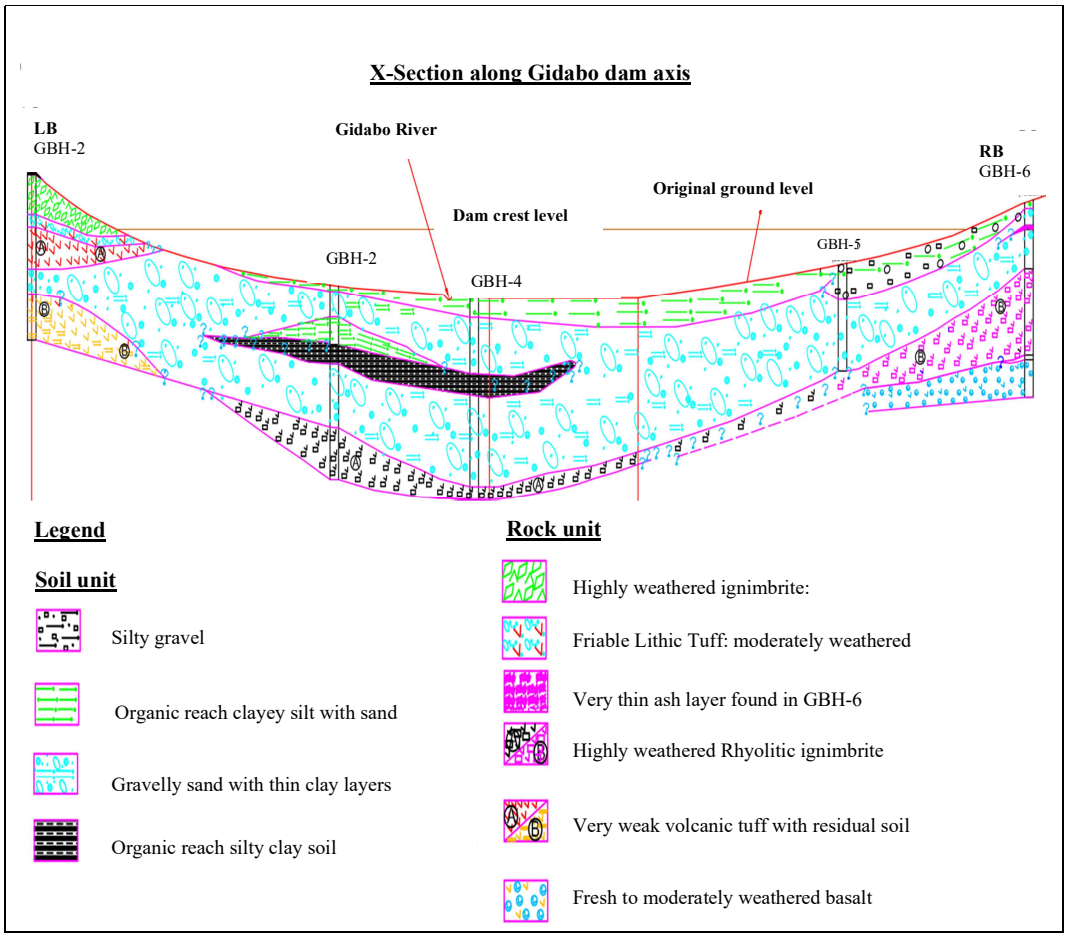

Figure 6.34: a) Geological map of Gidabo dam site showing the presence of alluvial deposit extensively covering the dam site and project area. b) Geological cross-section along the dam axis showing 40 m thick unconsolidated sediment at the center of dam axis (Modified from WWDSE, 2008).

Table 6.10: Peak ground acceleration of different design earthquakes proposed for the seismic design of Gidabo dam (WWDSE, 2008)

Design Earthquake	RP (years)	M	PGA (g)
MCE	10,000	7.5	0.7
OBE	145	5-	0.102

PGA: horizontal peak ground acceleration on rock surface, M: magnitude, RP: return period, MCE: maximum credible earthquake, OBE: operating basis earthquake

However, the recommended seismic hazard values of Table 6.10 were not considered in the design of the dam. Instead, a PGA-value of 0.3 g was used. The PGA-values estimated in the site investigation report exceed those of the current study significantly.

6.6.4 Results of the Seismic Hazard Analysis

The present (updated) site-specific seismic hazard analysis for Gidabo dam site is conducted based on the probabilistic approach following the procedures discussed in Chapter 4. Accordingly, the PGA-value for the SEE (10,000 years return period) is 0.4 g for the horizontal earthquake component on the outcropping rock (Fig. 6.34).

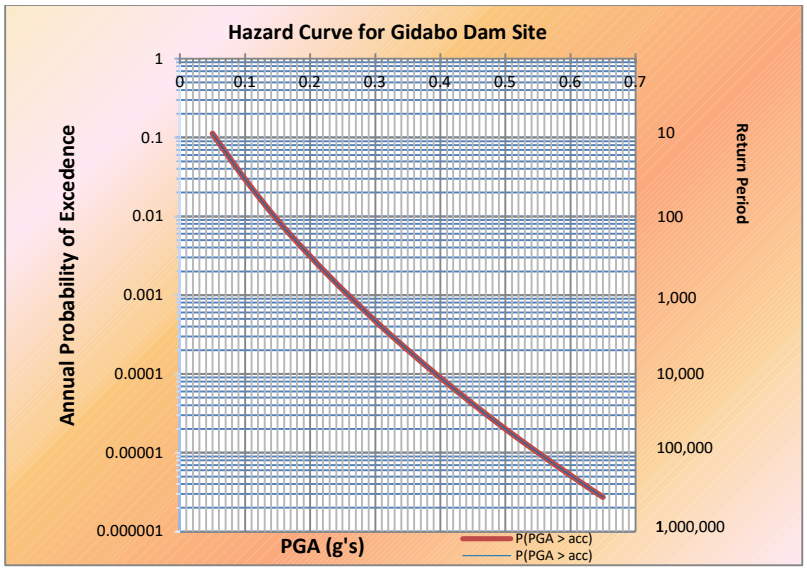

Figure 6.35: Horizontal peak ground acceleration at Gidabo dam site as a function of the return period.

The PGA-value of 0.3 g assumed in the dam design is less than the value obtained in the current seismic hazard study. Therefore, the dynamic response of the dam has to be checked for the updated PGA-value. For the Gidabo dam site, the results of the PSHA are also given in terms of uniform hazard spectra for 5% damping for various return periods (Fig. 6.35a). Furthermore, a deaggregation analysis was done to identify the magnitude and distance of seismic events with the greatest contribution to the seismic hazard at the site (Figs. 6.35b and 6.35c).

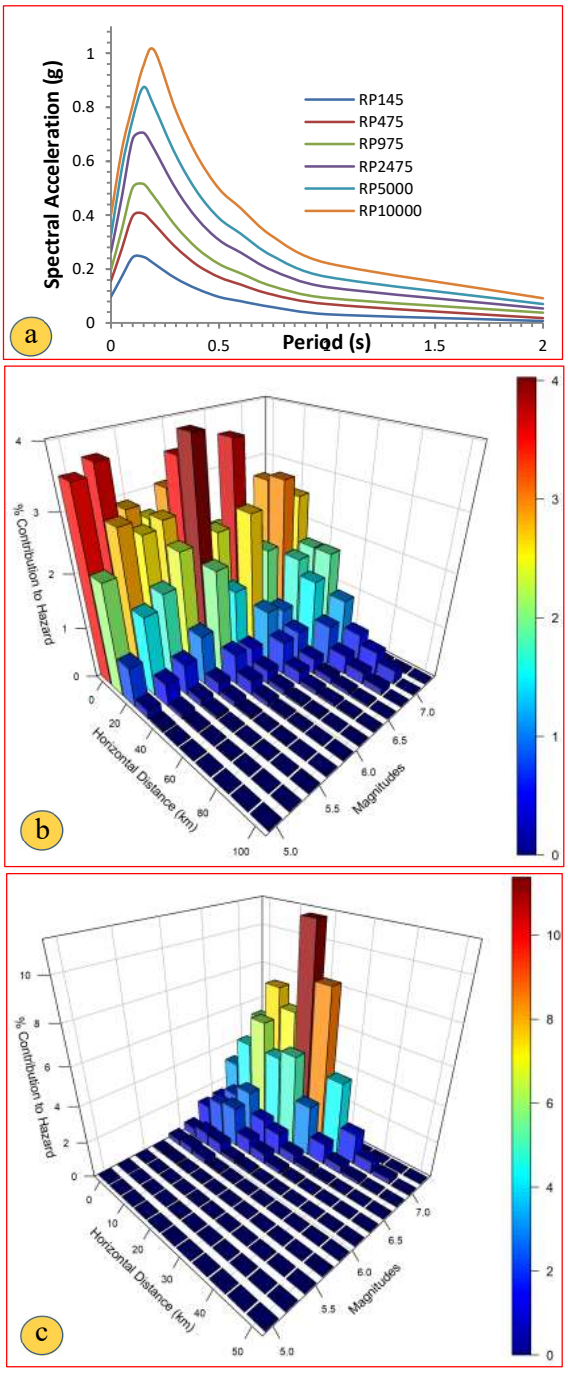

Figure 6.36: a. Uniform hazard spectra for various return periods for the Gidabo dam site for horizontal earthquake component on outcropping rock and 5% damping (RP: return period) b. Deaggregation result for 475 year return period c. Deaggregation result for 10,000 years return period.

The horizontal PGA-value is 0.40 g. For the vertical component 2/3 of the PGA and response spectra of the horizontal earthquake component are used, i.e. a vertical PGA-value of 0.27 g.

Table 6.11: Summary of earthquakes selected for time history development using spectral matching R: epicentral distance

No.	Earthquake	Station	Year	Mw	Earthquake Mechanism	R (km)	Site class/ Vs30 (m/s)
1	Imperial Val-06	El Centro Array St-2	1979	6.53	Strike slip	20	Soil (C)
2	Central Italy	Collecreta (MZ63)	2016	6.5	Normal	29	Soil (B)
3	Kobe-Japan	Morigawachi	1995	6.9	Strike slip	25	Soil (256)

Based on the magnitude and distance of the deaggregation analysis results, representative time histories are selected (table 6.11). The selected time histories are spectrally matched with the uniform hazard spectra of the dam site for 10,000 years return period (Fig. 6.36).

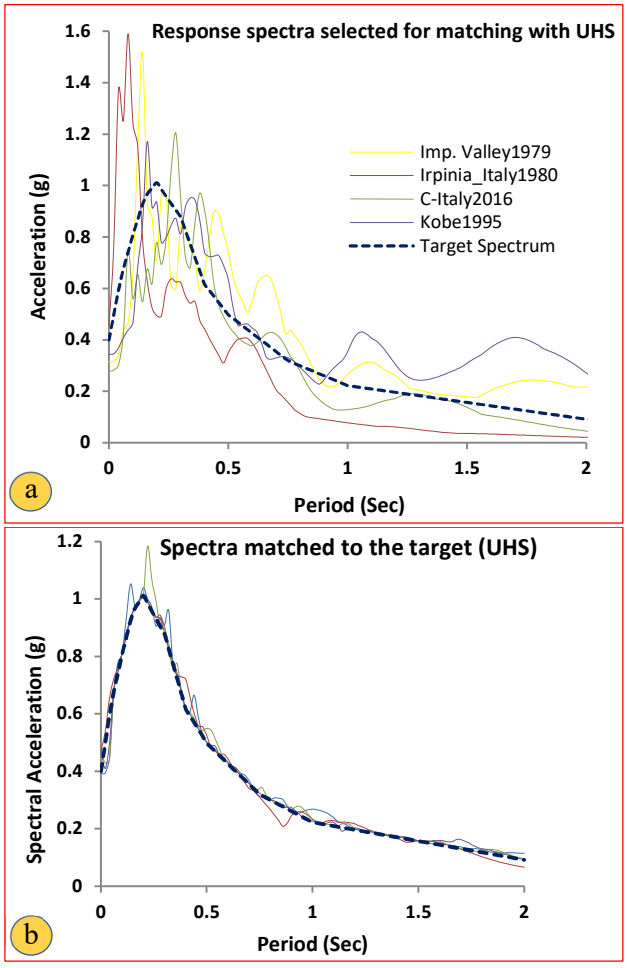

Figure 6.37: Horizontal acceleration response spectra of various earthquakes selected for time history analysis with UHS of Gidabo dam site for 10,000 years return period: a) response spectra of acceleration records, b) response spectra after matching with the target (UHS)

After spectrum matching, the acceleration time histories of the SEE were examined to ensure that they are reasonably close to the original time histories and target spectrum values in terms of peak values, waveform and strong shaking duration. As a result, three of the spectral matched time histories have been chosen and used for the stability analysis of the dam (Fig. 6.37).

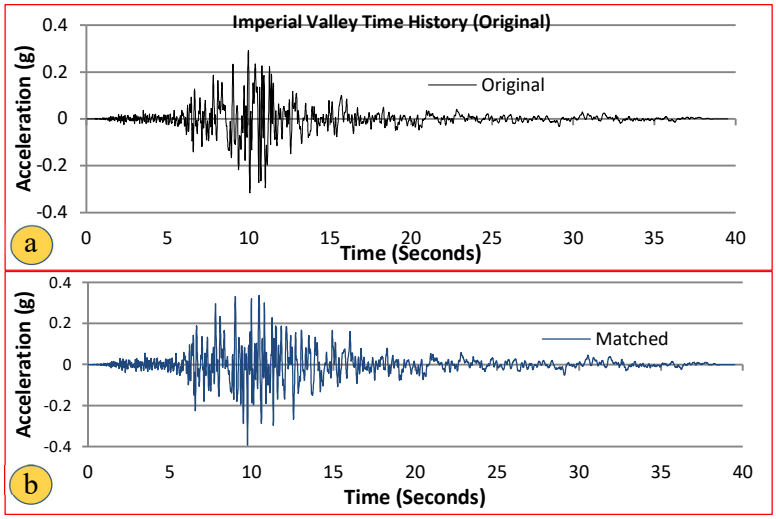

Figure 6.38: Comparison of pre and post spectral matching of acceleration time histories for Imperial Valley earthquake (El Centro Array 2 station) with SEE target spectrum for Gidabo dam site). a) recorded time history b) time history after spectral matching.

6.6.5 Seismic Analysis of Dam with Equivalent Linear Method

The two-dimensional (2D) dynamic analysis was conducted on the maximum cross-section of Gidabo dam using the spectrum matched acceleration time histories (Table 6.11 and Fig. 6.39). The earthquake analysis was carried out using a plane strain model of the dam and the soil foundation and the equivalent linear analysis concept with shear strain-dependent material properties was used.

6.6.5.1 Dam Zoning

The main features of the dam and maximum cross-section used for the analysis are given in Fig. 6.38. The dam geometry and the dam zoning were taken from the as-

built drawings, and the depth of the soil foundation is modeled based on the results of drillings and SPT tests.

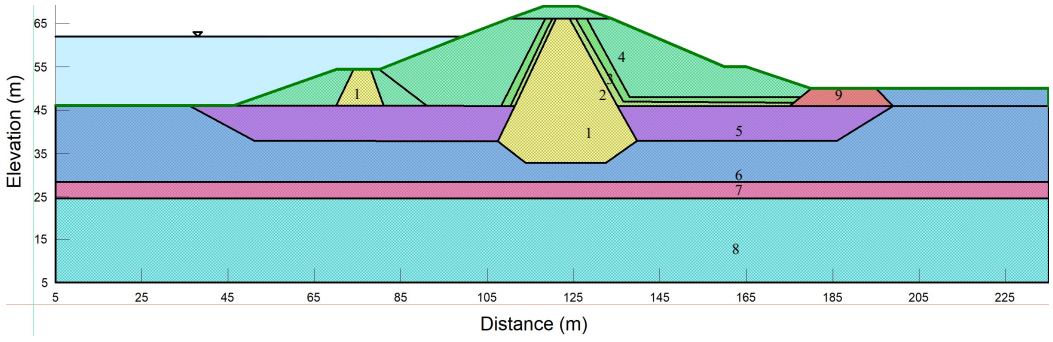

Max. height	27 m
Crest length	335 m
Dam volume	1 Mm^3
Crest width	8 m
Full supply level	1219.5 m
MWL (10,000 year)	1223.8 m
Dam crest	1226.9 m
Upstream slope	3/2.46:1
Downstream slope	3/2.46:1
Storage volume	62 Mm^3

1-Core
2-F1- Filter
3-F2-Filter
4-Shell
5-Backfill (clayey silt)
6-Upper alluvial foundation (medium dense)
7 - Organic silty clay (compressible)
8 - Lower alluvial material (dense)
9 - Rockfill toe

Figure 6.39: Maximum cross-section of Gidabo dam showing main features and material zoning.

6.6.5.2 STATIC DAM ANALYSIS

The static analysis was carried out by the computer program SIGMA/W (GEO-SLOPE International Ltd., 2019) using the Mohr-Coulomb elasto-plastic model. The material properties in different zones are obtained from the design reports, similar dam projects and published data from the literature (Table 6.12).

The static loads considered in the analysis are gravity load and water load. First, the dam body was built up in the FE model in one layer up to the level of the crest. The water load was applied as hydrostatic pressure acting on the upstream face of the core. A seepage analysis was performed in order to determine the water phreatic line within the dam body and to estimate pore pressures. The contour plot of the vertical stress due to dead load is shown in Fig. 6.39.

Table 6.12: Material properties for static deformation and stress analyses

Material Description	v	E (MPa)	γ (kN/m3)	C' (kPa)	Φ' (degrees)	K (m/s)
Impervious Core	0.40	20	16	10	20	1×10^{-9}
F1-filter	0.30	40	18	0	34	$1x\ 10^{-4}$
F2-Filter	0.30	50	19	0	35	$1x\ 10^{-4}$
Shell	0.30	50	19	0	25	2×10^{-5}
Backfill	0.40	6	16	26	10	1.5×10^{-7}
Upper Alluvial Foundation	0.30	22	16	0	28	1.5×10^{-5}
Organic Silty Clay	0.45	6	16	10	20	1.5×10^{-7}
Lower Alluvial Foundation	0.30	60	20	0	39	1.5×10^{-4}
Toe drain	0.30	60	22	0	40	$5x10^{-1}$

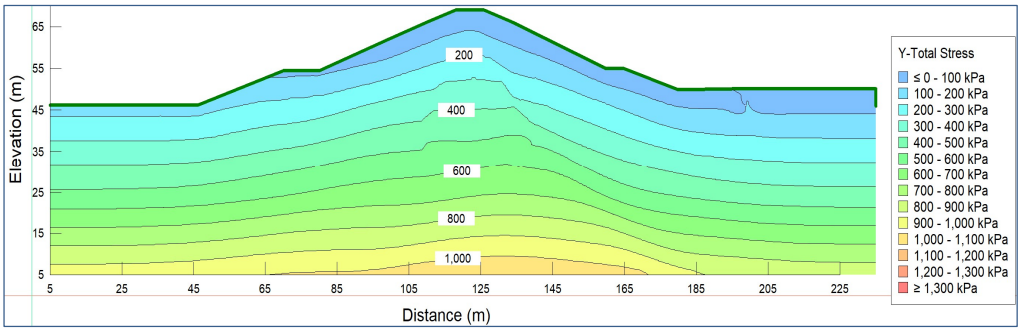

Figure 6.39: Contour plot of vertical stress from gravity load (dam body); maximum vertical stress 1100 kPa

6.6.5.3 Dynamic Material Properties

The dynamic material properties required for the earthquake response analysis are the dynamic shear modulus and the damping ratio; both are given as functions of the dynamic shear strain. The dynamic shear modulus G is commonly determined as the ratio G/G_{max} (reduction function) as a function of the cyclic shear strain and the maximum dynamic shear modulus G_{max}. The material parameters used for the earthquake analysis of Gidabo dam are obtained from design report, literature review and other dam projects and are given in Table 6.13. The dynamic shear modulus and the damping ratio of the embankment material were assumed to vary with the cyclic shear strain amplitude as depicted in Figure 6.28 and 6.40.

Table 6.13: Dynamic material properties in different zones of Gidabo dam

Material	K_{2max}	V	Modulus reduction (G/G_{max})	Damping	Material model
Impervious Core	50	0.40	1*	2*	Non-linear
F1-filter	60	0.30	3*	3*	Non-linear
F2-Filter	50	0.30	4*	4*	Non-linear
Shell	80	0.30	4*	4*	Non-linear
Backfill	50	0.40	1*	2*	Non-linear
Upper Alluvial Found.	70	0.30	3*	3*	Non-linear
Organic rich layer	40	0.45	3*	3*	Non-linear
Lower Alluvial Found.	130	0.30	4*	4*	Non-linear
Rock Toe	70	0.30	4*	4*	Non-linear

1*- Modulus reduction curve for clay (Sun et al., 1988) (Fig. 6.40a)
2*- damping ratio relationship for clay (Vucetic and Dobry, 1991) (Fig. 6.40b)
3*- Average relationship for sands by Seed and Idriss, 1970 (Fig. 6.28)
4* Seed et al., 1984 gravels (Fig. 6.28)

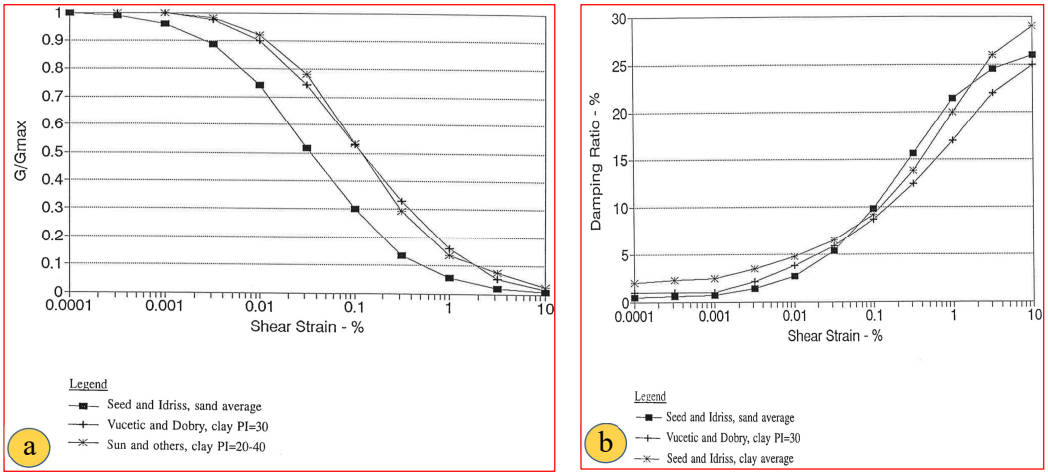

Figure 6.40: a) Modulus reduction curve for clay (Sun et al., 1988) b) damping ratio relationship for clay (Vucetic and Dobry, 1991).

6.6.6 Earthquake Response Analysis

The dynamic response of the maximum cross-section of Gidabo dam subjected to the SEE ground motion was carried out using the equivalent linear method (Seed and Idriss, 1970). The horizontal and vertical input acceleration time histories were applied at the base of the model. The vertical earthquake component was taken as 2/3 of the horizontal one. The boundary of the soil foundation is fixed in the vertical and horizontal direction at the base and the vertical direction is fixed in the two sides. The dynamic analysis was carried out by QUAKE/W computer program, (GEO-SLOPE

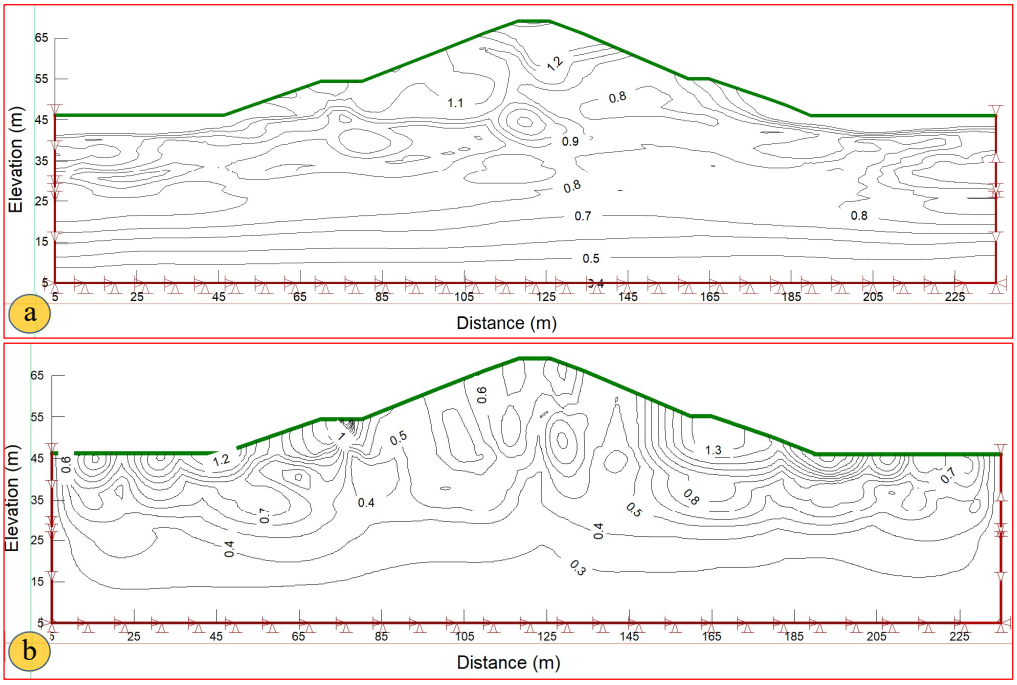

Figure 6.41: Contour plots of absolute maximum horizontal acceleration (a) and vertical accelerations (b) in dam body (SEE of 10,000 years return period): maximum horizontal and vertical accelerations: 1.2 g and 1.3 g.

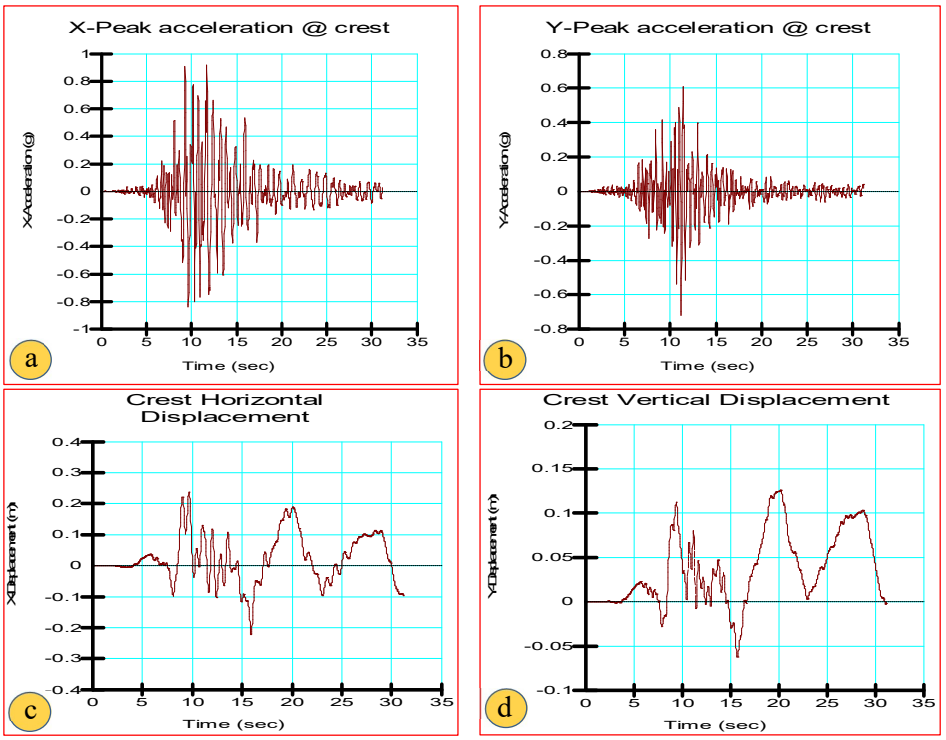

Figure 6.42: Acceleration time histories in the dam body for SEE of 10,000 years return period: horizontal acceleration at crest (top left), vertical acceleration at the crest (top right), horizontal crest displacement (c) and vertical crest displacement (d).

International Ltd., 2019). The main characteristics of the earthquakes are presented in Table 6.13. The contour plots of the absolute maximum horizontal and vertical accelerations in the dam body are given in Fig. 6.41. The peak absolute horizontal crest acceleration due to the SEE excitation is about 1.2 g (Fig. 6.42).

6.6.7 Dynamic Slope Stability Analysis

For the dynamic stability analysis of a potential sliding mass of the dam, its yield acceleration is determined first. The dynamic slope stability analysis of Gidabo dam is conducted using Newmark's Sliding Block Analysis. The shear strength parameters used for the dynamic slope stability analysis are given in Table 6.14.

Table 6.14: Material properties for dynamic slope stability analysis

Description	γ (kN/m3)	C' (kPa)	Φ′$_o$ (º)	Δ Φ′ (º)
Impervious core	16	10	20	0
F1-filter	18	0	34	4
F2-filter	19	0	35	4
Shell	19	0	27	2
Backfill	16	26	10	0
Upper alluvial foundation	16	0	28	5
Organic rich silty clay	16	10	20	7
Lower alluvial foundation	20	0	42	5
Toe drain	22	0	40	7

When the inertial forces acting on a potential sliding mass along the dam slope during earthquake event become sufficiently large, the total driving force (static plus dynamic) would exceed the available resisting force. In other words, once the horizontal acceleration is exceeds the yield acceleration, the factor of safety would drop below 1.0, implying that the potential sliding mass starts to move.

The relative velocity of the sliding mass increases as long as the earthquake acceleration remains above the yield value. When the acceleration falls below the yield level, the motion gets braked, and the sliding mass sticks to the underlying material after some time. The maximum sliding displacement of the critical blocks passing through full crest is 1.88 m downstream (yield acceleration 0.05 g) and 0.63

m upstream (yield acceleration 0.08 g). The main results of Newmark's sliding block analysis for the Gidabo dam are shown in Fig. 6.43.

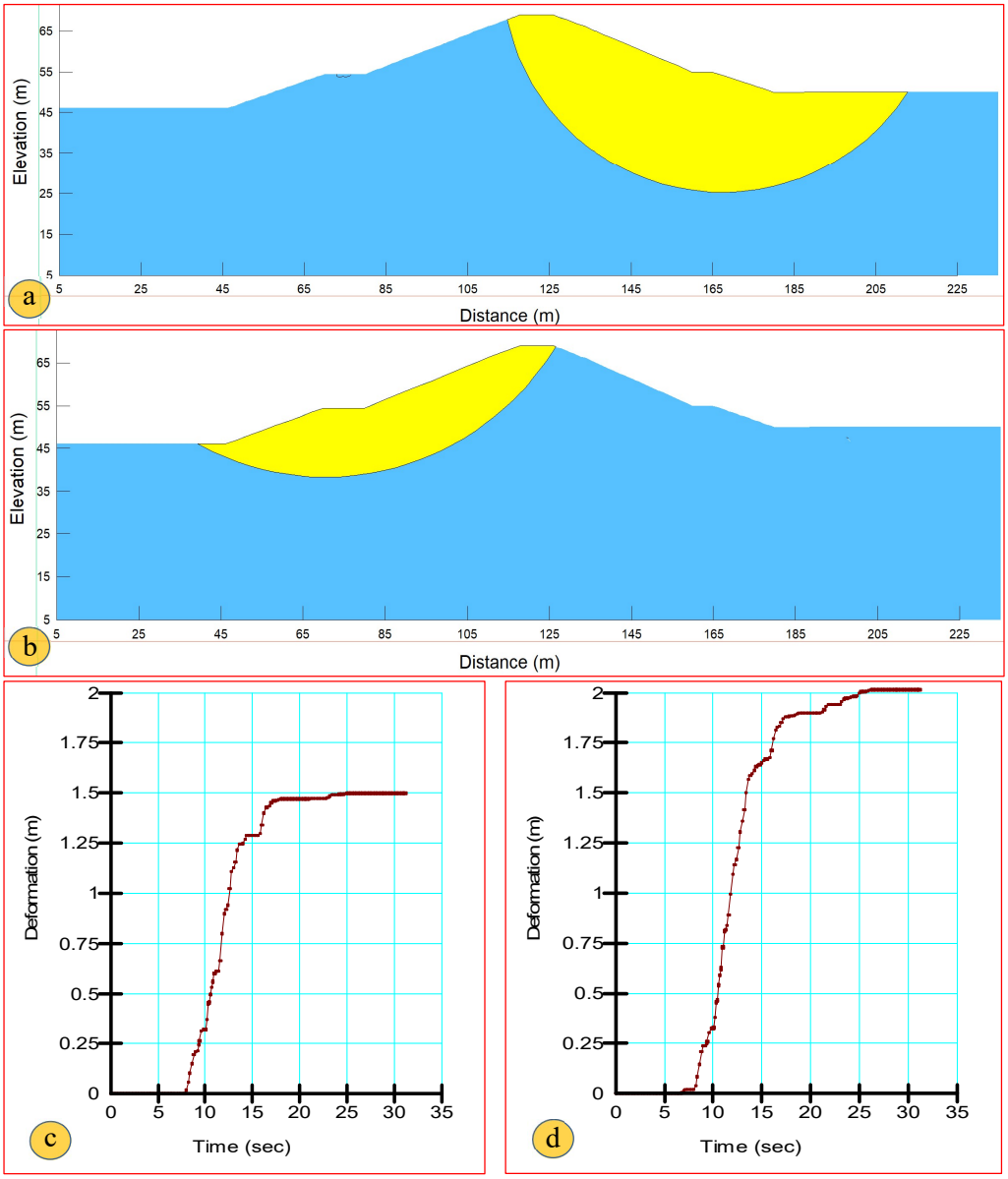

Figure 6.43*:* Newmark sliding block analysis results of Gidabo dam for SEE (Imperial valley earthquake): a) critical downstream slope (yield acceleration: 0.05 g), (b) critical upstream slope (yield acceleration: 0.08 g) (c) displacement time history of critical downstream slope, and (d) displacement time history of critical upstream slope.

The slope stability analysis is done for the horizontal and vertical earthquake components of the sliding mass. From Newmark sliding block analysis results of

Gidabo dam for three SEE time histories, the maximum deformation is obtained for Imperial Valley earthquake (Fig. 6.43).

6.6.8 Seismic Settlement and Loss of Freeboard

The estimate of loss of freeboard for Gidabo dam due to seismic sliding displacements of the critical downstream and upstream slopes was evaluated. During the SEE the upstream and downstream movements occur at different times and are assumed to have a cumulative effect on the vertical displacement of the crest. Therefore, the total reduction of the freeboard because of SEE induced sliding displacements is obtained as the sum of the vertical projections of the sliding movements of the two critical slopes.

The total vertical movement due to slope movements is 2.51 m which is the sum of the two vertical components, i.e. 1.88 m (downstream) and 0.63 m (upstream) slopes. The crest settlement due to densification can be determined using the empirical method by Bureau (1997), which results in a settlement of about 0.22% of the dam height (including soil foundation layer depth), therefore, a seismic settlement of 0.14 m has been estimated for the dam and soil foundation (65 m).

Thus, the total crest settlement of the dam is 2.65 m which is 2.51 m due to slope movement and 0.14 m due to material densification during earthquake.

6.6.9 Earthquake Safety

The main dynamic analyses results of Gidabo dam are discussed as follows:

- The maximum absolute horizontal crest acceleration due to the SEE is about 1.2 g,
- The total settlement due to the upstream and downstream slope movement (2.51 m) plus the vertical crest displacement due to densification of the dam body (0.14 m) is about 2.65 m.

The Gidabo dam is safe against overtopping during the SEE, as the freeboard provided is 4.5 m from the full supply level of the reservoir to the top of the impervious core. However, cracking of the clay core along the conduit due to differential settlement may lead to internal erosion. Moreover, offset of the conduit due to the settlement with intake structure will be significant and the conduit will not be adequate for lowering of the reservoir after the SEE. Thus, emergency outlet should be looked for evacuation of water from the reservoir.

In addition, liquefaction may also be possible due to presence of loose sandy layers susceptible to liquefaction between impermeable clayey layers including the backfill layers that prevent the dissipation of excess pore water pressure development during the SEE. Thus, an analysis of the liquefaction potential is needed.

6.6.10 Conclusions

Gidabo dam site is located in the seismically active southern part of MER. The project area is highly affected by tectonic faults. The dam must be able to withstand the effect of the SEE ground motion, which has a return period of 10,000 years according to ICOLD (2016). The present study shows that the dam can be subjected to significant earthquake ground motion which is estimated as 0.4 g for the horizontal earthquake component.

Based on the present (updated) seismic hazard analysis results, the dynamic response of the dam is checked for SEE ground motion. The dynamic analysis is conducted using equivalent linear analysis. The results of the SEE analyses show that the dam is safe from overtopping as an adequate freeboard is provided. However, the offset of the conduit with respect to the irrigation intake tower will be significant and the steel lining will be damaged such that it would become dangerous or impossible to use the irrigation outlet for lowering of the reservoir after a strong earthquake. Thus, as it will be difficult and very costly to improve the safety of the irrigation outlet system it is recommended to consider an alternative low-level outlet for evacuation of water from the reservoir and also to satisfy irrigation demand after strong earthquakes.

In addition, erosion of the core material along the contact with the conduit and through the alluvial foundation may be possible during SEE. Moreover, liquefaction may also be possible due to presence of loose sandy layers in between clay layers with low permeability including the backfill material that prevent the dissipation of excess pore water pressure development during earthquakes. Thus, liquefaction analysis should be carried out.

Furthermore, as the dam was constructed without any dam instrumentation, standard dam monitoring instruments shall be installed. In addition, strong motion instruments should be installed on the dam crest, at the base of the dam and on top of the spillway intake. Emergency action plan and early warning system should be in place.

6.7 Seismic Safety Analysis of Tendaho Dam

6.7.1 Introduction

Tendaho dam is a central core earthfill dam located in the seismically active part of the East African Rift, where the Red Sea Rift, Gulf of Aden Rift and the Main Ethiopian Rift intersect, forming the Afar Triangle. It is one of the largest irrigation dams in Ethiopia with a height of 53 m, a crest length of 412 m and a reservoir volume of 1.8 km^3(Fig. 6.44). The reservoir is used for the irrigation of 60,000 ha. The construction of the dam was completed in 2009. Following partial filling of the reservoir in 2010, leakage appeared on the abutment slopes and right ridge of the reservoir. As a consequence, different remedial measures were taken comprising grouting and slope stabilization works in the downstream slope of the dam. In contrast to extended grouting works, the leakage persisted to date and is one of the potential risks expected to worsen during major seismic events.

Figure 6.44: Tendaho earthfill dam(left), spillway (right) and intake tower in the middle.

In this section, the seismic safety evaluation of Tendaho dam is discussed. The seismic hazard includes both ground shaking and tectonic fault movements in the footprint of the dam. The site-specific seismic hazard analysis was conducted based on a probabilistic approach. The possible maximum size of fault displacement is estimated using the empirical relations by Wells and Coppersmith (1994). The seismic safety of the dam was checked using a two-dimensional (2D) dam model of the

highest cross section and the equivalent linear dynamic analysis method. The scope of work of the seismic safety analysis of Tendaho dam includes the following:

- Identification of the geological and tectonic setup;
- Site-specific seismic hazard assessment;
- Analysis of fault displacement in the footprint of the dam;
- Selection of appropriate acceleration time histories and spectral matching with response spectra obtained from the site-specific seismic hazard analysis;
- 2D seismic response analysis using the equivalent linear method;
- Selection of potential sliding masses and calculation of yield accelerations;
- Calculation of permanent earthquake-induced displacements of potential sliding masses;
- Estimation of seismic settlement due to vibration-induced densification of dam materials; and
- Determination of total reduction of freeboard and seismic safety of the dam.

6.7.2 Geology and Tectonics Background

The Tendaho dam site is underlain by the Afar Stratoid Series, which consists of various layers of basalts, volcanic breccias, and tuffs. The floor of the reservoir is underlain by down-faulted Afar Stratoid Series at depth, lacustrine sediments and quaternary superficial (alluvial and colluvial) deposits on top (WWDSE, 2005). The Afar Depression is one of the two places in the world where ocean floor spreading could can be observed on land. The current tectonic activity in Tendaho area is primarily related to the Afar Depression and includes the following: (1) passive rifting due to a far field stress exerted as a result of the Eurasian and the Arabian Plates convergence; (2) active rifting induced by a local rising plume under Afar Depression itself, and (3) a ridge push from the Indian Ocean spreading centres (Schilling et al., 1992). The tectonics, earthquakes and associated volcanism occurred in the Dabbahu-Manda Hararo rift segment in 2005 clearly indicates the geologic challenges for the safety of Tendaho dam found in the region. The structural analysis of Tendaho the dam site and its reservoir area shows that the area is highly affected by tectonic

fractures and faults. The details of additional work on the critical tectonic faults passing through the dam axis, spillway foundation, and the right and left abutments and their impact on the safety on the dam is discussed in Section 6.7.5.

6.7.3 Seismic Activity and Design Criteria

The seismicity of the dam site is controlled by three active rift systems that intersect at proximal distance to the site (MER, Red Sea, and Gulf of Aden). In the Afar area, the seismic activity is high and characterized by small and intermediate size earthquakes. In the past, several destructive earthquakes have occurred in this zone. The two most significant recent earthquakes occurred in 1969 and 1989. The 1969 Serdo earthquake had a magnitude of 6.1 and caused severe damage in the nearby town of Serdo. Out of its total population of 420, some 40 people lost their lives while some 160 persons were injured (Gouin, 1979). The 1989 Dobi Graben earthquake had a magnitude of 6.3. This event also caused deaths, injuries and major rockslides that blocked a 30 km segment of the main highway to the Red Sea port of Assab and destroyed six bridges (Asfaw and Ayele, 2004). The epicentres of the main shock of the 1969 Serdo earthquake and 1989 Dobi earthquake are only about 30 km and 100 km away from the Tendaho dam site, respectively.

For the maximum credible earthquake (MCE) and the operating basis earthquake (OBE), the peak ground acceleration (PGA) values were given as 0.3 g and 0.18 g, respectively (WWDSE, 2005). The methodology followed and the return period used were not mentioned. The seismic design criteria used for the seismic design of the dam and safety critical elements do not comply with current ICOLD guidelines (ICOLD, 2016). During dam construction (trench excavation), sandy material was found and dynamic analyses were conducted to identify the liquefiable nature of the soil (WWDSE, 2006). Material at a depth of 6 to 10 m was found to be liquefiable. Therefore, the liquefiable alluvial material was removed from critical zones of the dam foundation. In addition, the thickness of filter and transition zone was increased from 2 m to 3 m and the dam crest raised from 412 m to 413.5 m a,s,l, by replacing the 1.5 m high wave wall included in the original design (Hadush and Mesele, 2010).

Berhe and Wu (2009) also mentioned that the active fault passing through the dam body has historically produced earthquakes with magnitudes greater than 6 in the past, as cited in report (TTFR, 2011).

6.7.4 Results of the Seismic Hazard Analysis

The present (updated) site-specific seismic hazard analysis for Tendaho dam is conducted based on the probabilistic approach. Accordingly, the PGA-value for the SEE (10,000 years return period) is 0.61 g for the horizontal earthquake component on the outcropping rock, which differs from the previous works and the PGA-value of 0.3 g obtained during the design stage. The difference in the results is due to (i) difference in source zone model and earthquake return period, (ii) the attenuation relationships used, and (iii) the method of seismic hazard analysis. Therefore, the dynamic response of the dam must be checked for the ground motion parameters obtained from the current study.

The main results of the probabilistic seismic hazard analysis (PSHA) are uniform hazard spectra for 5% damping for various return periods (Fig. 6.45a). In addition, a deaggregation analysis was done to identify the magnitude and distance of seismic events with the greatest contribution to the seismic hazard at Tendaho dam site (Fig. 6.45b).

Table 6.15: Details of earthquakes selected for time history analysis

No.	Earthquake	Station	Year	M	Mechanism of Faulting	E.S. (km)	Site class/ Vs30 (m/s)
1	Central Italy	Accumoli(ACC)	2016	6.5	Normal	19	Rock
2	Hector Mine	Hector	1999	7.13	Strike Slip	11	726
3	Manjil-Iran	Abbar	1990	7.37	Strike Slip	13	724

Based on the magnitude and distance of the deaggregation analysis, representative acceleration time histories were selected. These time histories are spectrally matched with the site-specific uniform hazard spectra for a return period of 10,000 years (Fig. 6.46).

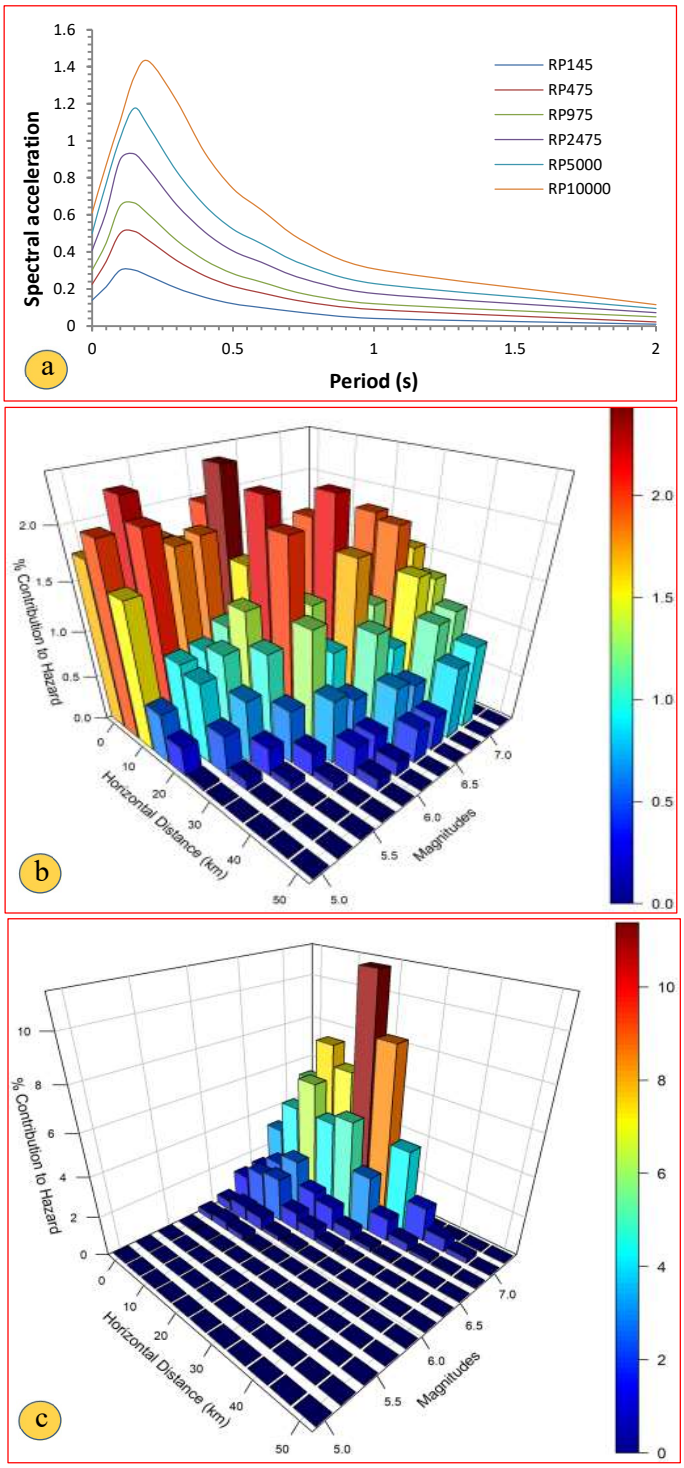

Figure 6.45: (a) Uniform hazard spectra for various return periods for the Tendaho dam site for horizontal earthquake component on outcropping rock and 5% damping (RP- return period). (b) Deaggregation result for 475 year return period earthquake ground motion. (c) Deaggregation result for 10,000 years return period earthquake ground motion showing the dominance of magnitude 7 earthquakes at epicentral distances of 10 to 20 km.

After spectrum matching, the acceleration, velocity, and displacement time-histories of the SEE were examined to ensure that they are reasonably close to the original time histories and target spectrum values in terms of peak values and waveform.

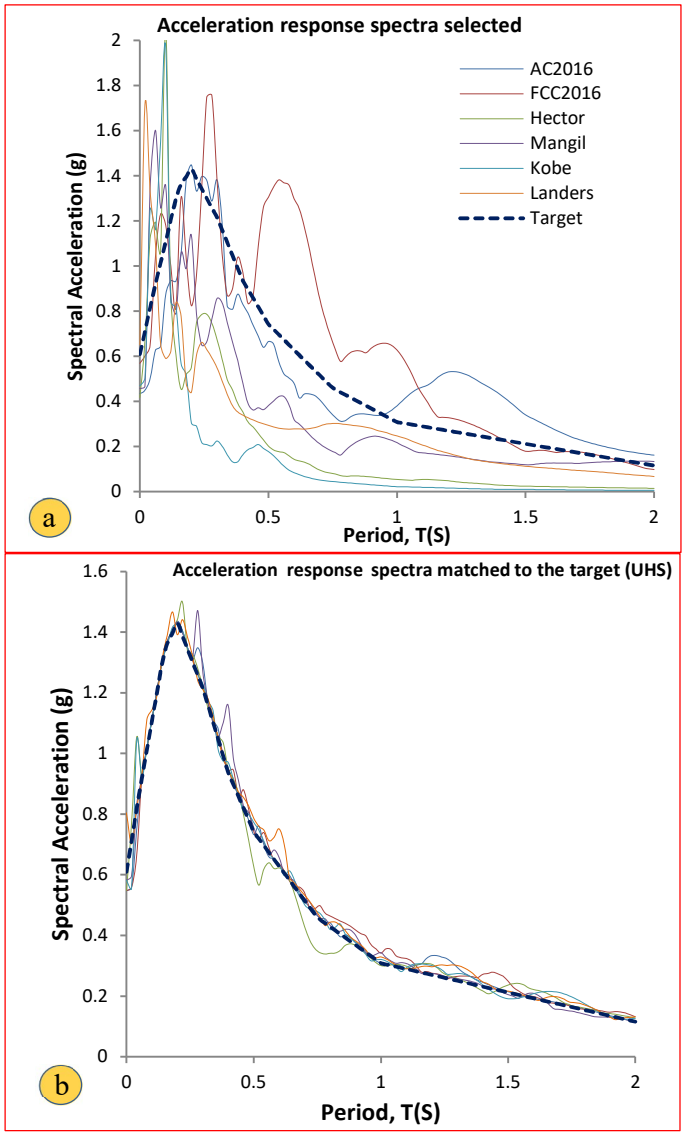

Figure 6.46: Acceleration response spectra of various earthquakes selected for time history analysis with UHS of Tendaho dam site for 10,000 years return period: a) response spectra of acceleration records, b) response spectra after matching with the target spectrum (UHS).

By checking the significant peaks and desired aspects of the ground motion were not altered too much, the acceleration time histories of three recoded earthquakes were selected and used for the dynamic dam stability analysis (Table 6.15 and Fig. 6.47).

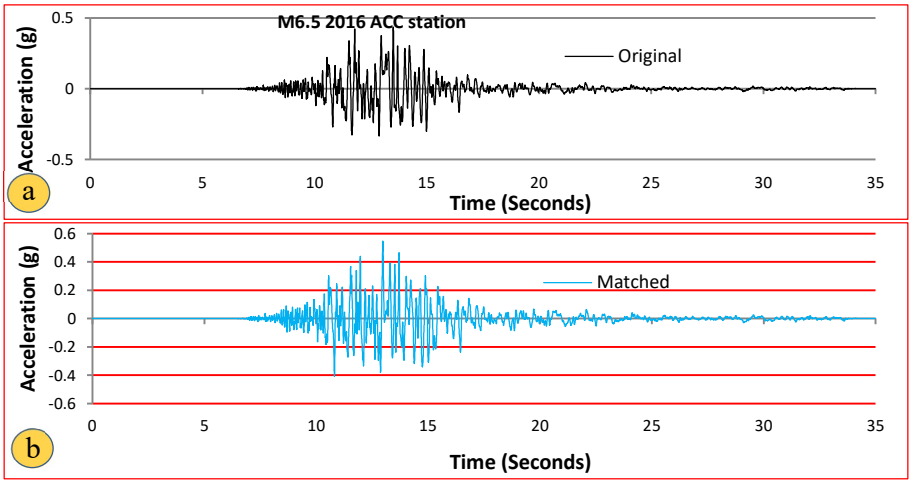

Figure 6.47: Comparison of pre (a) and post (b) spectral matching of acceleration time history for Mw 6.5 2016 Central Italy earthquake (recorded at ACC station) with Tendaho dam site 10,000 years return period uniform hazard spectrum (horizontal component).

6.7.5 Analysis of Fault Displacement in Dam Footprint

Faults with surface breaking capability crossing the dam site and potential block movements are the main points of interest for the safety of dams subjected to strong earthquakes (Wieland, 2013). From the structural geological data analysis, critical faults which pass through the dam and spillway foundation and abutments slope have been identified (Fig. 6.48). Images taken prior to the construction of the dam along with 5 m resolution SPOT images show fault lines that pass through the foundation of the dam and the spillway. The geophysical investigation during the design stage also confirms the presence of two faults in the dam foundation. The spillway is crossed by two faults that trend NNE-SSW and NNW-SSE following the Main Ethiopian and Red Sea trends, respectively. These faults were identified at an early stage of investigation. Faults crossing the dam site are evaluated for the maximum size of fault movements, as the size expresses its damaging potential.

The empirical correlations, developed by Wells and Coppersmith (1994) were used. The maximum fault displacement has been calculated for each fault shown in Fig. 6.48. The key element to be considered in the design of the dam is the shearing by

foundation fault rupture. It is important that the filter remains functional after offset and distortion to prevent internal erosion.

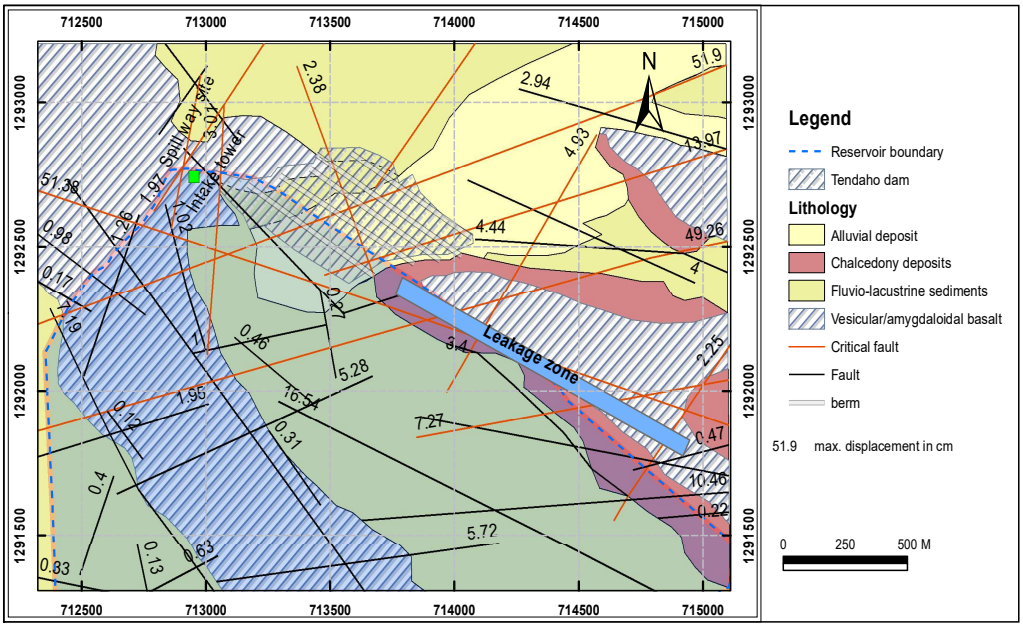

Figure 6.48: Critical faults passing through the dam and spillway foundation, abutment slopes and reservoir rim slopes with maximum displacement calculated for each faults.

6.7.6 Seismic Analysis of Dam Body with Equivalent Linear Method

The two-dimensional (2D) dynamic analysis of Tendaho dam was conducted for the maximum cross-section of the dam. The earthquake analysis is carried out using a plane strain model and the equivalent linear analysis concept with shear strain-dependent material properties to estimate deformations of the dam subjected to the ground motions of the SEE with 10,000 year return period and tectonic fault displacement.

6.7.6.1 Dam Zoning Used for Stability Analysis

The material used in different zones of Tendaho dam and the main features of the dam are given in Fig. 6.49.

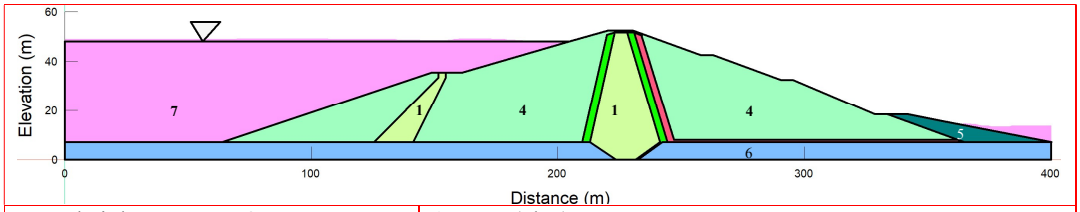

Max. height	53 m
Crest Length	412
Dam volume	1.96 Mm3
Crest Width	10 m
Full Supply level	408 m
MWL (10,000)	410.8 m
Dam Crest	413.5
U/S slope	2.75:1
D/s slope	3:1
Storage	1.86 km3

1. Core (clay)
2. F1- filter (sand)
3. F2- transition (gravel)
4. Shell (silt, sand and gravel)
5. Rockfill (cobble and boulder)
6. Foundation (lake sediment: siltstone, mudstone and sandstone)
7. Reservoir water

Figure 6.49: Maximum cross-section of Tendaho dam showing main features and material zoning

6.7.6.2 Static Deformation and Stress Analyses

The deformation analysis under static loading for Tendaho dam was carried out by the computer program SIGMA/W (GEO-SLOPE International Ltd., 2019) using the Mohr-Coulomb elasto-plastic model. The material properties in different zones and used for static deformation are obtained from the design report and other similar projects (Table 6.16).

Table 6.16: Material properties used for static deformation and stress analyses (v: Poisson's ratio, E: modulus of elasticity, U: weight density, C': cohesion, Φ': friction angle, K: permeability)

Material Description	v	E (MPa)	U(kN/m3)	C' (kPa)	Φ'	K (cm/s)
Clay core	0.4	20	16.0	7	25	$1x10^{-8}$
F1- filter (sand)	0.3	40	18.5	0	35	$1x10^{-2}$
F2- transition (gravel)	0.3	50	19.0	0	34	$6x10^{-2}$
Shell (silt, sand and gravel)	0.3	30	18.5	0	35	$1.2x10^{-7}$
Rockfill (cobble and boulders)	0.3	60	22.0	0	40	$1x10^{-1}$
Foundation	0.3	3,000	23.0	200	45	$1x10^{-5}$

The static loads considered in the analysis are gravity load and water load. The water load was applied as hydrostatic pressure acting on the upstream face of the core. The contour plot of the vertical stress due to gravity load is shown in Fig. 6.50.

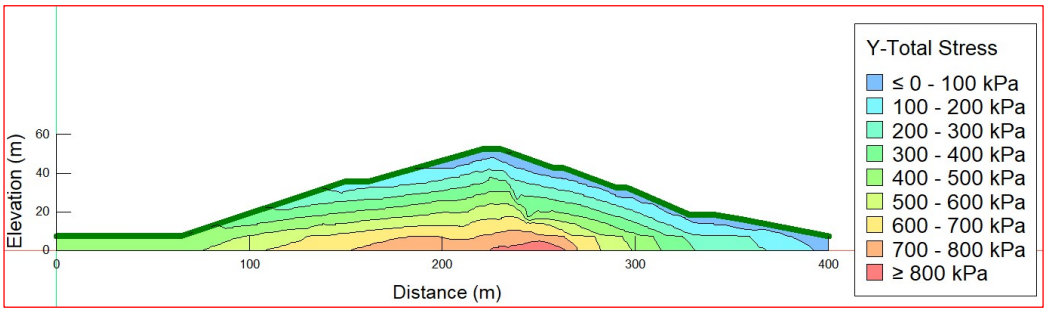

Figure 6.50: Contour plot of vertical stress from gravity load (dam body); maximum vertical stress in dam body: 860 kPa

6.7.6.3 Dynamic Material Properties

The dynamic material properties required for the earthquake response analysis are the dynamic shear modulus and the damping ratio; both are given as functions of the dynamic shear strain. The dynamic shear modulus G is usually given in the form of the shear strain-dependent ratio G/G_{max} (reduction function) where G_{max} is the maximum dynamic shear modulus. The material parameters used for the earthquake analysis of the dam by the equivalent linear method are obtained from the Tendaho design report, literature review and other dam projects and are given in Table 6.17.

Table 6.17: Dynamic material properties in different zones of Tendaho dam (K2max: material constant, v: Poisson‘s ratio).

Material	K_{2max}	v	Modulus reduction (G/G_{max})	Damping	Material model
Impervious clay core	40	0.40	1*	2*	Non-linear
F1-filter sand	60	0.30	3*	3*	Non-linear
F2-transition gravel	50	0.30	4*	4*	Non-linear
Shell gravel	80	0.30	4*	4*	Non-linear
Rockfill	50	0.30	4*	4*	Non-linear
Alluvial Foundation	70	0.30	4*	4*	Non-linear

1* Modulus reduction curve for clay (Sun and others, 1988)

2* Damping ratio relationship for clay (Vucetic and Dobry, 1991)

3* Average relationship for sands by Seed and Idriss, 1970

4* Properties for gravel by Seed et al., 1984

6.7.7 Earthquake Response Analysis

The dynamic response of the maximum dam cross-section subjected to the SEE ground motion was carried out using the equivalent linear method (Seed and Idriss, 1970). The method consists of an iterative computational process to adjust the damping ratio and the dynamic shear stiffness of each finite element until the dynamic properties are compatible with the dynamic shear strains. This method is extensively used in practice for the dynamic analysis of embankment dams. The 2D earthquake response analysis was carried out for the SEE ground motion only.

In the dynamic analysis, the horizontal and vertical acceleration time histories were applied at the base of the model. The acceleration response spectrum of the vertical component is taken as 2/3 of that of the horizontal component. The boundary condition is fixed at the base and the horizontal direction is fixed in the two vertical foundation boundaries. The dynamic analysis was carried out by QUAKE/W computer program, (GEO-SLOPE International Ltd., 2019). The main characteristics of these earthquakes are presented in Table 6.15.

The contour plots of the absolute maximum horizontal and vertical accelerations in the dam body are shown in Fig. 6.51. The maximum absolute horizontal crest acceleration due to the SEE excitation is about 1.49 g (Fig. 6.52).

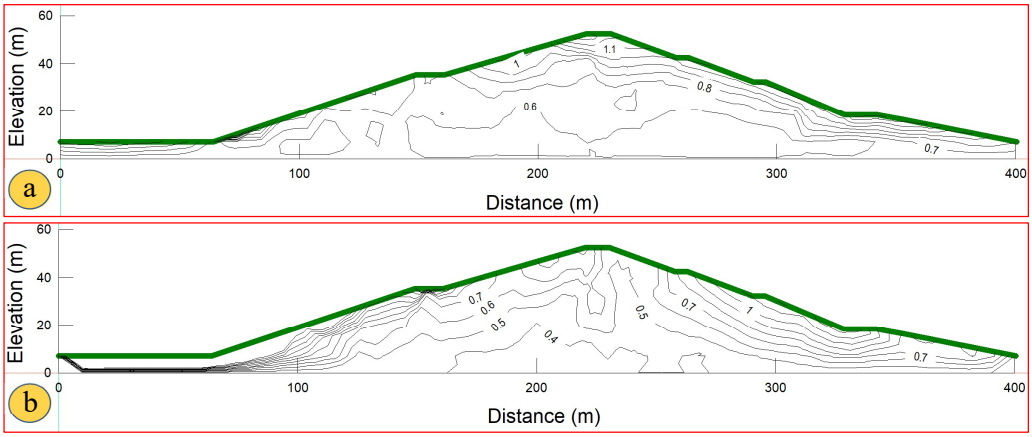

Figure 6.51: Contour plots of absolute maximum horizontal (top) and vertical (bottom) accelerations in dam body (SEE of 10,000 years return period): peak maximum horizontal and peak vertical accelerations 1.49 g and 1.23 g, respectively.

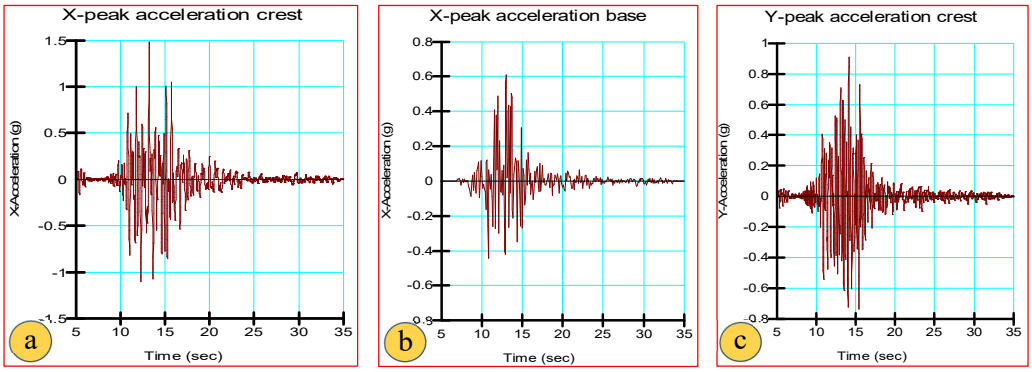

Figure 6.52: Acceleration time histories in the dam body: horizontal acceleration at crest (left), horizontal acceleration at the base (middle) and vertical acceleration at crest (right) for SEE of 10,000 return period.

6.7.8 Dynamic Slope Stability Analysis

The shear strength parameters used for the dynamic slope stability analysis of Tendaho dam are given in Table 6.18. For the dynamic stability analysis of a potential sliding mass of the dam, its yield acceleration is determined first (0.27 g downstream critical slope and 0.18 g upstream critical slope). The main results of Newmark's sliding block analysis are shown in Fig. 6.53.

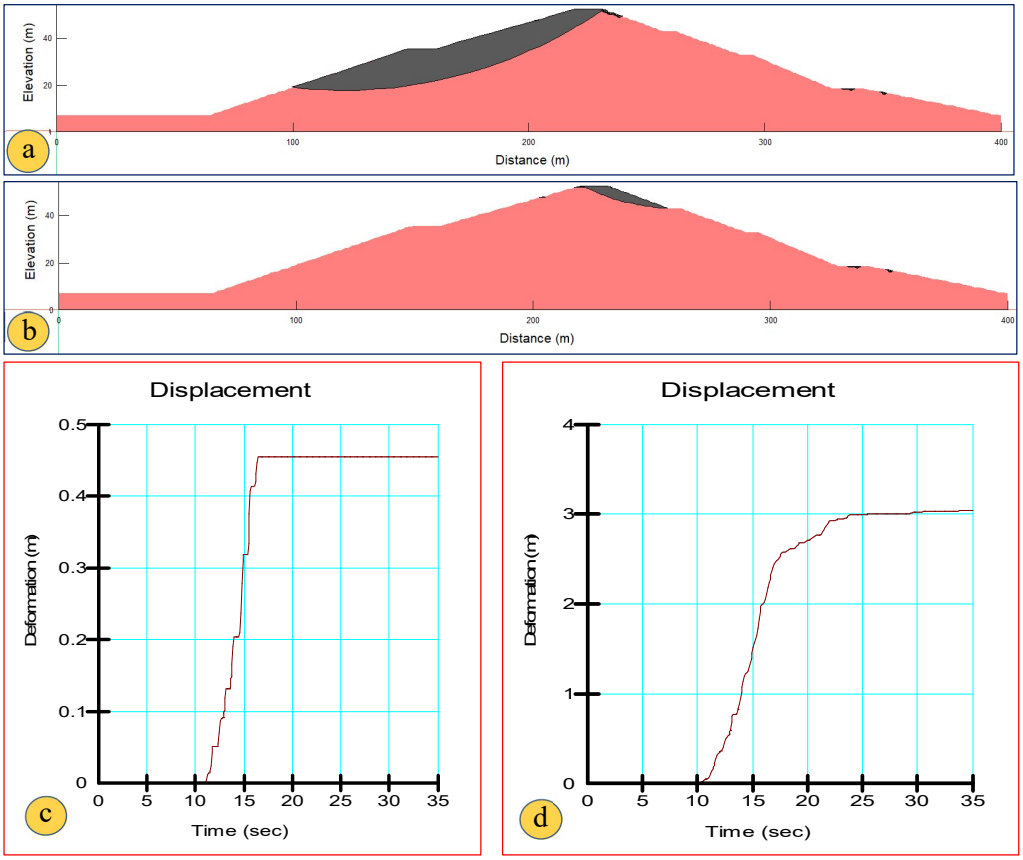

Figure 6.53: Newmark sliding block analysis results of Tendaho dam for SEE (Central Italy earthquake acceleration time history, ACC station): (a) critical downstream slope (yield acceleration: 0.27 g), (b) critical upstream slope (yield acceleration: 0.18 g), (c) displacement time history of critical downstream slope, and (d) displacement time history of critical upstream slope.

Table 6.18: Material properties for dynamic slope stability analysis

Description	Weight density γ (kN/m3)	Cohesion C' (kPa)	Initial friction angle Φ′$_o$ (º)	Friction angle reduction Δ Φ′ (º)
Clay core	18	7	25	0
F1- filter (sand)	18	0	35	3
F2- transition (gravel)	23	0	34	3
Shell (silt, sand and gravel)	23	0	35	4
Rockfill (cobble and boulders)	22	0	40	2
Foundation	21	200	45	0

6.7.9 Seismic Settlement and Loss of Freeboard Evaluation

Estimate of loss of freeboard for Tendaho dam due to seismic sliding displacements of the critical downstream and upstream slopes was evaluated. During the SEE the upstream and downstream movements occur at different times and are assumed to have a cumulative effect on the vertical displacement of the crest. Therefore, the total reduction of the freeboard because of SEE induced sliding displacements is obtained as the sum of the vertical projections of the sliding movements of the two critical slopes.

The total vertical movement due to slope movements is 95 cm which is the sum of the two vertical components, i.e. 78 cm (upstream) and 17 cm (downstream) slopes. The crest settlement due to densification can be determined using the empirical method by Bureau (1997), which results in a settlement of about 0.8% of the dam height, therefore, a seismic settlement of 42 cm has been estimated for the 53 m high dam. A maximum vertical fault displacement of 52 cm is obtained from the fault passing through the dam foundation.

The maximum crest settlement of the dam is 1.89 m which is 95 cm due to slope movement, 42 cm due to material densification, and 52 cm due fault displacement in the footprint of the dam. The 3 m freeboard provided for Tendaho dam is adequate to cope with the SEE ground motions with respect to overtopping.

6.7.10 Earthquake Safety

The dynamic analyses results of Tendaho are discussed as follows. The maximum absolute horizontal crest acceleration due to the SEE ground motion is 1.49 g. The dynamic slope stability calculations show that the maximum crest settlement resulting from the sliding of the critical masses at the upstream and downstream dam faces induced by the SEE ground motion is about 95 cm. The settlement resulted from earthquake vibration-induced densification of the dam body is estimated as 42 cm, using Bureau's empirical method. The settlement due to the vertical component of fault displacement in the footprint of the dam is about 52 cm. Therefore, the total loss

of freeboard for the combined worst case earthquake scenario (SEE of 10,000 years return period) is estimated as 1.89 m. The results of the dynamic stability analysis show that the dam is safe against overtopping during and after the SEE with a horizontal PGA of 0.61 g due to 3 m free board provided. However, from observed performance of the dam under normal operational condition with leakage in the foundation and dam contacts with the foundation and abutment slopes, there will be possibility of an increase in leakage due to the SEE, which may lead to dam failure due to internal erosion.

6.7.11 Conclusions

Tendaho dam site is located within the Afar Triangle, a tectonically active region in Ethiopia. The area has experienced damaging earthquakes in the recent past. Among these, the Serdo earthquake of 1969 and Dobi earthquake of 1989 with magnitudes of 6.1 and 6.3, respectively. The earthquake safety of Tendaho dam is very important because failure of such a structure may have disastrous consequences on life, property and economic activity in the downstream region of the dam. The updated seismic hazard studies carried out for the dam show that the dam can be subjected to stronger ground shaking (horizontal PGA of 0.61 g) than assumed during the original design phase (0.3 g) and the movements of faults and along other discontinuities in the footprint of the dam, spillway foundation and abutments slopes are possible during strong earthquakes. Furthermore, there is a high seepage risk along major tectonic fractures/faults following strong earthquake in the region.

Based on the present (updated) seismic hazard analysis results, the dynamic response of Tendaho dam is checked for the maximum cross-section of the dam subjected to the SEE ground motion. The dynamic analysis of the dam body is carried out using the equivalent linear analysis method. The results of the analyses show that the maximum loss of freeboard of 1.89 m due seismic actions can be accommodated by the available freeboard of 3 m, and therefore no overtopping has to be expected. However, piping through the foundation and erosion along the dam-abutment contact may be possible. Based on the current updated assessment it is recommended to

investigate methods for reducing the seepage in the dam foundation and the highly fractured abutments, and along the fault and shear zones. Furthermore, strong motion instruments should be installed in the dam body and the spillway. In addition, dam break analysis should be done and an early warning system (water alarm) should be considered.

6.8 Seismic safety evaluation of Tekeze Arch Dam

6.8.1 Introduction

Tekeze dam is the highest arch dam in Africa with the height of 188 m, crest length of 460 m and reservoir volume of 9,310 Mm^3 (Fig. 6.54). It is a double-curvature arch dam constructed on the Tekeze River, a tributary of the Nile, the longest river in the world. The main purpose of the dam is for power generation with installed capacity of 300 MW. The construction of the dam was completed in 2009. The dam site is at close distance to the seismically active East African Rift. Based on topographic study conducted at various dam sites and site assessment made during the present work, Tekeze dam site is located in mountainous terrain where earthquake triggered mass movements into the reservoir are possible.

Figure 6.54: View of downstream face of Tekeze arch dam with four orifice spillways

Many dams have been constructed in steep mountainous terrain where landslides can occur. Seismic activity is one of the major causes of landslides (Tiwari and Ajmera 2017). Most large and even moderate earthquakes trigger landslides, and these landslides may account for a significant portion of total earthquake damage in that region (Janusz et al. 2000). Furthermore, the effects of earthquake on slope stability are not only limited to the period of strong shaking but also have long-term consequences on slope stability. The Mw 7.8 Peru earthquake of 1970 triggered a

huge rock avalanche that killed at least 18,000 people (Janusz et al. 2000). The M8.3 Alaska earthquake of 1964 triggered numerous large landslides that caused widespread damage to buildings and infrastructure. The Mw 8.1 1989 Loma Prieta earthquake, the 1994 Northridge earthquake and the 1999 Taiwan earthquake triggered many landslides over a large area that caused massive damage. The 1961 Mw 6.3 Kara Kore earthquake recorded in the Rift Escarpment of Ethiopia has also caused several landslides (Gouin 1979).

Landslides, if large enough, can affect the safety of a dam or reservoir operation if they fail or move. Attention for reservoir slope stability started following the catastrophic event at Vajont dam of October 9, 1963 in Northern Italy that led to the loss of more than 2000 human lives in the downstream area of the dam. According to ICOLD (2002), the volume of landslide was more than 270 Mm^3 with sliding velocity up to 30 m/s. This landslide caused a huge impulse wave that overtopped the dam by more than 100 m.

During the 2008 Iwate-Miyagi earthquake (Mw 6.9) that struck the northern part of Japan, there was a massive landslide with slope length of 1.3 km, width of 0.9 km and a volume of 67 Mm^3, which occurred near Aratozawa Dam (Midorikawa et al. 2008). The portion of mass with volume of 1.5 Mm^3 moved into the reservoir causing a seiche that overtopped the spillway. The dam suffered only slight damage and the reservoir level was raised by 1.5 m (Matsumoto et al. 2011).

The above indicated earthquakes events have demonstrated that mass movement into the reservoir is one of the major hazard during major earthquake even more severe than ground shaking in some cases. In this regard, the Tekeze dam site is one of the dam site located in mountainous terrain and mass movements into the reservoir are possible during major earthquake in the region. Various small size landslides were also previously reported in the reservoir slopes under normal operational condition. In addition, the seismic hazard assessment result used for the design of the dam underestimated the seismic hazard and did not take into account reservoir slope stability under earthquake loading and potential impacts on the dam.

The present study is concerned with the seismic hazard evaluation at Tekeze dam site with particular emphasis on mass movement into the reservoir and the impulse wave that can be generated. For this purpose, the following tasks were carried out:

I. Identification of seismotectonic setup and landslide hazard at the dam site,
II. Site-specific seismic hazard evaluation based on probabilistic approach,
III. Stability analysis of abutment and reservoir slopes under static and earthquake loading conditions, and
IV. Analysis of impulse waves generated by earthquake triggered mass movement into the reservoir and possible risks on the safety of the dam.

6.8.2 Geology and Tectonic Background

The rocks at the dam site and reservoir area are Precambrian basement rocks, which comprise ancient meta-sediments, predominantly microcrystalline/crystalline limestones and sandstones that have been subject to tectonic deformations. The limestones are in a near vertically bedded and laminated series varying slightly in degree of crystallization, grain size, and texture. The most prominent of the discontinuities are the bedding and the stress relief joints parallel to the valley sides and affect the stability of valley side.

The tectonic features of the Tekeze dam site and reservoir area are taken into account in the slope stability analysis. Structural mapping conducted during the design stage showed that the dam site and the reservoir area are significantly affected by tectonic fractures and faults (Figs. 6.55 and 6.56). The faults are mainly, normal and strike slip faults. There are no tectonic faults passing through the dam foundation. However, there are slope instability problems that have been reported by previous works (Hailemariam, 2009).

6.8.3 Seismic Hazard Situation and Previous Studies

6.8.3.1 Seismotectonic Background

The regional geological structure that may influence the seismic hazard situation at Tekeze dam site has been reviewed. The reservoir area is structurally cut by a significant fault system and the eastern part is bounded by the East African Rift Margin which can generate significant earthquakes.

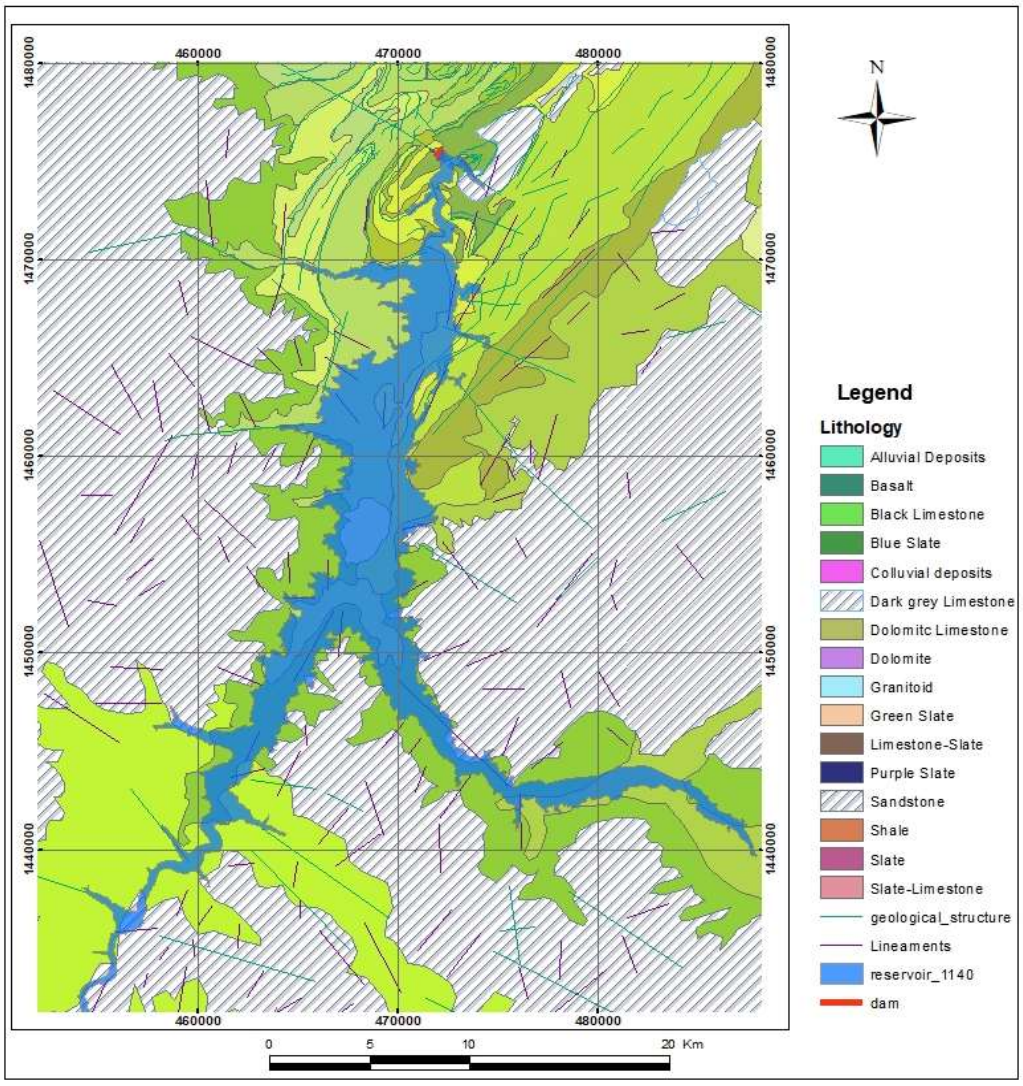

Figure 6.55: Geological and structural map of Tekeze dam and reservoir area

6.8.3.2 Seismic Activity in the Region

The seismicity at Tekeze dam site is controlled by the hazard from three seismogenic source zones. These are Escarpment, Afar Depression and Eritrea in order of their significance (Fig. 59). The earthquakes in the region are characterised by shallow depth of less than 30 km and intermediate magnitude. The Escarpment seismogenic zone is one of the most seismically active zones in Ethiopia, characterized by nearly N–S running faults.

Figure 6.56: View of reservoir from crest of Tekeze dam

The 1961 Kara Kore earthquake of M 6.3 is one of the major earthquakes in this region which caused significant damage. The epicentre of the main shock of the 1961 Kara Kore earthquake is about 280 km away from the Tekeze dam site.

6.8.3.3 Previous Seismic Hazard Study

At the design stage, the seismic hazard study for Tekeze dam site was conducted based on the deterministic approach. The estimated peak ground accelerations for

different return periods are given in Table 19 (EEPCO 1997). These values are very small. The absolute minimum PGA-value that should be used for dams is 0.15 g, which corresponds roughly to a seismic coefficient of 0.1. This seismic coefficient was used universally for the seismic design of dams since the 1930s almost irrespective of the often unknown seismic hazard at the dam site. Therefore, today, we should not use seismic hazard values that are lower than those used in the past for large dams.

Table 6.19: Peak ground acceleration values used for the design of Tekeze Dam (EEPCO 1997).

Design Earthquake	Peak Ground Acceleration	Return Period
OBE	0.01 g	145 years
MDE	0.02 g	975 years
MCE	0.03 g	10,000 years

6.8.4 Seismic Hazard Analysis

The present site-specific seismic hazard evaluation for Tekeze dam site was carried out to check the level of seismic hazard at the dam site. The main hazards considered were ground shaking hazard and mass movement into the reservoir. The ground motion parameters were calculated based on a probabilistic approach. Based on the ground motion parameters obtained from the seismic hazard analysis, the slope stability of the reservoir rim was assessed for the safety evaluation earthquake ground motion.

6.8.4.1 Probabilistic Ground Motion Estimation

The probabilistic seismic hazard analysis was performed using the Crisis 2018 seismic hazard analysis program following the procedures discussed under chapter 4. To account for site effects in the seismic hazard analysis, seismic refraction surveys were carried out in the right abutment. From the survey results the shear wave velocity of 1000 m/s was used as a representative value for Vs30 in the attenuation

models. From the seismic hazard analysis, the peak ground acceleration (PGA) of the horizontal earthquake component on rock outcrop was obtained for the following return periods: 145, 475, 1000, 2500, 5000 and 10,000 years. The Ethiopian Rift Escarpment seismic source zone mainly controls the seismic hazard at Tekeze dam site, with some contribution from the Afar Depression and minor contribution from Eritrea and Red Sea rifts in order of their significance due to attenuation of ground motion with distance from the sources at the dam site.

6.8.4.2 Slope Stability under Seismic Action

The stability of rock slopes is mainly governed by the geometry of the slope, discontinuity orientation, the shear strength parameters (cohesion (C) and angle of internal friction (φ) of the discontinuity planes) and water saturation conditions. Rock slopes falls in different forms whether it is under static or dynamic loading. Among the failure modes in rock slopes, the slope having plane mode of failure may easily destabilize under seismic loading. This commonly occurs in stratified layers when a discontinuity plane dips or daylights towards the valley at an angle lower than the slope angle and greater than the angle of friction of the discontinuity plane (Raghuvanshi 2017) (Fig. 6.57).

In the present study, the seismic stability of the slopes of the Tekeze reservoir was analysed. For this work, primary data were collected from the field and secondary data such as the topography of the area, the geometry of the slopes, structural discontinuities present in the rock mass and geotechnical properties of the rock mass were compiled from various sources. Eighteen potential slopes located up to 20 km upstream from the dam were checked whether the stability under kinematic condition is satisfied or not. For kinematically unstable slopes, the slope angle must be greater than the dip angle of the discontinuity/failure plane and the dip angle of discontinuity/failure plane must be greater than the angle of internal friction (i.e. αf>αp>F in Fig. 6.57). Based on this preliminary assessment, half of the slopes in the reservoir are found stable and excluded from the seismic stability analysis.

For the remaining nine slopes that are found unstable during the initial assessment, detailed stability analyses were worked out. These include stability analysis of the slope under static and dynamic loads and normal reservoir level. The following water contents were considered: dry, moderately saturated, and fully saturated. The modified technique of plane failure mode analysis proposed by Sharma et al. (1995) was used for the stability evaluation.

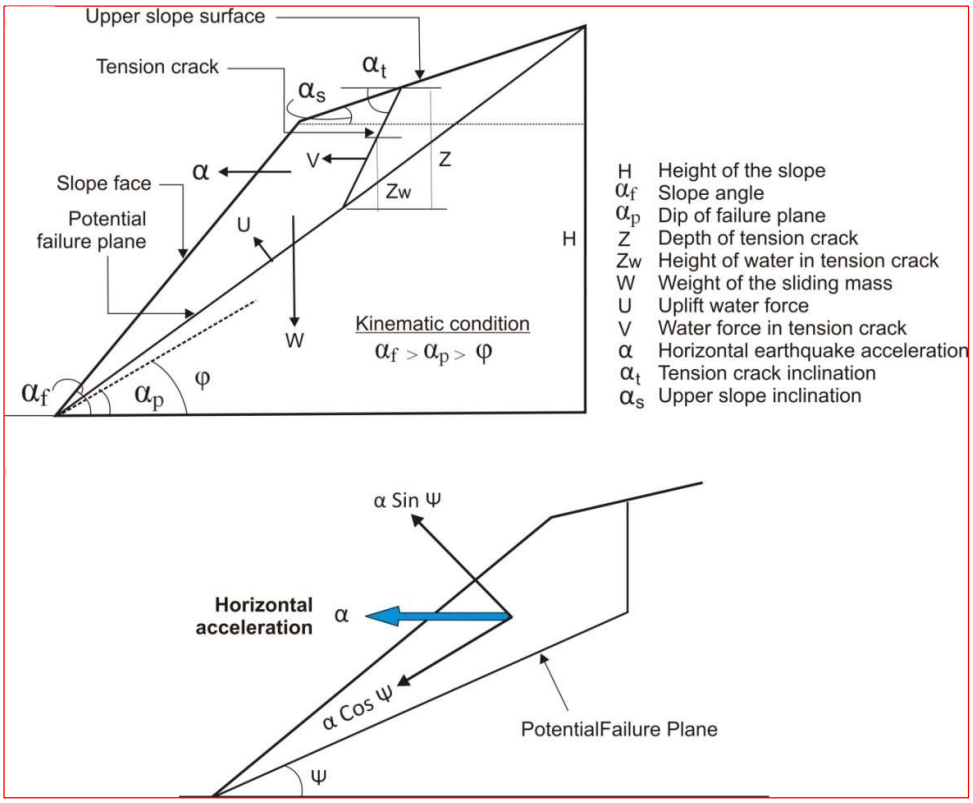

Figure 6.57: Sketch showing kinematic condition for plane mode of failure (top) and horizontal acceleration acting in center of gravity of sliding wedge (bottom) (Raghuvanshi 2017).

6.8.4.3 Impulse Wave Generation

Among the existing dam sites in Ethiopia, Tekeze dam is more prone to landslide-triggered impulse waves because of steep reservoir boundary, narrow reservoir geometry, possible large slide masses, and high impact velocities. Landslide-generated wave affects the safety of the downstream population when the dam will be overtopped.

Table 6.20. Main input data used for impulse wave analysis in Tekeze reservoir

Slope ID	$\forall_s$ [m3]	vs [m/s]	s [m]	b1 [m]	α [°]	h1 [m]	h2 [m]
TRS4	46.653	8.80	140	336	65	112	140
TRS7	36,503	6.00	55	525	30	105	140
TRS8	39,215	7.00	49	875	41	100	140
TRS10	26,349	17.00	83	700	48	90	140
TRS14	79,395	11.00	158	2150	55	95	140
TRS15	48,346	8.00	49	2100	46	90	140
TRS16	33,958	12.30	88	2400	50	80	140
TRS17	29,385	15.00	72	2334	44	70	140
TRS18	23,414	17.00	60	2900	40	60	140

b1 – reservoir width at impact point, h1 – water depth at landside point, h2 – water depth at impact point, s – slide thickness, $\forall_s$ - slide volume, vs - slide impact velocity, α - slide impact angle

Based on the review of existing methods on impulse wave generation, the simplified equations given by Heller (2007) (Fig. 6.58) and Muller (1996) were used in the present assessment.

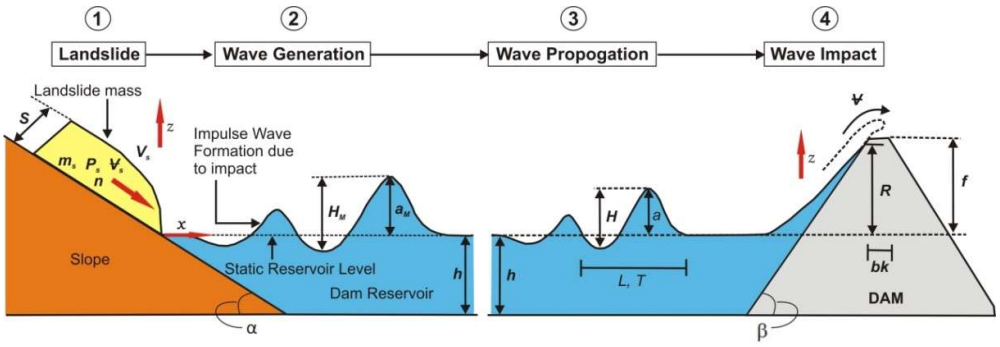

Figure 6.58: Sketches defining the most important impulse wave parameters. 1. Earthquake induced landslide (slide thickness(s), slide volume(Vs), slide impact velocity($\forall_s$), slide impact angle(α), slide density(ρ), slide porosity(n)) 2. Impulse wave generation (still water depth (h1), wave max. amplitude (HM) 3. Wave propagation (wave amplitude (a), wave length (L), wave period (T) 4. Wave impact (wave run-up(R), run-up angle (β), free board (f), crest width (b_k) and dam overtopping (V)) (after Heller 2007).

The landslide is modelled as a solid mass and three-dimensional (3D) free radial propagation of the impulse wave was considered for estimating the wave generation and wave propagation parameters. The parameters controlling the impulse waves on dams such as the wave height, wave amplitude, wave period and wave length were computed using equations of Heller (2007). The run-up height was computed according to Muller (1995) using the spread sheet program developed by Heller et al.

(2009). The main input data sets used for the analysis of wave run-up are given in Table 6.20.

6.8.5 Results and Discussion

6.8.5.1 Seismic Hazard Analysis Results

Tekeze dam must be able to withstand the effects of the ground motion of the safety evaluation earthquake (SEE), which has a return period of 10,000 years according to ICOLD (2016). The safety-critical elements such as bottom outlets, spillway gates, power supply and related control units must also be able to withstand the ground shaking of the SEE. According to the results obtained in the present hazard analysis for Tekeze dam site, the PGA-values of the horizontal earthquake component on the outcropping rock for different return periods are as follows: 0.06 g (145 years), 0.10 g (475 years), 0.138 g (1000 years), 0.184 g (2500 years), 0.224 g (5000 years) and 0.265 g (10,000 years). Tekeze dam should be designed for the SEE ground motion with a return period of 10,000 years, and a PGA of 0.265 g of the horizontal earthquake component.

For the Operating Basis Earthquake a return period of 500 years is advisable, which is equivalent to a PGA of 0.10 g. The PGA-values of 0.03 g obtained for MCE in the previous seismic hazard assessment report (Table 1) corresponds to a return period of less than 100 years as per the current seismic hazard analysis and is far below current seismic safety requirements for the dam. Therefore, the dynamic response of the dam and appurtenant structures must be rechecked for the increased level of ground motion.

The results of the PSHA are also given in terms of uniform hazard spectra for 5% damping for various return periods (Fig. 6.59 and Table 6.21). Furthermore, a deaggregation analyses was done to identify the magnitude and distance of seismic events with the greatest contribution to the seismic hazard.

As in the slope stability analysis only the horizontal earthquake component is used, therefore the PSHA is also only concerned with the horizontal earthquake component. However, for the dynamic analysis of the arch dam, which is best done by direct time integration, all three earthquake components are required. For that purpose, the earthquake input is required in the form of acceleration time histories. A discussion of how these time histories can be obtained from the acceleration response spectra is given in ICOLD (2016).

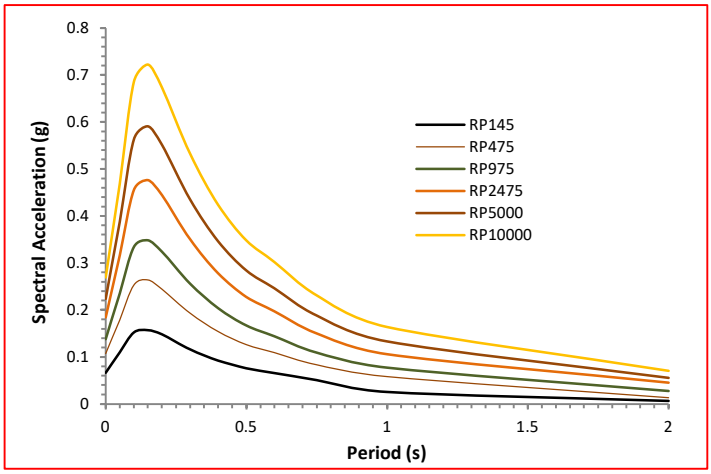

Figure 6.59: Uniform hazard spectra for various return periods for Tekeze dam site for horizontal earthquake component on outcropping rock and 5% damping (RP- return period)

Table 6.21: Spectral accelerations in percentage of g for different structural periods and earthquake return periods (horizontal EQ component on outcropping rock and 5% damping).

Structural period in seconds	Return period in years					
	145	500	1000	2500	5000	10,000
0.00	0.066	0.107	0.138	0.184	0.224	0.265
0.05	0.110	0.179	0.235	0.316	0.388	0.469
0.10	0.152	0.253	0.334	0.455	0.563	0.685
0.15	0.157	0.264	0.348	0.476	0.591	0.722
0.20	0.148	0.244	0.324	0.444	0.551	0.673
0.30	0.116	0.193	0.256	0.350	0.435	0.532
0.40	0.093	0.154	0.204	0.278	0.346	0.424
0.50	0.076	0.126	0.167	0.228	0.284	0.348
0.60	0.066	0.109	0.144	0.197	0.246	0.302
0.75	0.051	0.083	0.109	0.150	0.188	0.231
1.00	0.026	0.058	0.077	0.106	0.133	0.164
2.00	0.007	0.013	0.027	0.045	0.056	0.070

6.8.5.2 Slope stability Analysis Result during Earthquake

The slopes which are stable under static conditions may become unstable under seismic loading. The rock slopes under earthquake loading are subjected to accelerations which induce inertia forces and instability in the slope. For the seismic slope stability analysis, a conventional pseudo-static procedure was used with a horizontal peak ground acceleration of 0.265 g corresponding to the SEE.

The results of the slope stability analysis given in Table 6.22 show that most of the slopes are unstable under fully saturated or seismic condition and stable under dry or moderately saturated static condition. A factor of safety of less than one represents instability or failure.

6.8.5.3 Impact of Landslide-triggered Impulse Wave

Impulse waves generated by mass movements into the reservoir during earthquake may cause damages during run-up against dams. Particularly embankment dams may suffer serious damage or even fail completely due to overtopping and crest erosion. Based on the analysis of landslide-triggered impulse from potentially unstable slopes under earthquake loading, the maximum wave run-up was calculated. The result shows a maximum wave height and wave run-up between 0.4 to 2.1 m and 0.3 to 2.3 m, respectively (Table 6.23).

Table 6.22: Summary of slope stability analysis results

Slope ID	Weight of sliding mass (MN)	Surface area of failure plane (m^2)	Factor of Safety under different conditions			
			Conditions	Dry	Moderately Saturated	Fully Saturated
TRS4	1213	334	Static	1.81	1.12	0.37
			Dynamic	1.01	0.61	0.16
TRS7	964	662	Static	1.25	1.02	0.75
			Dynamic	0.65	0.51	0.37
TRS8	1051	472	Static	1.95	1.54	1.03
			Dynamic	1.02	0.80	0.55
TRS10	593	396	Static	1.00	0.62	0.23
			Dynamic	0.58	0.34	0.09
TRS14	1913	502	Static	2.00	1.45	0.80

			Dynamic	1.02	0.75	0.43
TRS15	1190	468	Static	1.42	1.07	0.66
			Dynamic	0.72	0.54	0.35
TRS16	863	384	Static	1.41	1.00	0.53
			Dynamic	0.79	0.56	0.29
TRS17	742	409	Static	1.43	1.06	0.62
			Dynamic	0.77	0.56	0.33
TRS18	591	392	Static	1.46	1.04	0.57
			Dynamic	0.81	0.56	0.28

The maximum wave run-up under the worst earthquake loading can be accommodated by the freeboard allowance of 5 m adopted in the design. Accordingly, there is no overtopping risk of the dam crest from landslides triggered by the worst earthquakes.

Table 6.23: Summary of results of impulse wave run-up analysis

Slope ID	Wave Height (m)	Wave Amplitude (m)	Run-up Height [m]
TRS4	2.1	1.7	2.3
TRS7	1.2	1	1.2
TRS8	0.7	0.6	0.7
TRS10	1.7	1.4	1.8
TRS14	1.7	1.4	1.7
TRS15	0.7	0.5	0.6
TRS16	0.8	0.6	0.7
TRS17	0.8	0.6	0.7
TRS18	0.4	0.3	0.3

6.8.6 Conclusions

Tekeze dam is located close to the Escarpment seismogenic source zone, which is one of the most seismically active zones in Ethiopia and characterized by nearly N–S running normal faults. The 1961 Kara Kore earthquake (M 6.3) is one of the major earthquakes in this region that caused significant damage in Ethiopia. The structural and topography analysis of the dam site and its reservoir area shows that the dam site and reservoir area are affected by tectonic faults. Moreover, steep slopes and older

landslides are also present that can affect the stability of the dam abutments and reservoir rim slopes.

Tekeze dam is the highest arch dam in Africa. The dam must be able to withstand the effects of the ground motion of the safety evaluation earthquake, which has a return period of 10,000 years according to ICOLD (2016). The present study shows that the dam can be subjected to significantly stronger ground shaking than assumed at the design stage. In addition, movements of faults and along other discontinuities in the abutments slopes can take place during strong earthquakes.

Furthermore, earthquake triggered landslides into the reservoir are possible, which may create impulse waves. However, the result show that the maximum wave run-up under worst earthquake action can be accommodated by the freeboard allowance of 5 m adopted in the design. As a result, there is no overtopping risk expected from landslide generated impulse waves in the reservoir.

Based on the present seismic safety assessment results, it is recommended that the dynamic response of the dam and appurtenant structures must be rechecked for the increased level of earthquake ground motion. As in the slope stability analysis only the horizontal earthquake component is used, therefore the PSHA is also only concerned with the horizontal earthquake component. However, for the dynamic analysis of the arch dam, which is best done by direct time integration, the acceleration time histories of all three earthquake components are required as input.

Chapter 7

7 General Conclusions

The specific conclusions are given in all main chapters and in Chapter 6, conclusions are also provided for each of the five dams. Therefore, these conclusions are not repeated in this Chapter. The objectives of this Chapter are (i) to give general conclusions, which are applicable to all dams in Ethiopia and (ii) to give a number of recommendations that shall be followed by all parties involved in the seismic safety of dams in Ethiopia.

Ethiopia has over 100 large storage dams and more are presently under construction and design. Earthquake hazard is one of the major safety concerns for these dams due to the seismically active EAR system that experienced damaging earthquakes in the past. In this thesis, seismic safety study conducted for large Ethiopian dams is presented. Accordingly, the following tasks were carried out:

- Review of the international state of practice on seismic design and lessons learned from the observed performance of dams from past earthquakes;
- Evaluation of seismic hazard assessment and seismic analysis reports conducted for various dams in Ethiopia and identification of main gaps in the hazard assessment and seismic analysis and design of large dams;
- Assessment geological and seismotectonic setup and related hazards at dam sites;
- Initial seismic hazard evaluation at 110 dam sites;
- Development of reference seismic zoning map for dams based on the probabilistic hazard analysis approach for earthquake return period of 10,000 years;

- Seismic risk analysis for 30 dams based on current seismic hazard analysis results and using Bureau (2003) method;
- Site-specific seismic hazard analysis at five selected dam sites;
- Two-dimensional seismic stability analysis of 4 dams for SEE ground motion;
- Stability analysis of abutment and reservoir slopes under earthquake loading and analysis of impulse waves generated by earthquake-triggered mass movement into the reservoir and possible risks on the safety of the dam.

The general conclusions and recommendations are highlighted in the subsequent sections.

1. Seismic Performance of Dams

Earthquakes have always played an important role in the design of new dams and safety evaluations of the existing ones. However, only few dams have experienced damaging earthquakes. From these few cases, some were damaged under earthquake loads that were less than the design loads. Others performed well under earthquake ground shaking that greatly exceeded the seismic design values witnessing that well-designed and well-constructed dams can perform well during strong earthquake.

2. Geological Considerations

The experience obtained from previous dam failures shows the need for extensive geological investigations at dam sites. The dam sites in Ethiopia are located in variable geological and tectonic settings, which play a key role in the safety of dams under normal operational and seismic conditions. In steep terrain, it is important to look specifically for potential sliding mass in the reservoir and stability of the abutment slopes under saturated and seismic conditions. Possibility of excessive settlement, pore water pressure development and liquefaction must be considered. Detailed geological mapping of the dam foundation and abutment slopes, to define the

discontinuities and potential sliding blocks, is essential. The impact of discontinuities in the dam foundation and uplift pressures must be considered in the sliding stability analysis of concrete dams.

In tectonically active regions like MER, faults are often found in dam foundations. Tectonic faults close to dam sites must be studied carefully. Sites with active faults in dam foundations should be avoided if possible. However, when a better site is not available, it is recommended to construct a conservatively designed embankment dam. The maximum fault displacement should be considered in the dam design. Concrete dams are not suitable for such sites.

3. Seismicity of the Region

The available earthquake catalogue of the East African Rift System is too short and the information on the historical seismicity is limited and incomplete. Strong earthquakes may have return periods of several hundred to thousands of years, depending on the seismotectonic conditions. Considering the short earthquake catalogue and the incomplete information on seismicity, the estimate of the seismic hazard is difficult and involves major uncertainties particularly for earthquakes with long return periods. Thus, additional information from the geological and tectonic history of the region is required for a proper seismic hazard analysis. This includes Quaternary geology and tectonic setup, seismic energy release, geothermal activity and observed seismicity.

4. Seismic Hazard Analysis

Site-specific seismic hazard analysis is usually recommended for large dam projects. Multiple earthquake effects on dams, such as ground shaking, fault displacement and mass movement into the reservoir etc. must be taken into account in the design and safety evaluation of dams. The seismic hazard analysis should be done for 10,000 years return period if a probabilistic seismic hazard analysis is carried out as

recommended by ICOLD (2016). It is assumed that no region is basically free from earthquakes and, therefore, all dams must be able to withstand some level of earthquake action. Where the seismicity is low and the information on historical seismicity is scarce, a longer return period should be used for large storage dams with high consequences like recommended in UK. The horizontal PGA-value of the SEE should not be less 0.15 g, as this corresponds roughly to a seismic coefficient of 0.1 used in the past for the seismic design of most dams.

5. Seismic Design Criteria

The present seismic hazard study shows that the seismic hazard is underestimated in most of the dam sites in Ethiopia. The seismic design criteria used during the construction of many dams do not comply with today's recommended state of practice. For older dams, the seismic design criteria used are unknown. Based on the present seismic hazard assessment results, it is recommended that the seismic safety of existing dams and the safety-critical elements like spillways and low level outlets must be rechecked for the updated earthquake ground motion. The dams can be subjected to stronger earthquakes than what is assumed in their design. Inelastic deformations may occur in dams; therefore, the seismic stability analysis has to be carried out in the time domain for dams with high-risk classes. Thus, the earthquake input must be in the form of acceleration time histories that match the target response spectra obtained from the site-specific seismic hazard analyses.

The safety-relevant elements used for controlling of the reservoir after a strong earthquake must be able to withstand the ground motions of the SEE. However, some of large storage dams in Ethiopia were constructed without bottom outlet. Therefore, lowering of the reservoir may not be possible after the SEE.

6. Seismic Failure Modes of Dams and Improvement Measures

An earthquake may cause deformations, settlement, liquefaction, etc. in a large dam. During strong earthquakes, an embankment or its foundation may lose its shear

strength due to the build-up of the pore pressure in sandy-silty material, which leads to excessive settlement and loss of freeboard followed by overtopping failure. Overtopping may also be caused by slope failures or rockfalls into the reservoir during an earthquake, displacing a large volume of water or due to impulse waves in the reservoir. Fault rupture in the footprint of a dam may cause differential settlement and cracking leading to internal erosion and piping in the foundation in embankment dams. Weak layers and discontinuities in the dam foundation may cause sliding of concrete gravity dams. Slope failures close to the dam may block the spillway and/or the intakes of low level outlets etc.

According to ICOLD (2001), a favorable seismic performance of gravity dams can be attained by the following design measures: maintenance of low concrete placing temperatures to reduce initial heat-induced tensile stresses and shrinkage cracking; including a good drainage system to reduce uplift pressure, providing well-prepared lift surfaces to maximize bond and tensile strength; utilization of shear keys in vertical construction joints; minimizing of discontinuities in the dam body to prevent local stress concentrations; increasing the crest width to improve the dynamic stability of the dam crest and avoiding a break in slope on the downstream faces of gravity dams to eliminate local stress concentration.

The main recommendations for the design and construction of embankment dams subjected to severe earthquake shaking are the following: foundation must be excavated to very dense layer; the loose foundation materials must be densified or removed to avoid excessive settlement and possibility liquefaction; fill materials that to build up significant pore water pressures during strong shaking must be avoided; different zones of the embankment must be thoroughly compacted to prevent excessive settlement during an earthquake; high capacity internal drainage zones to capture seepage from any transverse cracking caused by earthquakes; widened core sections at abutments to provide additional width at contacts; provision of filters on fractured rock to prevent piping of embankment materials into the foundation, wide filter and drain zones must be used to overcome offset of filter due to fault displacement at the footprint of the dam; a wide grout curtain (double or triple line) to minimize leakage of water through the dam foundation; sufficient freeboard should be

provided in order to compensate the settlement likely to occur during the earthquake and to prevent overtopping of the crest due to impulse waves in the reservoir; wide crest and compacting at optimum moisture or slightly above will help the embankment to be more flexible under seismic loading.

7. Dam Safety and Instrumentation

Several dams were constructed without any dam instrumentation. Standard dam monitoring instruments shall be installed including strong motion instruments (accelerographs). Different alarm levels must be specified for each instrument. An emergency action plan and early warning system should be in place, which is standard practice for large dam projects today.

A dam safety program based on a legal framework and design guidelines should be put into operation in Ethiopia by the dam safety supervisory authority. As the life-span of a large dam can be several hundred years, different seismic hazard analyses and seismic safety checks will be necessary when (i) new data are available, (ii) the risk classification of a dam has changed due to on-going developments, and (iii) new seismic safety and performance criteria have been introduced.

References

Abrahamson, N.A., Silva, W.J. and Kamai, R., 2014, Summary of the ASK14 Ground Motion Relation for Active Crustal Regions: Earthquake Spectra, v. 30, No. 3, p. 1025-1055.

Abrahamson, N. A., 1992, Non-stationary Spectral Matching: Seismological Research Letters, v. 63, No. 1, p. 30.

Asfaw, L. and Ayele, A., 2004, Report of the Dobi Graben Earthquake Swarm of August 1989: Proceedings of the Fourth EGMEA Congress, Addis Ababa, Ethiopia.

Ayele, A., 2017, Probabilistic seismic hazard analysis (PSHA) for Ethiopia and the neighboring region: Journal of African Earth Sciences, v. 134, p. 257–264, doi:10.1016/j.jafrearsci.2017.06.016.

Ayele, A., Ebinger, C., Alstyne, C., Keir, D., Nixon, W., Belachew, M. and Hammond, S., 2015, Seismicity of the central Afar rift and implications for Tendaho dam hazards, Geological Society, London, Special Publications.

Ayele, A., Alstyne, C., Ebinger, C. and Belachew, M., 2012, Seismicity and the Tendaho Dam Safety, Magmatic Rifting and Active Volcanism, Addis Ababa, Ethiopia, 11-13 January 2012.

Ayele, A., 1995, Earthquake catalogue of the horn of Africa for the period 1960–1993, Seismological Department Uppsala, Report 3-95.

Boccaletti, M., Mazzuoli, R., Bonini, M., Trua, T. andand Abebe, B., 1999, Plio-Quaternary volcanotectonic activity in the northern sector of Main Ethiopian Rift: Relationships with oblique rifting: Journal of Africa Earth Science, V. 29, p. 679 – 698.

Boccaletti, M., Bonini, M., Mazzuoli, R., Abebe, B., Piccardi, L. and Tortorici, L., 1998, Quaternary oblique extensional tectonics in the Ethiopian Rift (Horn of Africa): Tectonophysics, v. 287, p. 97–116.

Bohnhoff, M., Martínez-garzón, P., Bulut, F., Stierle, E., and Ben-zion, Y., 2016, Tectonophysics Maximum earthquake magnitudes along different sections of the North Anatolian fault zone: Tectonophysics, v. 674, p. 147–165, doi:10.1016/j.tecto.2016.02.028.

Bommer, J.J., Scherbaum, F., Bungum, H., Cotton, F., Sabetta, F. and Abrahamson, NA., 2005, the use of logic trees for ground-motion prediction equations in seismic-hazard analysis: Bulletin of the Seismological Society of America, Vol. 95, No. 2, p. 377–389, doi: 10.1785/0120040073.

Boore D.M., Stewart J.O., Seyhan E. and Atkinson G.M., 2014, NGA-West2 Equations for Predicting PGA, PGV, and 5% Damped PSA for Shallow Crustal Earthquakes, Earthquake Spectra, v. 30, p. 1057-1085.

Boore, D. and Joyner, W., 1997, Site amplifications for generic rock sites: Bulletin of the Seismological Society of America, v. 87 (2), p. 327−341.

Bureau, G.J., 2003, In: Chenh, W.F., Scawthorn, C. (Eds.), Dams and Appurtenant Facilities in Earthquake Engineering Handbook. CRS press, Bora Raton, p. 26.1–26.47.

Bureau, G., 1997, Evaluation Methods and Acceptability of Seismic Deformations in Embankment Dam, Proceedings of the 19th Congress on Large Dams, Florence, Italy.

Bureau, G and Ballentine, G.D., 2002, A Comprehensive Seismic Vulnerability and Loss Assessment of the State Of South Carolina Using HAZUS, Part VI, Dam Inventory and Vulnerability Assessment Methodology, 7th National Conference on Earthquake Engineering, July 21-25, Boston, Earthquake Engineering Research Institute, Oakland, CA.

Campbell K.W. and Bozorgnia Y., 2014, NGA-West2 Ground Motion Model for the Average Horizontal Components of PGA, PGV and 5% Damped Linear Acceleration Response Spectra, Earthquake Spectra, v. 30, p. 1087-1115.

Chiou B.S.J. and Youngs R.R., 2014, Update of the Chiou and Youngs NGA model for the average horizontal component of peak ground motion and response spectra. Earthquake spectra, v. 30, n. 3, p. 1117–1153.

Cornell, C.A., 1968, Engineering seismic risk analysis: Bulletin of the Seismological Society of America, v. 58, p. 1583-1606.

Delavaud, E., Cotton, F., Akkar, S., Scherbaum, F., Danciu, L., Beauval, C., Drouet, S., Douglas, J., Basili, R., Sandikkaya, MA., Segou, M., Faccoli, E. and Theodoulidis, N., 2011, Toward a ground-motion logic tree for probabilistic seismic hazard assessment in Europe: Journal of Seismology v. 16, p. 451–473. DOI 10.1007/s10950-012-9281-z.

EEP, 2014, Grand Ethiopian Renaissance Dam Hydroelectric Project, Seismic Hazard Analysis Report, Ethiopia electric Power, Addis Ababa.

EEP, 2013, Grand Ethiopian Renaissance Dam Hydropower Project, Seismic Hazard Analysis Report, Ethiopia electric Power, Addis Ababa.

EEP, 2013, Grand Ethiopian Renaissance Dam project site model, GERD hydropower project, Ethiopia electric Power, Addis Ababa.

EEP, 2012, Geological investigation report, GERD hydropower project, Ethiopia electric Power, Addis Ababa.

EEPCO, 2009. Gibe III project site model, Gibe III Hydroelectric Project, Ethiopia Electric Power Corporation, Addis Ababa.

EEPCO, 2008, Dam stability analysis report, Level 1 design, Gibe III Hydroelectric Project, Ethiopia Electric Power Corporation, Addis Ababa.

EEPCO, 2007, Seismic Hazard Analysis Report, Gibe III Hydroelectric Project, Ethiopia Electric Power Corporation, Addis Ababa.

EEPCO, 1997, Tekeze Feasibility Study Seismology Report, Hydroelectric Project, Ethiopia Electric Power Corporation, Addis Ababa.

Flagg, C.G., 1979, Geological cause of dam incidents: Bulletin of Association of Engineering Geology, v. 20, p196-201. https://doi.org/10.1007/BF02591282

Gani N.D., Abdelsalam M.G., Gera S., and Gani M.R., 2008, Stratigraphic and structural evolution of the Blue Nile Basin, Northwestern Ethiopian Plateau: Geological Journal. DOI: 10.1002/gj.1127.

Gardner, J.K., and L. Knopoff, 1974, Is the sequence of earthquakes in Southern California, with aftershocks removed, Poissonian? Bulletin of the Seismological Society of America v. 64 (5): p. 1363–1367

Gasparini, D., and Vanmarcke, E. H., 1976, SIMQKE: A Program for Artificial Motion Generation, Department of Civil Engineering, Massachusetts Institute of Technology.

Gazetas, G., and Dakoulas, P., 1992, Seismic analysis and design of rockfill dams: state-of-the-art: Soil Dynamics and Earthquake Engineering, v. 11, p. 27–61, doi:10.1016/0267-7261(92)90024-8.

GEO-SLOPE International Ltd., 2019, Seepage Modelling with SEEP/W 2019, An Engineering Methodology, Calgary, Alberta, Canada.

GEO-SLOPE International Ltd., 2019, Stress-Deformation Modelling with SIGMA/W 2019, An Engineering Methodology, Calgary, Alberta, Canada.

GEO-SLOPE International Ltd., 2019, Stability Modelling with SLOPE/W 2019, An Engineering Methodology, Calgary, Alberta, Canada.

GEO-SLOPE International Ltd., 2019, Dynamic Modelling with QUAKE/W 2019, An Engineering Methodology, Calgary, Alberta, Canada.

Goitom, B., Werner, M.J., Goda, K., Hammond, J.O.S., Ogubazghi, G., Oppenheimer, C., Helmstetter, A., Keir, D., and Illsley-kemp, F., 2017, Probabilistic Seismic-Hazard Assessment for Eritrea: v. 107, doi:10.1785/0120160210.

Gouin, P., 1979, Earthquake History of Ethiopia and the Horn of Africa, IDRC, Ottawa, 259.

Grünthal G., 1985, The up-dated earthquake catalogue for the German Democratic Republic and adjacent areas - statistical data characteristics and conclusions for hazard assessment, 3rd International Symposium on the Analysis of Seismicity and Seismic Risk, Liblice/Czechoslovakia, 17–22 June 1985, Proceedings Vol. I, p. 19–25.

Hagos, L., Arvidsson, R. and Roberts, R., 2006, Application of the spatially smoothed seismicity and Monte Carlo methods to estimate the seismic hazard of Eritrea and surrounding areas: Natural Hazards, v. 39, p. 395–418.

Hailemariam, T., 2009, Slope rock mass characterization in Tekeze hydropower reservoir: Implication to GIS based slope stability and reservoir impounding induced hazard analyses, PhD Dissertation, Department of Civil Engineering and Natural Hazards, University of Natural Resources and Applied Life Sciences, Vienna.

Heller, V., Hager, W. H., and Minor, H. E., 2009, Landslide generated impulse waves in reservoirs: basics and computation, Technical report, VAW, ETH Zurich.

Heller, V., 2007, Landslide generated impulse waves: prediction of near field characteristics, Dissertation 17531, ETH Zurich, Zurich

Hinks, J., Wieland, M. and Matsumoto, N., 2012, Seismic Behaviour of Dams, Proc. Int. Symposium on Dams for a Changing World, 80th ICOLD Annual Meeting, Kyoto, Japan.

Hofmann, C., Courtillot, V., Feraud, G., Rochette, P., Yirgu, G., Ketefo, E., and Pik, R., 1997, Timing of the Ethiopian flood basalt event and implications for plume birth and global change: Nature, v. 389, p. 838-841.

Hofstetter, R. and Beyth, M., 2003, The Afar Depression: Interpretation of the 1960–2000 earthquakes: Geophysical Journal International, v. 155, p. 715−732.

Huggett, R., 2007, Fundamentals of geomorphology, 2nd edition, Routledge Taylor and Francis Group, London and New York, p. 458.

ICOLD, 2016, Selecting seismic parameters for large dams, Guidelines, Bulletin 148, International Commission on Large Dams, Paris.

ICOLD, 2010, ICOLD position paper on dam safety and earthquake, ICOLD committee on seismic aspect of dam design, International Commission on Large Dams, Paris.

ICOLD, 2005, Dam foundations, Geologic considerations, investigation: methods, Treatment, Monitoring, Bulletin 129, International Commission on Large Dams, Paris.

ICOLD, 2002, Reservoir landslides: investigation and management, Guidelines and case histories, Bulletin 124, International Commission on Large Dams, Paris.

ICOLD, 1998, Neotectonics and Dams, Bulletin 112, Committee on Seismic Aspects of Dam Design,ICOLD, Paris.

ICOLD, 1989, Selecting Seismic Parameters for Large Dams, Guidelines, Bulletin 72, Committee on Seismic Aspects of Dam Design, ICOLD, Paris

Janusz, W., David, K. K, and Chyi-Tyi, L., 2000, Special Issue from the Symposium on Landslide Hazards in Seismically Active Regions: Journal of Engineering Geology, v. 58, p. 1-8, ELSEVIER.

JCOLD, 2014, Current Situation of JCOLD Activity about Seismic Data - Relevance of New Bulletin, Seismic Interpretation of Integrated Observation Data, Japan Committee on Large Dams, p. 1–7.

Kazmin, V., 1973, The geological map of Ethiopia, 1:2,000,000. Ethiopian Institute of Geological Surveys, Addis Ababa.

Kazmin, V., Shifferaw, A. and Balcha, T., 1978, The Ethiopian Basement: Stratigraphy and possible manner of evolution. Ethiopian Institute of Geological Surveys, Addis Ababa, P 1-9.

Kebede, F., and Asfaw L.M., 1996, Seismic Hazard assessment for Ethiopia and the neighbouring countries: Ethiopia Journal of Science, V. 19 (1), p. 15-50.

Keir, D., Ebinger, C., Stuart, G., Daly, E., and Ayele, A., 2006, Strain accommodation by magmatism and faulting as rifting proceeds to breakup: Seismicity of the northern Ethiopian rift: Journal of Geophysical Research, v. 111.

Lilhanand, K., and Tseng, W. S., 1988, Development and Application of Realistic Earthquake Time-Histories Compatible with Multiple-Damping Design Spectra, Proceedings of the 9th World Conference of Earthquake Engineering, Tokyo-Kyoto, Japan, August 2-9, Japan Association for Earthquake Disaster Prevention.

Lubkowski, Z., Villani, M., Coates, K., Jirouskova N, and Willis, M., 2014, Seismic design consideration for East Africa, 2nd European conference on earthquake engineering and seismology, 25-29 August 2014, Istanbul.

M. Leclerc, P. Leger, R.Tinawi, 2002, RS-DAM user's manual, University of Ecole Polytechnique of Montreal, Canada, (http://www.struc.polymtl.ca/rsdam/)

Makdisi, F., and Seed, H., 1977, A Simplified Procedure for Estimating Earthquake-Induced Deformations in Dams and Embankments, Report No. UCB/EERC-77/19, University of California, Department of Earthquake Engineering, p. 62.

Mammo, T., 2005, Site-specific ground motion simulation and seismic response analysis at the proposed bridge sites within the city of Addis Ababa: Journal of Engineering Geology, v. 79, p. 127–150.

Manighetti, I., Tapponnier, P., Courtillot, V., Gruszow, S., and Gillot, P.G., 1997, Propagation of rifting along the Arabia–Somalia plate boundary: Gulfs of Aden and Tadjoura: Journal of Geophysical Research 102, 2681–2710.

Matsumoto, N, Yoshida, H. and Kasai, T., 2011, Performance of the Ishibuchi CFRD during the Miyage earthquake. The International Journal of Hydropower and Dams, v. 18, Issue 1, p 52-55.

Midorikawa, S., Miura, H. and Ohmachi, T., 2008, Report on the 2008 Iwate-Miyagi-Nairiku, Japan Earthquake, Tokyo Institute of Technology, Japan.

Midzi, V., Hlatywayo, D., Chapola, L.S., Kebede, F., Atakens, K., Lombe, D. K., Turyomugyendo, G. and Tugume, F.A., 1999, Seismic hazard assessment in eastern and southern Africa, Annales di Geofisica, v. 42, p. 1067–1083.

Mohr, P.A., 1967, The Ethiopian Rift System: Bulletin of Geophysical Observatory v. 11, p. 1 – 65, Addis Ababa University.

Mohr, P., 1983, Ethiopian flood basalt province: Nature, v. 303, p. 577–584.

Mohr, P.A., 1989, Patterns of faulting in the Ethiopian Rift Valley: Tectonophysics v. 143, p. 169 – 179. Addis Ababa.

Monobe, N., Takata, A. and Matumura, M., 1936, seismic stability of earth dam, Trans. 2nd congress on large dams, Washington, D.C., Q VII, p. 435-444.

Müller, D., 1995, Auflaufen und Überschwappen von Impulswellen an Talsperren. VAW Mitteilung 137, Vischer, D., ed. ETH Zurich, Switzerland.

Mulargia F. and Tinti S., 1985, Seismic sample areas defined from incomplete catalogues: An application to the Italian territory, Physics of the Earth and Planetary Interiors, v. 40, p. 273-300.

MWH and Energoprojekt JV, 2011, Technical Record of Design and Construction. Tekeze Hydroelectric Project. Ethiopia Electric Power Corporation, Addis Ababa

Nuttli, O.W., Bollinger, G.A., and Herrmann, R.B., 1986, The 1886 Charleston, South Carolina, earthquake - A 1986 perspective: U.S. Geological Survey Circular, v. 985.

Newmark, N.M., 1965, Effects of Earthquakes on Dams and Embankments, Geotechnique, V. 15, No. 2, p. 139-160.

Ordaz, M., Martinelli, F., Aguilar, A., Arboleda, J., Meletti, C. and D'Amico, 2018, CRISIS Program for Computing Seismic Hazard, Instituto de Ingeniería, Universidad Nacional Autonoma de Mexico.

Poggi, V., Durrheim, R.,Tuluka, G.M., Weatherill, G., Gee, R., Pagani, M., Nyblade, A. and Delvaux, D., 2017, Assessing seismic hazard of the East African Rift: a pilot study from GEM and Africa Array: Bulletin of Earthquake Engineering, Springer Science.

Raghuvanshi, T. K., 2017, Plane failure in rock slopes – A review on stability analysis techniques: Journal of King Saud University – Science, King Saud University, v. 31(1), p. 101–109, Elsevier.

Reiter, L., 1994, Earth Hazard Analysis, Columbia University Press, New York.

Reasenberg P., 1985, Second-order moment of central California seismicity, 1969–1982, Journal of Geophysical Research, Solid Earth, v. 90, 3–18.

Sharma, S., Raghuvanshi, T. and Anbalagan, R., 1995, Plane failure analysis of rock slopes: Geot. Geol. Eng., V. 13, p. 105–111.

Schilling, G., Kingsley, H., Hanan, B., McCully, L., 1992, Nd–Sr–Pb isotopic variations along the Gulf of Aden: evidence for Afar mantle plume-continental lithosphere interaction: Journal of Geophysical Research, v. 97, p. 10,927–10,966.

Scordilis, E.M., 2006, Empirical global relations converting MS and mb to moment magnitude: Journal of Seismology, v. 10 (2), p. 225–236. https://doi.org/10.1007/ s10950-006-9012-4.

Seed, H.B., Wong, R.T., Idriss, I.M., and Tokimatsu, K., 1984, Moduli and damping factors for dynamic analyses of cohesionless soils. Report no. UCB/EERC-84/14, University of California, Berkeley.

Seed, H. B. and Idriss, I. M., 1970, Soil moduli and damping factors for dynamic response analysis. Report No. EERC 70-10. Berkeley: Earthquake Engineering Research Center, University of California, 1970.

Seged, H. and Haile, M., 2010, Earthquake induced liquefaction analysis of Tendaho earth-fill dam, Department of Civil Engineering, Addis Ababa University, v. 27.

Seismosoft Ltd., 2018, SeismoMatch, http://www.seismosoft.com/

Silva, W., and Lee, K., 1987, State-of-the-art for Assessing Earthquake Hazards in the United States, Report 24, WES RASCAL Code for Synthesizing Earthquake Ground Motions, Miscellaneous Paper S-73-1, U.S. Army Engineer Waterways Experiment Station, Vicksburg, MS.

Sun, J., Golesorkhi, R. and Seed H. B., 1988, Dynamic Moduli and Damping Ratios for Cohesive Soils, Earthquake engineering research center, Report no. UCB/EElC•881/5, University of California, Berkeley.

Tefera, M., Negussie T., Kebede, W., Teshome, K., 1996, Geological map of Ethiopia, Ethiopian Institute Geological Serveys, Addis Ababa.

Tiwari, B. and Ajmera, B., 2017, Landslides Triggered by Earthquakes from 1920 to 2015, Advancing culture of living with landslides, DOI 10.1007/978-3-319-53498-5. Springer International Publishing.

TTFR, 2011, Assessment of technical problems around the dam and proposed mitigation measure. Tendaho dam and irrigation project report, Ministry of water, irrigation and energy, Addis Ababa.

Uhrhammer, R.A., 1986, Characteristics of Northern and Central California Seismicity (abs), Earthquake Notes, V. 57, No. 1, p.21.

USACE, 2003, Time-History Dynamic Analysis of Concrete Hydraulic Structures, US Army Corps of Engineers, EM 1110-2-6051.

USACE, 2007, Earthquake Design and Evaluation of Concrete Hydraulic Structures, US Army Corps of Engineers, EM 1110-2-6053.

USSD, 2014, Observed performance of dams during earthquakes, v. III. US Society on Dams, Denver, p 130

USCOLD, 2000, Observed performance of dams during earthquakes. US Committee on Large Dams, v. II, Denver, p. 162

USCOLD, 1992, Observed performance of dams during earthquakes, US Committee on Large Dams, Denver, v. I, p 129

Van Stiphout, T., J. Zhuang, and D. Marsan, 2012, Seismicity declustering, Community online resource for statistical seismicity analysis, doi:10.5078/corssa52382934. Available at http://www.corssa.org.

Vucetic, M. and Dobry, R., 1991, Effect of Soil Plasticity on Cyclic Response: Journal of Geotechnical Engineering, v. 117, no. 1, ASCE.

Wells, D. and Coppersmith, K., 1994, New empirical relationships among magnitude, rupture length, rupture width, rupture area, and surface displacement: Bulletin of the Seismological Society of America, v.. 84, No. 4, p. 974−1002.

Wesnousky, S.G., 1986, Earthquakes, Quaternary Faults, and Seismic Hazard in California: Journal of geophysical research, v. 91, n. B12, p.12,587-12,631.

Westergaard, H., 1933, Water pressure on dams during earthquakes, Transaction of ASCE, v. 98.

Wieland, M., 2019, Limitations of risk and probabilistic safety analyses for large storage dams, International Dam Safety Conference proceedings, Bhubaneswar, Odisha, India, 13-14 February 2019.

Wieland, M. and Brenner, R.P., 2015, Performance criteria for rockfill dams subjected to multiple seismic hazards. Proc. ICOLD Congress, Stavanger, Norway, June 2015

Wieland, M., 2008a, Large dams the first structures designed systematically against earthquakes, Special Session S13, Proc. 14th World Conf. on Earthquake Engineering, Beijing, China, Oct. 12-17, 2008

Wieland, M., Brenner, R.P. and Bozovic, A., 2008, Potentially active faults in the foundations of large dams part I: Vulnerability of dams to seismic movements in dam foundation, Special Session S13, Proc. 14th World Conf. on Earthquake Engineering Beijing, China, Oct. 2008

Wieland, M. and Brenner, R.P., 2005, Earthquake aspects of concrete-face rockfill dams, diaphragm walls and grout curtains, Proc. Symposium on CFRD and 20th Anniversary of China's CFRD Construction, Yichang, China, Sept. 19-24, 2005

Wiemer, S., 2001, A software package to analyse seismicity: ZMAP. Seismological Research Letters: 373–382. https://doi.org/10.1785/gssrl.72.3.373.

Wolfenden, E., Ebinger, C., Yirgu, G., Deino, A., and Ayalew, D., 2004, Evolution of the northern Main Ethiopian rift: birth of a triple junction: Earth and Planetary Science Letters, v. 224, p. 213–228, doi:10.1016/j.epsl.2004.04.022.

Wright, T.J., Ebinger, C., Biggs, J., Ayele, A., Yirgu, G., Keir, D., Stork, A., 2006, Magma-maintained rift segmentation at continental rupture in the 2005 Afar dyking episode: Nature, v. 442, p. 291–294.

WWDSE, 2007, Geology and Structure of the Tendaho Dam and Irrigation Project Area with Particular Emphasis to Evaluating Reservoir Area Water Tightness. Tendaho dam and Irrigation Project, Ministry of Water Resources, Addis Ababa

WWDSE, 2006, Dynamic analysis conducted to identify liquefiable soil, Tendaho dam and Irrigation Project, Ministry of Water Resources, Addis Ababa

WWDSE, 2005, Tendaho Dam Final Design Report, Tendaho dam and Irrigation Project, Ministry of Water Resources, Addis Ababa

Yamaguchi, Y.; Kondo, M. and Kabori, T., 2012, Safety Inspections and Seismic Behavior of Embankment Dams during the 2011 off the Pacific Coast of Tohoku Earthquake, The Japanese Geotechnical Society Soils and Foundations, December, http:www.elsevier.com/locate/sandf

Yegian, M.K., Marciano, E.A. and Ghahraman, V.G., 1988, Integrated seismic risk analysis of earth dam, Department of Civil Engineering, Northeastern University Boston, Massachusetts, Report no. CE-88-15.